UNITED STATES DEPARTMENT OF THE INTERIOR

GEOLOGICAL SURVEY

CHEMICAL AND MINERALOGICAL VARIATION IN THE PIONEER BATHOLITH, SOUTHWEST MONTANA

by

Jane Marie Hammarstrom

82-143

Open-File Report ~~81-~~

This report was originally submitted in partial fulfillment of the requirements for the degree of Master of Science from Virginia Polytechnic Institute and State University, August, 1981. This report is preliminary and has not been reviewed for conformity with U.S. Geological Survey editorial standards or stratigraphic nomenclature. Any use of trade names is for descriptive purposes only and does not imply endorsement by the USGS.

1981

Contents

Contents (Continued)

Introduction

The Pioneer Batholith is a Late Cretaceous to Paleocene composite batholith located in the Pioneer Mountains of southwestern Montana. Interest in this batholith stems from its proximity and gross similarities to the larger Boulder and Idaho Batholiths and from the diversity of rocks emplaced in a relatively short geologic time span. The spatial relationship of the Pioneer Batholith to other major intrusions in the area is shown in Fig. 1.

Recent studies in the eastern Pioneer Mountains by Zen and others (1975), Zen (1977, 1980) and Snee (1978) reveal more than 15 mappable granitoid plutons ranging from Cretaceous hornblende gabbros, quartz diorites, granodiorites and granite to Paleocene muscovite granites. Concurrent investigations of whole rock initial strontium ratios and radiometric ages led Zen, Arth and Marvin (1980) to suggest that two magmas were active in the upper crust contemporaneously. Mixing of magmas, differentiation within each magma, assimilation of country rock, or a combination of processes may account for the diversity of rock types and initial strontium values.

This study was undertaken to 1) characterize major plutons in the northeastern part of the Pioneer Batholith in terms of modal mineralogy and rock chemistry, 2) determine mineral compositions by microprobe analysis, and 3) assess minerals as indicators of intensive parameters during crystallization. Results of this study will contribute to a larger study aimed at defining the tectonic framework of the Pioneer Mountains.

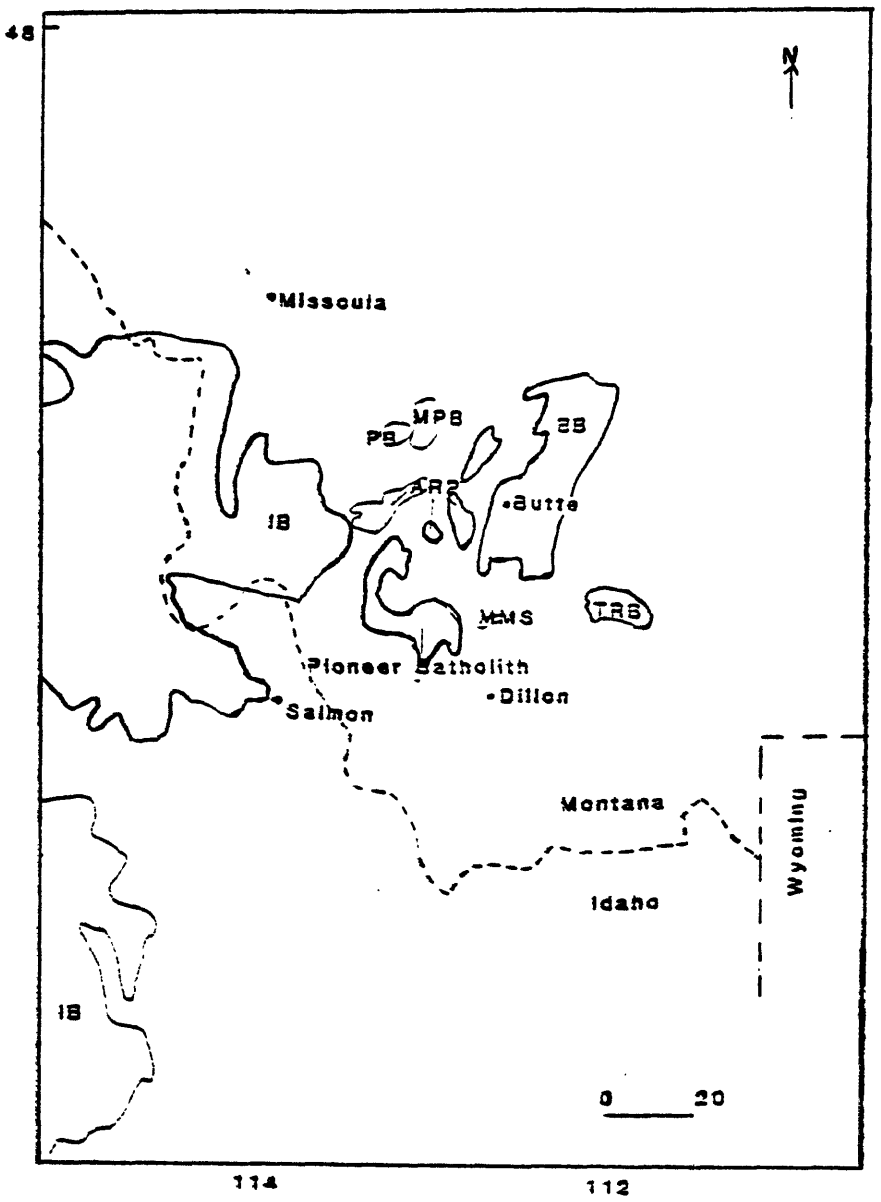

Figure 1. Map of major intrusions in southwestern Montana and eastern Idaho. Symbols for intrusions are as follows:

IB: Idaho Batholith
BB: Boulder Batholith
MPB: Mount Powell Batholith
PB: Philipsburg Batholith
ARP: Anaconda Range Plutons
TRB: Tobacco Root Batholith

Previous work

Early geologic investigations in the Pioneer Mountains concentrated on the geology of the mining centers in the area (Karlstrom, 1948; Myers, 1952; Theodosis, 1956; Pattee, 1960) and grouped most of the granitoid rocks as quartz monzonite, presumably related to the Butte Quartz Monzonite of the nearby Boulder Batholith. Myers (1952) distinguished granite from quartz monzonite (granodiorite by Streckeisen's 1973 classification of plutonic rocks) at Brown's Lake in the southeastern corner of the Vipond Park quadrangle where scheelite-bearing skarns occur at the contact of the intrusion with carbonate rocks of the Pennsylvanian Amsden Formation. Collins (1975, 1977) studied these garnet-pyroxene skarns and concluded that mineralization resulted from fluids diffusing outward from the intrusion at temperatures in the range 400 to 725°C at an oxygen fugacity (f_{O2}) around 10^{-20} and total pressure on the order of 0.75 kilobars, based on observed mineral assemblages and stratigraphic thickness. In 1970, E-an Zen began a study of the tectonic framework of the Pioneer Mountains. This study involved mapping of the Vipond Park, Maurice Mountain and Stine Mountain quadrangles at a scale of 1:62,500 and concomitant studies of the age, chemistry and isotope systematics of the intrusive and volcanic rocks. Table I summarizes these studies to date. Zen and others (1975) published a preliminary report on the age, chemistry and petrography of intrusive and contact-metamorphosed rocks. Zen reported on the volcanic rocks in the Vipond Park quadrangle (Zen and others, 1979) and summarized the initial strontium data (Zen, Arth and Marvin, 1980). Snee (1978) mapped parts of the Torrey Mountain, Twin Adams and Polaris quadrangles

TABLE I. Summary of current studies on the Pioneer Batholith

METHOD OF STUDY	SCOPE	REFERENCE
1. mapping	northeastern Pioneer Batholith	Zen, 1975-1980
	southeastern Pioneer Batholith	Snee, 1978
2. radiometric ages	K/Ar on mineral separates	Marvin, in Zen and others (1975) Snee, 1978
	K/Ar on whole rock splits	Marvin, unpublished
	fission track on sphene	Naesar, unpublished
	Rb/Sr on whole rock splits	Arth, unpublished
3. initial strontium	whole rock splits	Arth, (in Zen and others, 1980)
4. lead isotopes	potassium feldspar separates	Doe, unpublished
	galenas	
5. oxygen isotopes	δO^{18} on whole rock splits	O'Neil, unpublished
6. major element	rapid rock analyses	this study, analyses by Analytical Laboratories, USGS
7. trace element	instrumental neutron activation analyses	this study, analyses by Analytical Laboratories, USGS
8. mineral chemistry	microprobe analyses	this study
9. petrography	modal analyses	this study
	thin section study	

which cover the southeastern portions of the batholith. Snee reported on petrography and K/Ar ages for intrusive and volcanic rocks in his map area. Snee and Sutter (1978) presented data on whole rock chemistry for the southeastern part of the batholith. Snee is currently continuing his mapping to the west and conducting an extensive study of the cooling history of the batholith. Regional geochemical studies in the Pioneer Mountains are being conducted as part of the U.S. Geological Survey's CUSMAP* program. Berger and others (1979) reported preliminary results of reconnaissance geochemical exploration in the southern Pioneer Mountains where several important mining districts (Au,Ag,Cu, Pb,Zn, W) are located. Berger and others describe two main phases of mineralization: 1) an early contact metasomatism represented by high temperature (400-600°C) skarns rich in tungsten and molybdenum and poor in base metals and 2) a lower temperature system of fracture controlled vein deposits which cut the skarns and host base metal deposits. On the basis of similarities in trace element suites from one deposit to another, Berger and others suggested that a common genetic process may account for much of the mineralization in the area.

Pearson and Berger (1980) reported on three bodies of hydrothermally altered rock which contain molybdenite. All three are located in the central Pioneer Range and are associated with quartz porphyries intruded into the main granodiorite pluton of the batholith. K/Ar dates of 66 and 69 Ma on muscovite from altered rock led Pearson and

*CUSMAP: Conterminous United States Mineral Assessment Program

Berger to suggest that the quartz porphyry may represent a late stage in the crystallization of the Pioneer Batholith. Although the rocks have a greisen-like appearance, no actual greisen minerals, such as tourmaline, fluorite or topaz, were found.

Farther north, at Cannivan Gulch in the Vipond Park quadrangle, a molybdenum deposit associated with potassic alteration of a Late Cretaceous biotite granodiorite stock is currently being developed. Schmidt and Worthington (1977) described this deposit and reported K/Ar ages in biotite from the granodiorite (67-68 Ma), coarse hydrothermal vein muscovite (59-62 Ma) and vein adularia (55 Ma) and concluded that mineralization post-dated granodiorite emplacement by at least 6 million years.

Geology of the Pioneer Batholith

The Pioneer Range trends north-south and is divided in half along its length by the Wise River valley. The western Pioneer Range is largely composed of Precambrian quartzites thrust eastward over Paleozoic sedimentary rocks and intrusive rocks. The eastern Pioneers consist of Phanerozoic sedimentary rocks and granitoid rocks of the batholith. Snee (1978) described the regional geolgic and structural setting of the Pioneer Batholith.

A modified compilation of Zen's map of the Vipond Park, Maurice Mountain and Stine Mountain quadrangles and Snee's 1978 map of parts of the adjacent Torrey Mountain, Twin Adams and Polaris quadrangles is shown in Fig. 2. Four groups of plutonic rocks (field names) are indicated on the map: 1)Cretaceous quartz diorites and more mafic rocks (Kpd), 2) Cretaceous tonalites (Kpt) and granodiorites (Kpgr), 3) Cretaceous granites (Kpg) and border phase porphyritic granodiorite (Kpp) and 4) Tertiary muscovite granites (Tpg). Areally minor ultramafics of uncertain association occur as xenoliths in quartz diorite at Cherry Lake in the Vipond Park quadrangle. Snee mapped hornblende gabbro along the southern margins of the batholith in the Polaris quadrangle. Other mafic rocks (pyroxenites, gabbros) occur just north of the the northern boundary of the Vipond Park quadrangle, near Dewey, Montana; these are currently under study by Glen Zinter of SUNY, Buffalo. The largest plutons in the eastern Pioneers are the granodiorite pluton (Kpgr) that occupies most of the southeastern corner of the batholith and the Cretaceous granite (Kpg). Porphyritic variants of both these plutons occur. The map unit "Kpgr" includes Snee's (1978) major granodiorite

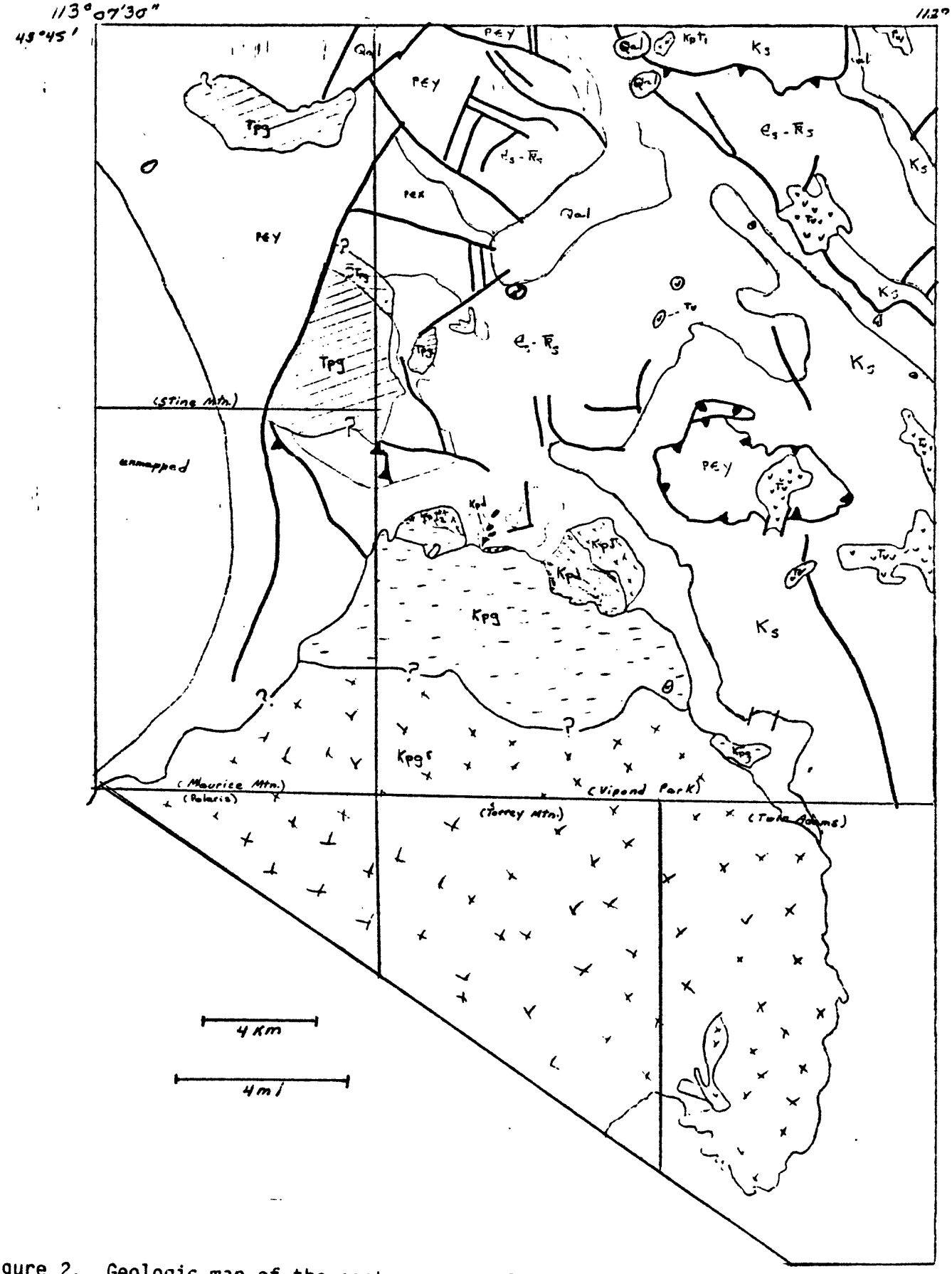

Figure 2. Geologic map of the eastern part of the Pioneer Batholith. This map is a simplified compilation of maps by Zen (unpublished) and Snee (1978). Quadrangle names shown in parentheses.

pluton which is continuous into Zen's map area to the north, as well as several fine-grained biotite tonalites and another granodiorite of local occurrence which are intrusive into the main granodiorite. Snee (1978) observed that internal variations in texture and mineralogy in the major granodiorite are of local occurrence in areas bounded by different types of country rock. He proposed the possibility that these variations may represent assimilation of different types of country rock into the magma by stoping during emplacement. Textural variations may also result from tapping of different levels of the magma chambers, i.e., fine-grained variants may have cooled quickly as the result of a pressure quench. Alaskites, pegmatites and a variety of dikes crosscut the plutons.

The area immediately east and north of the batholith is occupied by Cambrian (C_S - Tr_S) to Cretaceous (K_S)sedimentary rocks and Tertiary volcanics (Tv). Zen and others (1979) reported on these volcanics which consist of several fields of Eocene (47-51 Ma, K/Ar whole rock) flows ranging from andesite to rhyodacite, one area of Miocene (21 Ma, K/Ar whole rock) basalt, and a 50 Ma (K/Ar biotite) shallow rhyolite vitrophyre intrusion. Initial strontium ratios for these rocks range from .7064.7098, similar to ranges observed for the post-intrusive Lowland Creek Volcanics associated with the Boulder Batholith. No extensive pre-intrusive volcanic field comparable to the Elkhorn Mountain Volcanics of Boulder Batholith terrane is observed in the Pioneers. However, Snee (1980) mapped volcanics along the southern margins of the batholith which include a 70 Ma dacite (whole rock $^{40}Ar/^{39}Ar$ age). This is the only evidence for volcanism associated with plutonism in the

Pioneer Batholith encountered so far.

On the west, the batholith intrudes Precambrian rocks. Zen (written communication) has mapped two groups of Precambrian rocks, which are indicated as PCY and PCX on the map. PCY rocks are predominently quartzites, similar to the rocks of the Belt Series. PCX rocks consist of feldspathic gneisses and amphibolites (1634 m.y. Rb/Sr isochron, Arth, written communication). Arth investigated the Rb/Sr systematics of these rocks and Zen and others (1980) suggested that such terranes are candidate source rocks for the granitoids on isotopic grounds.

Field Relations

The batholith intrudes a sequence of Paleozoic sedimentary rocks with little accompanying deformation. Contacts with country rock are generally sharp and in places a narrow, high temperature-low pressure contact aureole represented by the assemblage cordierite-andalusite-biotite is developed (Zen and others, 1975). In the Vipond Park quadrangle Zen worked out an intrusive sequence based on field relations and presented supporting radiometric ages on biotite and hornblende. Inclusions of quartz diorite were observed in the porphyritic granodiorite border phase of the main Cretaceous granite pluton. The relationship between the two major plutons, the Cretaceous granite and granodiorite, is less clear. In places, the granite cuts the grandiorite and truncates the primary foliation in it; elsewhere, the conact appears to be gradational. Mafic schlieren and discoid mafic inclusions, many of which are probably cognate, are common to both rocks. Miarolitic cavities, though restricted in occurrence are observed in the granodiorite.

Age

K/Ar ages on biotite and hornblende mineral separates from plutonic rocks range from 65 to 78 million years (calculated using current decay constants). Data are taken from Zen, Marvin and Mehnert (1975), Snee (1978), and Zen, Arth and Marvin (1980). Snee (1978) reported a disturbed age of 116 Ma for hornblende from a hornblende gabbro in the southernmost part of the batholith. This is the oldest age reported for such rocks from the area, but Ar release studies by Snee indicate that it is not a geologically significant age. Ages for the main granodiorite and granite plutons overlap. Agreement between biotite and hornblende ages from a typical granodiorite (sample IVP) and for a porphyritic border phase of the main Cretaceous granite pluton (sample BH9850) is within experimental error.

Snee (1978) analysed four biotite-hornblende pairs in the extensive granodiorite pluton in the southeastern part of the batholith (same pluton as sample IVP) by conventional K/Ar methods and found hornblende ages slightly older (~2 Ma) than ages for coexisting biotite. Snee (1978) discussed two possibilities for this discrepancy: 1) post-crystallization reheating may disturb biotite ages more readily than hornblende ages because hornblende has a higher "closing" temperature with respect to K/Ar or 2) differences in age may represent actual time involved in cooling from hornblende (400-500°C) to biotite (180-260°C) closing temperatures.

Zen and others (1975) suggested that the large age discrepancy between hornblende (78.3 ± 2.1 Ma) and biotite (72.6 ± 2.7 Ma) in the

quartz diorite probably results from metamorphism of the quartz diorite by later intrusion of the granite. Zen mapped a contact-metamorphosed dioritic border facies of the granite.

Ages of the two muscovite granite plutons are around 65 Ma (K/Ar on biotite).

Strontium isotopes

Initial strontium (S_i) ratios on dated whole rock samples were determined by Arth (Zen and others, 1980). The values for the intrusive rocks cluster in two distinct groups. The main Cretaceous granite pluton and a small, porphyritic granodiorite border pluton have S_i = 0.7132-0.7138 whereas the quartz diorite and granodiorite and Paleocene muscovite granite have S_i = .7113-.7118. Zen and Arth suggest that the tight clustering of S_i values as two contemporaneous magmas, which may have mixed to produce a gradational zone between granite and granodiorite in places. Suspected "mixed" rock has characteristics of both adjacent rocks and an intermediate S_i. All initial strontium values are significantly higher than those observed for the Boulder Batholith, which range from 0.705 for Rader Creek granodiorite to 0.710 for the leucocratic rocks of the Donald and Hell Canyon plutons (Doe and others,1968).

Initial strontium ratios for the extensive Butte Quartz Monzonite range from 0.7065-0.7077.

Modal Analyses

Representative samples of the major plutons were chosen for modal analysis of stained slabs (Fig. 3). Table II contains the results of counting a minimum of 1000 points on slabs selectively stained for potassium feldspar and plagioclase. The area counted for each rock exceeded 150 cm^2. Biotite, hornblende and accessory minerals are grouped as "mafic" minerals as they cannot be adequately distinguished on stained slabs. Normalized quartz-potassium feldspar-plagioclase ratios are plotted in Fig. 4 on the ternary diagram used by Streckeisen (1973) to classify plutonic igneous rocks. Most of the rocks fall within the granodiorite field; rocks referred to in the field as granite (Kpg) actually fall within the granodiorite field on the diagram near Streckeisen's granite boundary. There is no distinct clustering of points by map unit. The samples from the southern part of the Kpgr pluton plot closest to the quartz diorite field on the diagram; samples from the northern part of the pluton, closest to the granite contact are relatively richer in "granite" components (alkali feldspar, quartz). The rocks south of the inferred granite-granodiorite contact are typically medium-grained to locally porphyritic granodiorites and tonalites composed of plagioclase, anhedral white potassium feldspar megacrysts which host inclusions of all other minerals in the rock, quartz, hornblende, biotite, sphene, magnetite and accessory minerals (apatite, epidote, allanite, zircon). Rocks north of the contact contain relatively clean pink potassium feldspar phenocrysts, less hornblende and more epidote than Kpgr. The Tertiary muscovite granites occur in discrete plutons north of the main Cretaceous granite pluton.

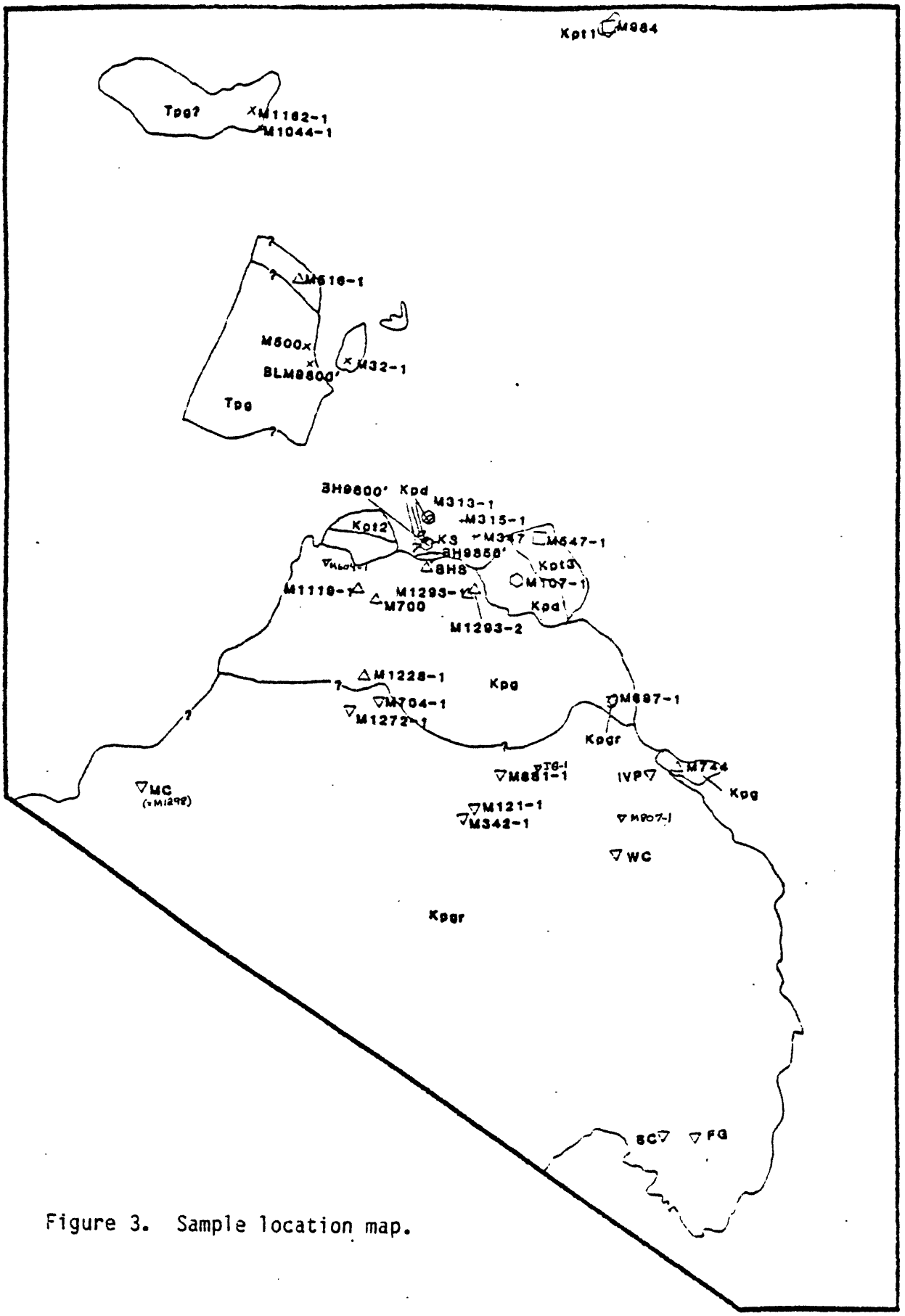

Figure 3. Sample location map.

Table II. Modal analyses of stained slabs from representative samples of major plutons in the Pioneer Batholith (volume per cent)

MAP UNIT	Kpd	Kpt_1	Kpt_3	Kpgr				
SAMPLE	M313-1	M984-1	M547-1	M807	FG	IVP	IVP	M1272-1
ALKALI FELDSPAR	0	0.1	5.8	13.0	13.4	13.2	9.3	16.1
PLAGIOCLASE	55.9	51.0	50.6	53.3	51.8	49.6	50.0	45.9
QUARTZ	7.4	9.6	19.6	23.0	20.7	23.7	24.8	27.3
MAFIC MINERALS	36.3	39.2	24.0	10.4	13.9	13.4	15.3	10.5
OTHER	0.4	0	0	0.3	0.2	0.1	0.6	0.1

MAP UNIT	Kpgr							Kpp	Kpg
SAMPLE	M121-1	M881-1	M342	M1298-1	M704-1	BC	JG1	BH9850-1	M1228-1
ALKALI FELDSPAR	18.6	17.7	14.9	14.7	19.3	7.4	15.2	12.5	15.4
PLAGIOCLASE	45.6	45.0	44.3	40.6	39.6	49.4	46.8	47.5	46.6
QUARTZ	24.7	28.7	28.7	31.6	29.5	30.4	26.0	21.2	27.9
MAFIC MINERALS	10.6	8.4	11.7	12.9	11.4	12.7	11.6	18.5	10.3
OTHER	0.4	0.2	0.4	0.1	0.2	0	0.3	0.2	0.1

MAP UNIT	Kpg						Tpg		
SAMPLE	M1293-1	M1293-2	M700-1	M604-1	BHS	M1120	M500	BLM 9800	M32-1
ALKALI FELDSPAR	13.3	14 .2	12.5	17.4	23.3	26.2	21.9	19.5	20.2
PLAGIOCLASE	45.9	42 .7	41.5	38.8	37.7	35.2	34.3	36.7	47.2
QUARTZ	28.2	31 .4	30.3	35.0	34.2	34.5	34.8	35.8	27.5
MAFIC MINERALS	12.5	11 .6	15.4	8.6	4.7	4.0	8.8	7.2	4.9
OTHER*	0.1	0 .1	0.2	0.2	0.1	0.1	0.2	0.8	0.2

*Includes muscovite

Modal analyses show that these are granites; they consist of plagioclase, white potassium feldspar phenocrysts, quartz, biotite, muscovite and accessory minerals.

Although the more mafic rocks form small plutons at the outer margins of the batholith, no simple zoning pattern of rock type from rim to core of the whole batholith is observed. Concentrically zoned plutons, where temperature decreases from rim to core as magma solidifies inward from quartz diorite margins through granodiorite and granite to a porphyritic granite core have been described for similar calc-alkalic complexes (e.g., Tuolumne Series in the Sierra Nevada Batholith, Bateman and Chappell, 1979). In the Pioneers, neither granites nor porphyritic phases are confined to interior regions. The crude south to north trend of increasing volumes of exposed granite may reflect structural control on emplacement or post-emplacement modification.

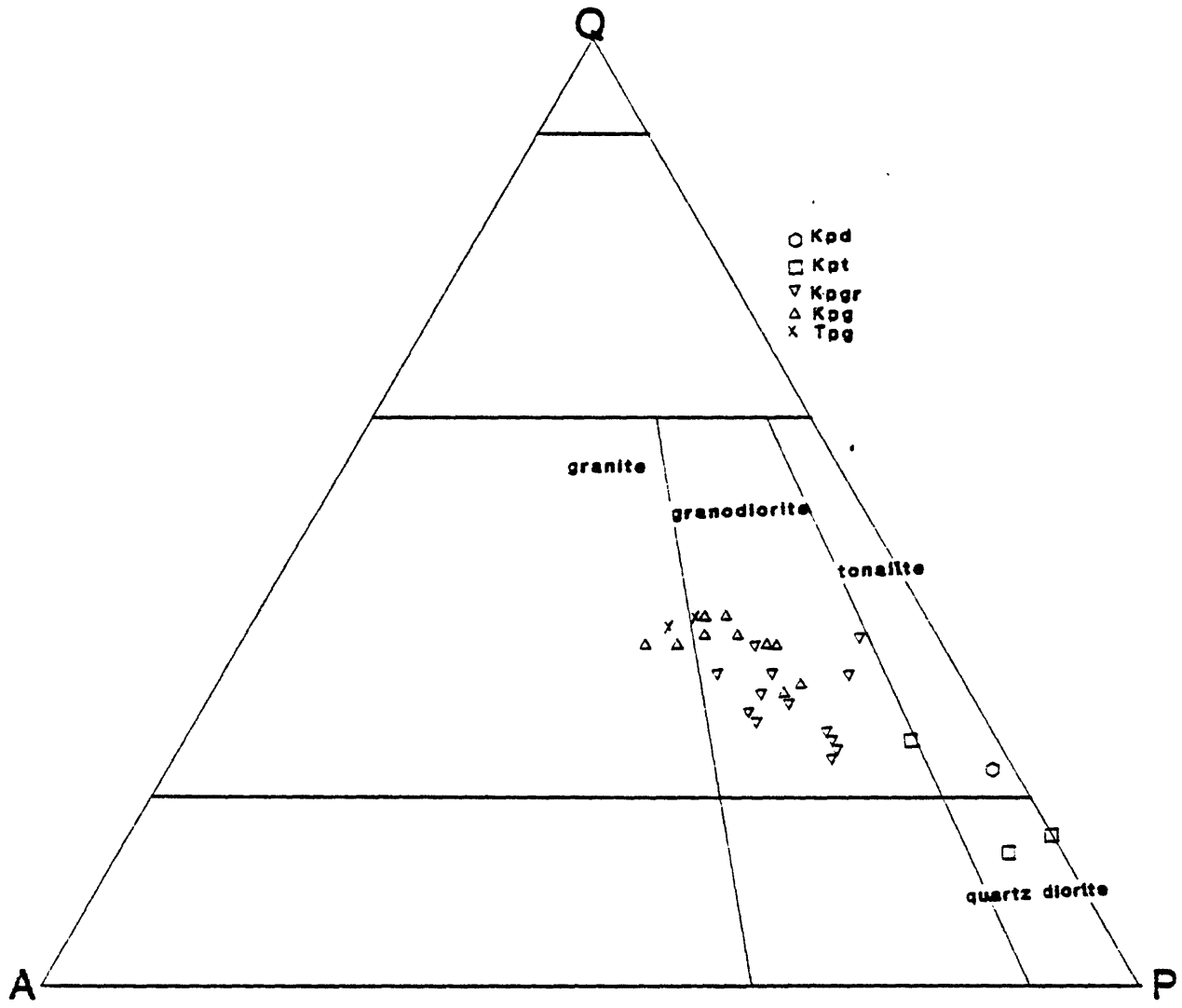

Figure 4. Quartz-alkali feldspar-plagioclase (Q-A-P) diagram for Pioneer rocks based on modal analysis of stained slabs. Rock names and field boundaries from Streckeisen (1973).

Petrography

Zen, Marvin and Mehnert (1975) briefly described representative samples of 5 major intrusive rock types in the Pioneer Batholith and presented age, chemical, and modal data on them. Snee (1978) described rocks in the southern part of the batholith. The following descriptions of the major rock units reflect study of samples collected by Zen and Snee, as well as their earlier observations. Modal analyses were performed on representative samples of each pluton (see Fig. 3 for locations) to estimate biotite, hornblende and accessory mineral abundances. A minimum of 1000 points was counted per thin section. Table III summarizes the modal data.

The following petrographic descriptions are based on thin section study of about 100 samples. Only those samples for which other types of data are available are indicated on the sample map in Fig. 3.

Cretaceous quartz diorite

Three small areas of outcrop of medium to fine grained dark grey quartz diorite occur near the northeastern edge of the batholith in the Vipond Park quadrangle. All three are separated from the main body of the batholith and from each other by Paleozoic sedimentary rocks. A larger area of quartz diorite, sandwiched between tonalite on the northeast and metamorphosed quartz diorite on the southwest, lies a few kilometers away. The altered quartz diorite was presumably hydrated by intrusion of the adjacent Cretaceous granite.

The quartz diorites are heterogeneous, ranging from fine to medium grained to porphyritic. Zen, Marvin, and Mehnert (1975) presented modal data on sample 313, from one of the small plugs farthest away from the

granite. Other samples of quartz diorite exhibit varying degrees of alteration. Typical textures are shown in the photos in Fig. 5. Pleochroic subhedral to anhedral hornblende is the most abundant mafic mineral in the quartz diorite. In some samples, hornblende is characterized by brownish cores with green rims; in other samples, all hornblende is green but displays patchy coloration. A high-relief, non-pleochroic colorless to light green mineral forms the the core of some hornblendes and may represent relict augitic-diopsidic pyroxene. Small grains of an iron oxide are concentrated in light green altered areas (felted mat texture) in some hornblende cores. Hornblendes are commonly twinned and often host patches of brown biotite. Apatite and small opaque inclusions are common. A distinct blue-green rim is observed on parts of some hornblende grains and may be another (sodic?) amphibole. Biotite is brown, pleochroic, generally ragged in appearance.Some biotite is bent and shows sweeping extinction. Much of the biotite is disrupted at plagioclase contacts where small (<0.1 mm), anhedral grains of sphene are concentrated. Chlorite and granular sphene occur along biotite cleavages and epidote is observed with chlorite. Larger (up to 0.5 mm across) anhedral grains of sphene occur with magnetite adjacent to biotite and hornblende.

Euhedral zoned and twinned plagioclase laths (length to width 2:1 or greater) appear to be an early phase. Degree of alteration varies from sample to sample. Inclusions of magnetite and apatite are common.

Potassium feldspar is rare to absent. Where present, it is anhedral, non-perthitic, untwinned, occasionally zoned, occupies areas up to 1mm across and is interstitial to all other minerals in the rock. Though generally clean, potassium feldspar sometimes contains inclusions of plagioclase.

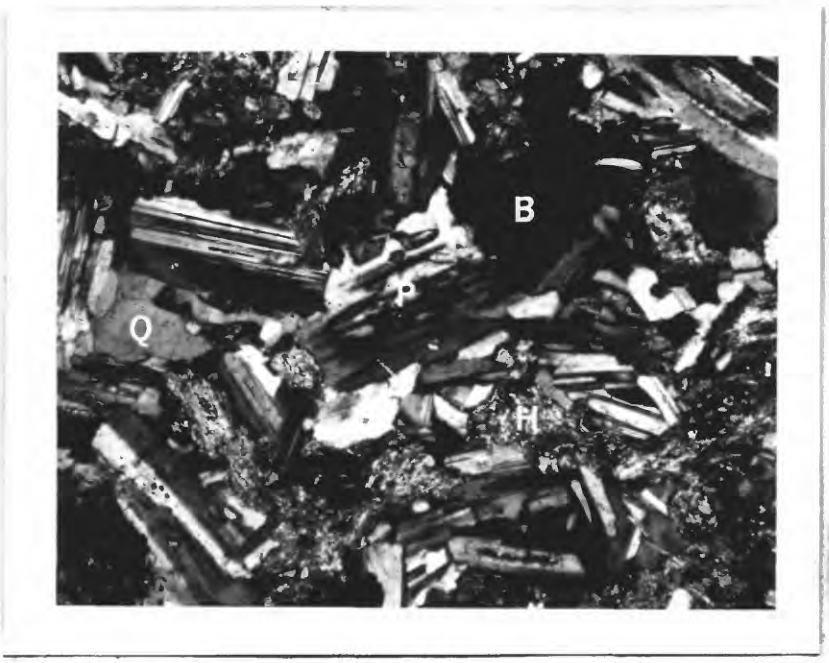

Figure 5. Photomicrograph of Kpd sample M130-2 showing typical quartz diorite texture. Field of view is 3mm wide. Crossed nicols.

P=plagioclase H=hornblende Q=quartz

B=biotite

Quartz occurs in anhedral grains displaying sweeping extinction and also occurs interstitially. Apatite is ubiquitous as euhedral hexagons and 0.2mm rounded grains.

Heterogeneity of quartz diorite samples precludes a generalized sequence of crystallization for the rock. However, textural relations suggest that plagioclase, at least some of the iron oxide (?magnetite) and apatite began to crystallize early. Biotite-hornblende relations are unclear. Hornblende appears to be replacing an early pyroxene phase; patches of biotite in hornblende are more common than hornblende in biotite. The interstitial nature of quartz in samples lacking potassium feldspar suggests that it began crystallizing late, and where potassium feldspar is present, it appears to come in later than quartz. The intimate association of sphene with ferromagnesian minerals and the lack of euhedral sphene rhombs suggest that sphene may have formed during subsolidus reequilibration reactions involving Ti-bearing biotite and plagioclase rather than a primary magmatic phase.

Cretaceous tonalites

Three separate plutons of tonalite, designated Kpt_1, Kpt_2 and Kpt_3 on the map in Fig. 3, were outlined by Zen. Kpt_1 is a small, highly weathered pluton with poor outcrop at the northern edge of the Vipond Park quadrangle. Kpt_1 has not been dated; it is probably Cretaceous, but may be related to a more mafic group of rocks just to the north. Kpt_2 and Kpt_3 are medium- to fine-grained border phases lying north and east of the main Kpg pluton. Kpt_1 is spatially and petrographically distinct from the others and will therefore be discussed separately. Kpt_1 is characterized by the presence of distinctly colored 1+ mm

subhedral hornblendes. Hornblende cores are generally brown and grade outward to green rims. Some cores are altered to chlorite, a highly birefringent phase and opaques. No pyroxene was observed, but altered hornblende cores may represent relict pyroxene.

Twinned and zoned plagioclase laths average 1.5mm in length and commonly occur as inclusions in hornblendes. No potassium feldspar was observed. Quartz fills interstices between other minerals, suggesting that crystallization of quartz began relatively late in the course of solidification of the rock.

Pleochroic epidote (to 3mm across) occurs in hornblende. Epidote also occurs along biotite cleavages and in some plagioclase cores. Apatite is ubiquitous within and adjacent to biotite as laths and hexagonally-shaped crystals. Biotite and hornblende generally form discrete clots with blocky magnetite grains.

Kpt_2 is a biotite-rich border phase of the Cretaceous granite (Fig. 6). In one Kpt_2 sample, hornblendes occur as 1mm+ twinned euhedral to subhedral rhombs. Hornblende cores generally have a brownish cast, whereas rims are green. Plagioclase, biotite and anhedral sphene are observed in hornblende.

Biotite is dark brown, twinned, and forms 1mm long subhedral books. Concentrations of granular sphene are observed along biotite cleavages and at some biotite-feldspar contacts, where the biotite grain feathers out into the feldspar.

Zoned, twinned plagioclase crystals occur in synneusis intergrowths. Cores often have a mottled appearance; both biotite and hornblende are observed within plagioclase cores.

Potassium feldspar (~2mm across) is slightly perthitic, lacks microcline twinning, and contains partly resorbed plagioclases, hornblende and quartz. Myrmekite is developed on plagioclase rims at potassium feldspar contacts.

Four occurrences of sphene are noted: 1) as 0.3mm long euhedral rhombs not in contact with mafic silicate minerals, 2) as granules in biotite, 3) as rhombs which are anhedral against mafic silicate minerals and euhedral against quartz and feldspar, and 4) as thin rims around blocky opaque (probably magnetite) minerals.

Zoned allanite, rimmed with epidote is observed adjacent to biotite. Subhedral epidote (0.4mm across) is noted in potassium feldspar and small patches of epidote occur in plagioclase.

No muscovite is observed.

Apatite is common in biotite and hornblende.

Thin section study of another sample from the same pluton revealed the same mineralogy with several textural differences. Hornblende in this sample is evenly colored green and occurs as patchy grains, never as rhombs. Biotite is much more abundant than hornblende, and as above, occurs in hornblende. Potassium feldspar grains are smaller (~1mm across), non-perthitic, and myrmekite at plagioclase contacts is very rare. Kpt_3 forms a N-S elongated pluton on the northeastern edge of the Batholith in the Vipond Park quadrangle. Quartz diorite separates Kpt_3 from the large Cretaceous granite pluton.

Hornblende in Kpt_3 is green, commonly twinned and intergrown with dark brown biotite. Rhombs up to 1mm long and lath-shaped

grains occur. Patches of biotite in hornblende are common.

Plagioclases occur as zoned, twinned crystals up to 1.2mm long, generally occurring in clusters. In one sample, a clearly terminated plagioclase crystal is observed at a contact with quartz and potassium feldspar.

Potassium feldspar is less abundant than quartz, which tends to fill interstices between other minerals.

Sphene occurs as rhombs in some samples, but is only observed in mafic silicate minerals in others.

Anhedral allanite (0.5mm across) rimmed with epidote is noted in association with hornblende. The abundance of anhedral epidote in biotite and hornblende varies from sample to sample.

Figure 6. Photomicrograph of Kpt_1 sample M984-1 showing zoned and twinned plagioclase (P) and large hornblende (H) with brown core (c) and green rim (r). Field of view is 3mm wide. Crossed nicols.

Cretaceous granodiorite

Cretaceous granodiorite (Kpgr), a medium-grained heterogeneous rock which forms the largest pluton of the batholith, occupies most of the area of the southeastern Pioneers. The northeastern edge of this pluton was mapped in the southern part of the Vipond Park quadrangle by E-an Zen, who has proposed the name "Uphill Creek granodiorite" for the pluton. Snee (1978) mapped and described the central and southern parts of the pluton (Snee's Kgdl map unit) as well as several hornblende-free tonalites and a porphyritic granodiorite that lie within it. Zen and others (1975) described a typical specimen of granodiorite from Ivanhoe Pit and the porphyritic granodiorite from Birch Creek. The granodiorite pluton is heterogeneous as indicated by the spread of slab modes on the Streckeisen plot in Fig. 4. In the southern and eastern parts of the pluton, the granodiorite is quite distinct from the major granite pluton in the Vipond Park quadrangle. It is medium grained and composed of plagioclase, white potassium feldspar, hornblende, biotite, sphene, opaques, apatite, zircon and epidote minerals. As the granite contact is approached, the granodiorite becomes less distinct - it is slightly coarser and contains pinkish potassium feldspars. Hornblende occurs throughout the granodiorite but is always subordinate to biotite in abundance. Snee (1978) found an average of 2.5 times as much biotite as hornblende based on modal analysis of thin sections spanning the granodiorite in his map area. Hornblende is green, pleochroic, twinned and generally occurs as subhedral pseudohexagonal rhombs or as laths. Chlorite and rarely epidote are observed in hornblende cores. No pyroxene or alteration suggestive of relict pyroxene is observed. Clots of

hornblende, biotite and sphene where hornblende averages 0.3x0.7mm are common; smaller, more euhedral hornblendes are observed in potassium feldspar. Inclusions of other minerals in hornblendes are generally limited to apatites and opaques.

Brown, pleochroic biotite forms subhedral books measuring up to 1mm across. "Swallowtail" twinning is common. Small grains of opaque minerals and apatite are usually included; inclusions of 0.05mm long plagioclases are occasionally observed. Degree of chloritization (in patches and along cleavages) varies from sample to sample.

No muscovite is observed.

Plagioclase forms as blocky to lath-shaped zoned and twinned, rarely terminated crystals. Though it is generally inclusion-free, tiny grains of opaque minerals and apatite and rarely mafic silicates in a rim area are observed. Degree of alteration (sericite, saussurite causing cloudiness) varies within any given thin section. Large, anhedral grains of potassium feldspar contain inclusions of all other minerals in the rock, including quartz. Plagioclases within potassium feldspar are anhedral, resorbed to varying degrees and develop a thin rim of albite at the grain contact with the potassium feldspar. Myrmekite is sometimes observed on these plagioclases; most commonly it occurs as well-developed lobe-like protrusions on plagioclases which occur around the margins of large potassium feldspars. Grid twinning is generally lacking and perthite is only weakly developed, if observed at all. Sphene is readily visible in hand speciman as clove brown euhedral crystals and forms 0.2-0.6 volume % of the thin section mode. Euhedral faces of 0.5mm long sphene rhombs are observed against quartz and

feldspars (Fig. 7). Crystal faces against mafic silicates are generally anhedral. Sphene also forms thin bands around blocky magnetite grains and occurs as granules in mafic silicates and with tiny opaque grains at ragged biotite contacts against feldspar. Inclusions of apatite and zircon in sphene rhombs are common. Examination of polished sections in reflected light, x-ray diffraction of magnetic heavy mineral separates and microprobe analyses reveal that the blocky opaque grains are magnetite. Rarely, a narrow band of hematite is observed in magnetite. No euhedral, discrete crystals of hematite were seen, nor were iron-titanium oxide minerals observed in this rock.

Distinctive reddish-brown allanites are common as blocky or cigar-shaped grains. Many are zoned and partly rimmed by epidote. Epidote is common in biotite, generally associated with chlorite.

Based on observed inclusion relationships and the nature of grain contacts, plagioclase, some magnetite, apatite and zircon appear to be minerals which began to crystallize early. Hornblende, biotite and sphene probably began to crystallize later, followed by quartz and lastly, potassium feldspar. Chlorite, feldspar alteration, hematite in magnetite, epidote and granular sphene formation are likely late magmatic or subsolidus in origin.

Figure 7. Photomicrograph of Kpgr sample from Ivanhoe Pit (IVP). Note euhedral rhomb of sphene (S), interstitial nature of potassium feldspar (K), coarse biotite (B), zoned, twinned plagioclase (P) and quartz (Q). Field of view is 5.5mm wide. Crossed nicols.

Cretaceous granites

Two plutons of Cretaceous granite outcrop in the Vipond Park quadrangle one is a major pluton of the batholith and the other is a smaller body cut off from the main pluton by the major granodiorite near Ivanhoe Pit at the eastern margin of the batholith. Field observation, age, whole rock chemistry and initial strontium ratios indicate that these two bodies of granite are indistinguishable.

The granite is typically coarse-grained and is characterized by pink potassium feldspar phenocrysts. The pink color of the feldspar probably represents a late stage oxidation of iron oxide mineral inclusions to hematite under conditions of water saturation, as suggested by Barker and others (1975) for similar observations in the Pikes Peak Batholith.

Hornblende is always less abundant than biotite in the granite and was absent in several thin sections.Modal hornblende ranged from 0-4% in analysed sections and biotite/hornblende ratios range from 2-5 where both minerals are present.

Hornblende is green, pleochroic, forms subhedral rhombs and laths and is commonly twinned. Occasionally, euhedral rhombs are observed as inclusions in potassium feldspar phenocrysts (Fig. 8); such hornblende is always smaller and less ragged than hornblende outside of potassium feldspar. Maximum length of hornblendes is about 3.0mm; in potassium feldspar, hornblendes are usually <0.3mm long.

Pleochroic brown biotite forms 8-10 volume % of the mode. Biotite usually occurs as 1-3mm long subhedral books, enclosing 0.05 mm rounded or hexagonal apatites and 0.02mm zircons surrounded by pleochroic haloes.

Much of the biotite exhibits sweeping extinction and some grains are bent. In some samples, biotite displays a reaction relationship with adjacent potassium feldspar grains. Small opaque minerals (probably magnetite) occur within biotite and near biotite grain contacts with potassium feldspar. No feldspars were observed within biotite grains. Grain contacts between biotite and plagioclase are generally sharp as opposed to ragged contacts observed for biotite-potassium feldspar contacts.

Large laths of plagioclase averaging 2-3 mm in length, with a maximum length of 6mm display both simple and polysynthetic twins and zoning. Plagioclase is generally free of inclusions with the exception of rare tiny opaque grains or zircons. In some crystals, oval, fractured cores are separated from clean rims by a prominent band of sericite. Patches of plagioclase, some of which are rounded and embayed, suggesting resorption, occur within large potassium feldspar phenocrysts. Well-developed lobes of myrmekite are common at contacts of plagioclase with potassium feldspar phenocrysts, but myrmekite is relatively rare at margins of plagioclase enclosed by potassium feldspar. Potassium feldspar lacks grid twinning, frequently displays Carlsbad twins and is only weakly perthitic.

Epidote is ubiquitous in Cretaceous granite, forming up to 0.8 volume % of the thin section mode. Most of the epidote occurs as coarse, yellow-green subhedral crystals or in "sunburst" texture in biotite, usually associated with chlorite; some epidote is zoned. This epidote may represent late-magmatic alteration which caused chloritization of biotite and sericitization of feldspars. Alternatively, all, or some of the coarse epidote may be a primary magmatic phase (Zen, 1980).

Epidote also occurs as rims on allanite crystals, which commonly have hornblende cores, and small anhedral grains of clearly late epidote (saussurite) are observed in plagioclase.

Muscovite is rare to absent in the granite. Two textural occurrences of muscovite in granite have been noted: 1) muscovite interleaving with biotite and chlorite along biotite cleavages and 2) patches of muscovite in altered feldspars. No muscovite is associated with chlorite-free biotite and both occurences of muscovite in this rock unit are probably subsolidus alteration effects.

Granular sphene occurs in biotite and sphene rims blocky magnetite grains. Euhedral sphene rhombs characteristic of the granodiorite are less well-developed in the granite; subhedral sphene is occasionally seen adjacent to hornblende. Euhedral rhombs do occur in a small porphyritic border pluton of the granite.

Euhedral and rounded 0.05 mm hexagonally shaped apatites are commonly included in biotite and less commonly in hornblende. Rounded apatites form "windows" in and around blocky magnetite grains.

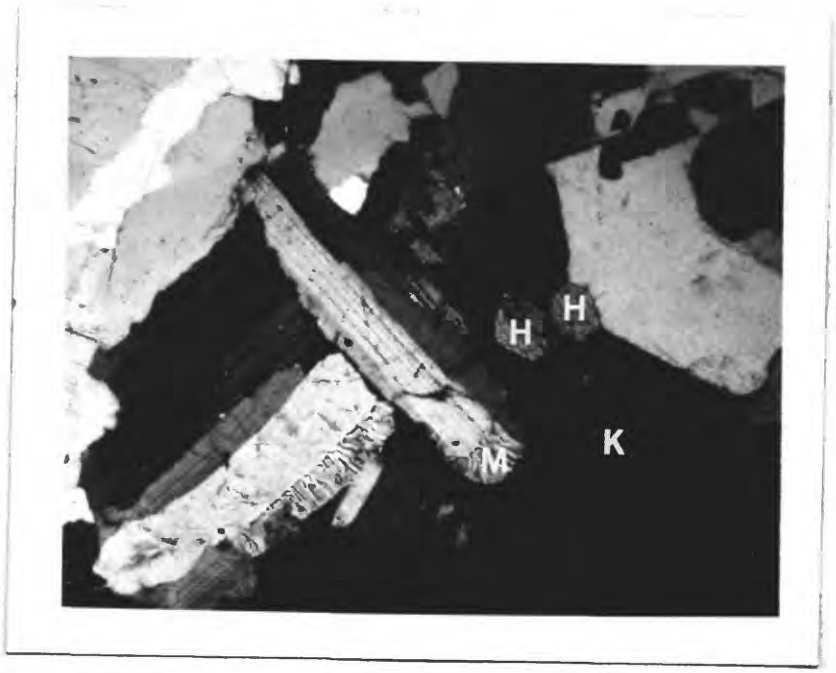

Figure 8. Photomicrograph of Kpg sample M1306-2. Note homogeneity of potassium feldspar (K), subhedral hornblendes (H) within potassium feldspar, and well-developed lobelike protrusions of myrmekite (M) on plagioclase in contact with potassium feldspar. Field of view is 3mm wide. Crossed nicols.

Paleocene granite

Three discrete plutons of muscovite granite are indicated on the map in Fig. 2. The largest of these plutons is a 65 Ma (K/Ar on biotite) medium to coarse grained granite in contact with Paleozoic sediments to the east, Precambrian "Y" rocks to the south and truncated by a prominent NE-SW fault on the west. Due east of this pluton lies a smaller body of porphyritic two-mica granite, also 65 Ma. Another muscovite bearing granite, age uncertain, occurs in the Stine Creek area, northwest of the other two plutons. Fine-grained muscovite-bearing dikes (Tda) have been mapped by Zen and Snee and reconnaissance mapping by them shows that these granites are more extensive than indicated on the existing maps. Muscovite is generally visible in hand specimen, although it is locally variable in abundance throughout the plutons. Mineralogically, the two-mica granites are distinguished from the Cretaceous rocks by presence of coarse muscovite and lack of amphibole and generally sphene.

Biotite is brown, pleochroic, usually subhedral, and occurs in books up to 1mm long. Chlorite is common along cleavages and in the porphyritic pluton chlorite has completely replaced much of the biotite. Biotite forms 2-3 volume % of the mode.

Muscovite occurs in several textural relations. Coarse-grained (up to 1mm long) muscovite occurs in intimate association with biotite, often interleaving along cleavages or cross-cutting a biotite grain. Discrete, euhedral books of muscovite are less common, but by no means rare. Opaque inclusions, 0.05mm in length or smaller, are common. Muscovite which is clearly of secondary origin occurs as coarse to fine sericite

in feldspars. Muscovite is also observed rimming large, blocky magnetite grains. Fig. 9 shows examples of textural variants. Muscovite forms 2 volume % of the thin section mode.

Interpretation of muscovite textures is problematic. Miller and others (1981) attempted to set down textural criteria for distinguishing primary (crystallized from a magma) from secondary (subsolidus formation) muscovite. They proposed that relatively coarse, euhedral muscovites which occur as discrete grains in unaltered igneous rocks should be primary, whereas smaller, less well-defined grains enclosed by other minerals suggest a secondary origin. In the easternmost Tertiary plutons of the Pioneer Batholith, discrete muscovite grains and muscovites which cut across biotite with euhedral termination against the biotite are interpreted as primary magmatic muscovite. Interleaving biotite-muscovite intergrowths where one mineral occurs along cleavages of the other, are more ambiguous to interpret. In the Stine Creek pluton, only this latter texture was observed and epidote and chlorite in biotite are common, suggesting that muscovite may have formed under subsolidus conditions. All occurrences of muscovite in feldspars and rimming large, blocky magnetites are interpreted as secondary.

Deuteric alteration involving biotite + H_2O reacting to form muscovite + chlorite + K_2O is possible; however, muscovite-biotite intergrowths are generally free of chlorite.

Strongly zoned, twinned plagioclase crystals as large as 3x4mm are common. Plagioclase often appears cloudy in plane polarized light, especially in core areas where sericite is concentrated.

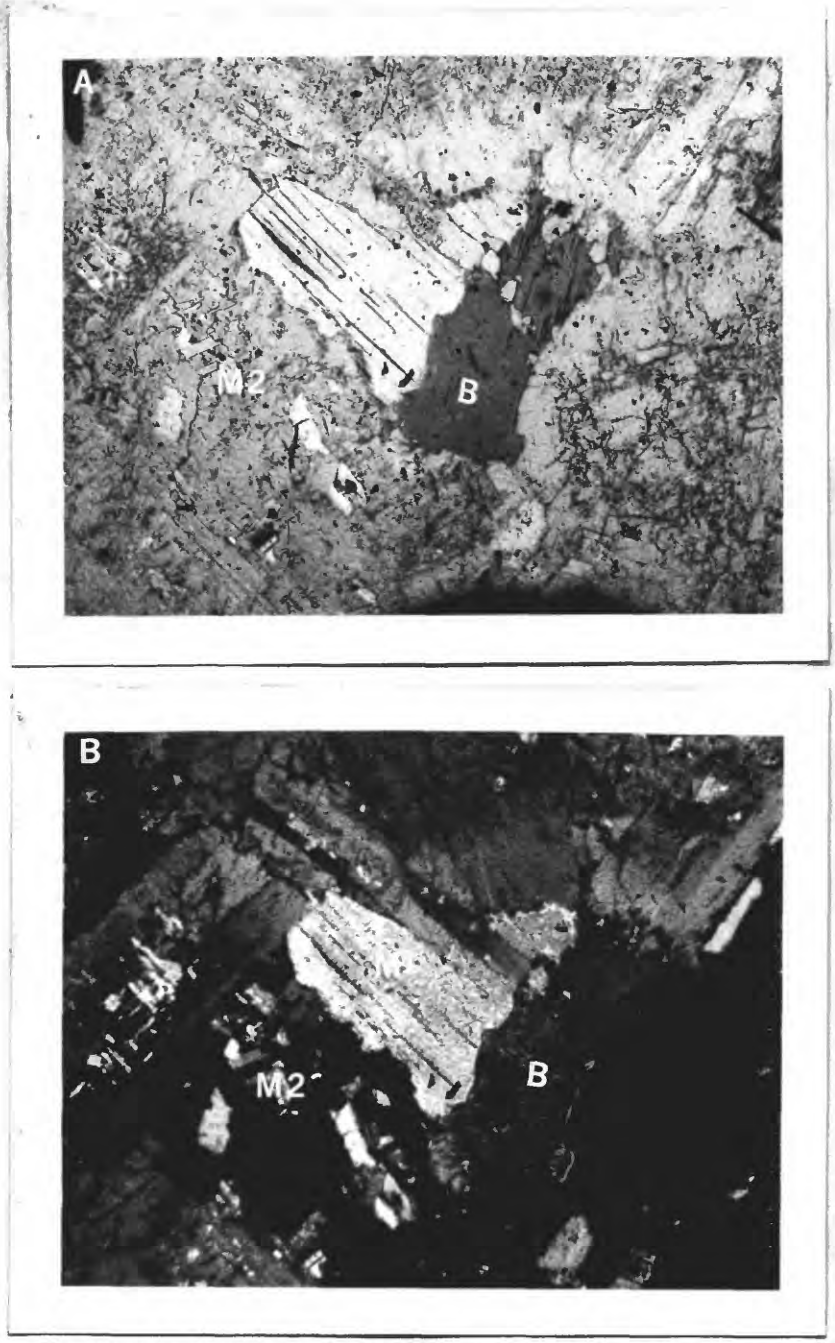

Figure 9. Photomicrograph of Tpg sample M500-2. A)plane polarized light B) crossed nicols. Note two textures of muscovite illustrated: M1 represents typical primary magmatic texture of muscovite-biotite intergrowth; biotite cross-cuts muscovite rather than interleaves along cleavages
M2 represents secondary muscovite replacing plagioclase.
Field of view is 3mm wide.

Potassium feldspar forms large subhedral phenocrysts, frequently displays Carlsbad twins, rarely microcline twins. Perthite is more common than in the Cretaceous rocks. Myrmekite and inclusions other than plagioclase are relatively rare in potassium feldspar in the eastern plutons, more common in the Stine Creek pluton. The sphene and epidote which characterize the Cretaceous granite are rare in the Paleocene granite; sphene occurs as small, anhedral grains rather than as euhedral rhomb-shaped crystals. Opaque minerals consist of blocky magnetites, similar to opaques in Cretaceous rocks, and small grains (0.1mm maximum length) of ilmenite and titanohematite within and adjacent to biotite-muscovite intergrowths. Apatite occurs in both biotite and muscovite; zircon is observed in biotite, and more rarely in muscovite.

In the porphyritic pluton, a purple isotropic mineral identified as fluorite is observed in a chloritized biotite. Sagenitic rutile needles are also observed in chlorite in this rock. Quartz and potassium feldspar relations are not clear cut with regard to which commenced crystallizing first. Potassium feldspar grains do not host quartz inclusions in these rocks and occur as more discrete phenocrysts than in the Cretaceous granodiorite; potassium feldspar probably began crystallizing before quartz.

Sequences of crystallization

Generalized sequences of crystallization for the minerals in rocks forming the major plutons of the Pioneer Batholith are shown in Fig. 10. Barker and others (1975) presented such diagrams for the Pikes Peak Batholith and emphasized that such diagrams are only approximations and that onset, cessation and overlap of crystallization of phases

Table III. Modal analyses of thin sections from representative samples of major plutons in the Pioneer Batholith (volume per cents)

MAP UNIT	Kpd*	Kpgr							
SAMPLE	M313	M121 -1-78	M122 -1	M122 -2	M881 -1-78	IVP*	IVP	BC*	BC
ALKALI FELDSPAR	0.0	24.3	32.8	24.0	18.5	4.3	8.5	17.3	10.4
PLAGIOCLASE	64.9	30.0	30.1	36.8	44.7	51.0	48.8	47.1	51.5
QUARTZ	4.3	37.1	30.9	33.7	23.9	26.0	26.9	28.5	31.6
BIOTITE	7.7	4.0	2.3	3.1	5.8	7.8	7.4	4.5	4.3
HORNBLENDE	17.2	2.7	2.3	0	4.3	4.3	5.2	0.3	0.2
MUSCOVITE		0	0	0	0		0		0
CHLORITE	0.0	0.2	0.3	1.1	1.5	1.2	0.7	0.9	0.4
SPHENE	0.4	0.3	0.3	0.6	0.2	0.8	0.4	0.3	0.1
OPAQUES		1.2	0.9	0.7	0.9		1.8		1.3
EPIDOTE		0.3	tr		tr		0.1		
ALLANITE		0.3		tr					
APATITE							0.2		
MYRMEKITE									
OTHER	5.6					4.7		1.9	
#POINTS		1739	2008	1000	2085		1916		

*from Zen, Marvin and Mehnert, 1975

Table III continued.

MAP UNIT	Kpp*	Kpg					Tpg	
SAMPLE	BH9850	M98-1	M98-2	BHS*	MT293 -1	MT293 -2	M500-2 -78	M32-1 -1
ALKALI FELDSPAR	17.9	14.4	20.5	29.0	15.0	24.5	36.2	9.9
PLAGIOCLASE	39.9	47.7	47.5	31.5	37.2	56.1	34.3	56.7
QUARTZ	34.1	26.0	23.1	34.1	32.0	10.4	23.6	28.9
BIOTITE	15.4	10.6	8.2	4.3	8.7	4.6	3.2	1.7
HORNBLENDE	2.3	0.2	0	0.0	4.2	0.9	0	0
MUSCOVITE		0	0.1		0	tr	2.3	2.2
CHLORITE	0.0			0.3	1.0	1.4	0.2	0.4
SPHENE	0.6	0.7	0.4	0.0	0.2	0.4	0	0
OPAQUES		0.4	0.2		1.0	0.5	0.2	0.2
EPIDOTE					0.2	0.8	0	
ALLANITE					tr	tr	0	
APATITE					tr		0	
MYRMEKITE					0.5	0.2	tr	
OTHER	1.4			0.8		tr		
#POINTS		1000	1000		2000	1824		

*from Zen, Marvin and Mehnert, 1975

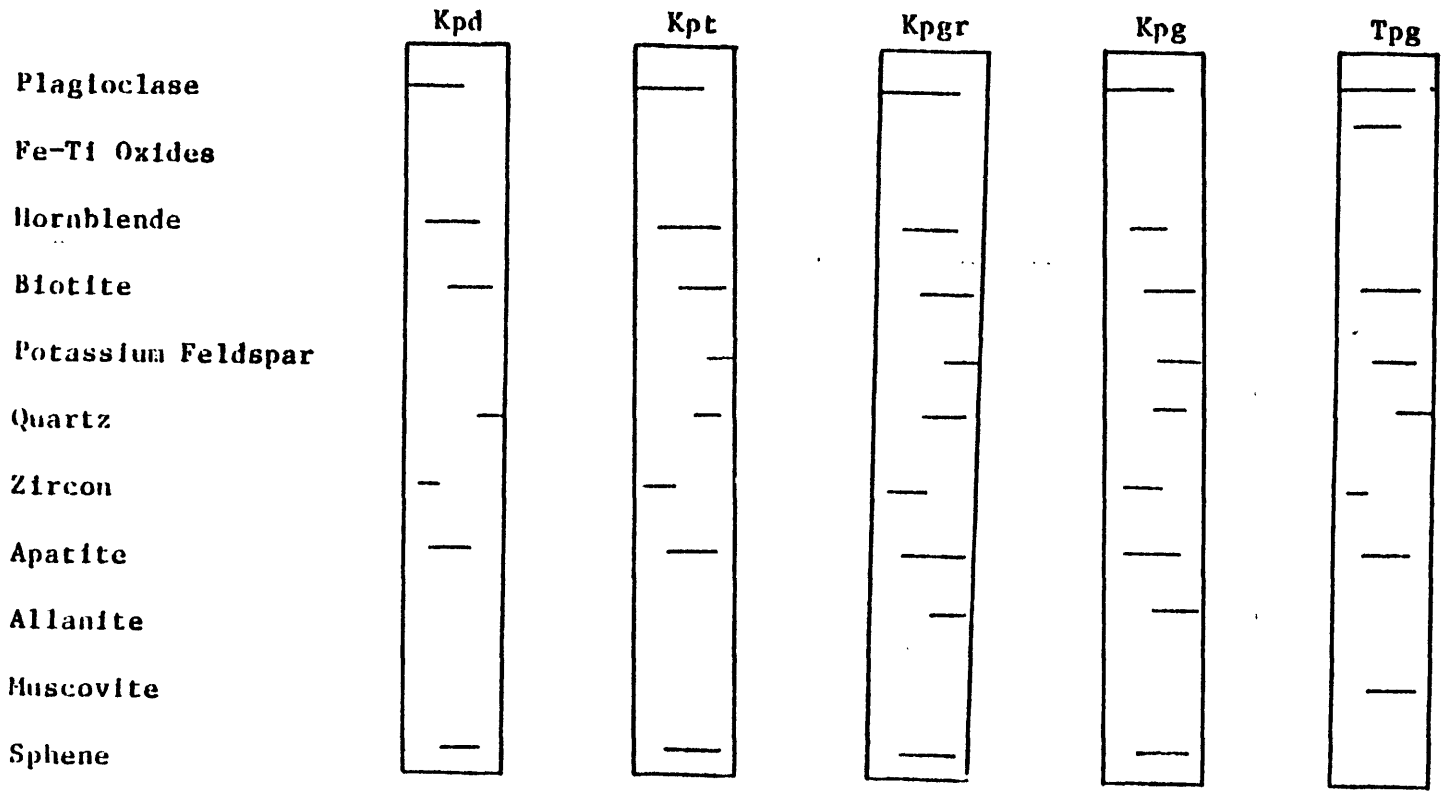

Figure 10. Generalized sequence of crystallization of minerals for major plutons in the Pioneer Batholith based on petrographic observations.

cannot be precisely determined. Diagrams for the Pioneer rocks are based on observations of 1) inclusion relations, 2) development of crystal faces of one mineral against another, 3) intergrowths of phases, and 4) interstitial textures of one phase relative to other phases in the rock.

Only those phase believed to have crystallized from a melt are indicated on the diagram in Fig. 10; anhedral sphene, muscovite in feldspar, epidote and chlorite are therefore not represented.

Major element whole rock chemistry

Twenty-five representative whole rock samples from various plutons were analysed by the rapid rock method (Shapiro, 1975) in the Analytical Laboratories of the U.S. Geological Survey in Reston, Va. Separate splits of four samples were also analysed by x-ray fluorescence by Bruce Chappell of the Australian National University. Sample locations are indicated on the map in Fig. 3. CIPW norms and the Thornton-Tuttle differentiation index (D.I.) were calculated using Bowen's (1971) graphic normative analysis computer program. Results are summarized in Table IV. Harker plots and pertinent ternary diagrams are shown in Figs. 11 - 16.

Silica content ranges from 49 to 74 weight per cent. Total alkalis (Na_2O+K_2O) increase from 4% in quartz diorite to 6% in granodiorite to up to 8-9% in muscovite granite. FeO/Fe_2O_3 ratios are variable (0.4 to 1.5).

In terms of Peacocks's (1931) alkali-lime index based on the silica content at which $CaO = Na_2O + K_2O$, the Pioneer rocks are calc-alkalic, i.e., the intersection of CaO and total alkalis occurs between 56 and 61 weight per cent SiO_2.

All of the rocks are quartz-normative and about half are slightly corundum-normative (2.6% maximum). Thus the Pioneer rocks are slightly peraluminous in terms of chemistry. No aluminum silicates or garnet have been observed in plutonic rocks. Only the Tertiary granites host primary looking muscovite, thus there is no correlation between presence of muscovite and amount of normative corundum. Some clearly secondary muscovite is present in the Cretaceous granites.

Table IV. Major element rock analyses and normative minerals for rocks of the Pioneer Batholith

Map Unit	Kpd	Kpd	Kptl	Kptl	Kpt3
Sample	BH9800	M313-1	M984-2	M984-2+	M547-1
Plot symbol	A	B	C	C	D
SiO_2	49.50	52.40	56.70	52.23	61.10
Al_2O_3	18.30	18.20	17.00	17.92	15.70
Fe_2O_3	4.90	5.10	3.30	3.17	2.30
FeO	6.40	5.40	4.30	4.45	3.60
MgO	5.00	3.90	2.90	3.07	2.40
CaO	9.20	8.70	6.00	6.22	5.60
Na_2O	2.40	3.00	3.50	3.55	3.30
K_2O	1.40	1.30	2.10	2.05	3.00
H_2O	1.10	1.00	1.20	1.50	0.66
TiO_2	1.20	1.20	0.97	0.98	0.72
P_2O_5	0.26	0.35	0.28	0.26	0.20
MnO	0.16	0.11	0.17	0.13	0.14
ZrO_2	n.d.*	n.d.	n.d.	0.03	n.d.
CO_2	0.03	0.02	0.08	0.12	0.06
BaO	n.d.	n.d.	n.d.	0.08	n.d.
F	n.d.	n.d.	0.05	n.d.	0.05
Total	99.85	100.68	98.53	99.76	98.81
normative minerals					
Q	2.98	6.54	11.21	9.29	15.59
C					
Z				0.05	
Or	8.29	7.63	12.60	12.14	17.94
Ab	20.34	25.21	30.06	30.11	28.26
An	35.08	32.14	34.84	26.97	19.40
Wo	3.65	3.48	1.18	0.69	2.83
En	12.47	9.65	7.33	7.66	6.05
Fs	6.03	3.90	3.94	4.19	3.83
Mt	7.12	7.35	4.86	4.61	3.38
Hm					
Il	2.28	2.26	1.87	1.89	1.38
Ap	0.62	0.82	0.67	0.62	0.48
Fr			0.05		0.07
Cc	0.07	0.04	0.19	0.27	0.14
Total	98.93	99.02	98.80	98.49	99.35
D.I.	32	39	54	52	62
Analyst	H. Smith	L. Artis	Z. Hamlin	B. Chappell	Z. Hamlin

* n.d. = not determined + x-ray fluorescene analysis

Table IV. Continued

Map Unit	Kpt	Kpp	Kpgr	Kpgr	Kpgr
Sample	M547-1+	BH9850	M121-1	FG	IVP
Plot symbol	D	E	F	G	H
SiO_2	61.27	64.70	65.50	65.50	65.70
Al_2O_3	16.55	16.40	15.40	15.90	16.20
Fe_2O_3	2.40	2.10	2.40	1.90	2.80
FeO	3.65	2.90	1.90	2.30	2.10
MgO	2.53	1.80	1.50	1.60	1.50
CaO	5.45	4.20	3.70	4.20	4.50
Na_2O	3.38	3.30	3.70	3.30	3.00
K_2O	2.26	2.80	3.50	2.40	2.60
H_2O	0.93	0.75	0.70	0.42	0.80
TiO_2	0.73	0.59	0.42	0.45	0.42
P_2O_5	0.17	0.14	0.16	0.20	0.21
MnO	0.11	0.10	0.10	0.08	0.08
ZrO_2	0.01	n.d.	n.d.	n.d.	n.d.
CO_2	0.14	<0.05	0.02	0.08	0.02
BaO	0.09	n.d.	n.d.	n.d.	n.d.
F	n.d.	n.d.	n.d.	n.d.	n.d.
Total	99.67	99.78	99.00	98.33	99.93
normative minerals					
Q	17.07	22.28	21.14	26.02	26.63
C		0.64		0.92	0.82
Z	0.02				
Or	13.40	16.58	20.89	14.23	15.38
Ab	28.70	27.98	31.62	28.40	25.40
An	23.39	19.96	15.23	19.35	20.84
Wo	0.79		0.89		
En	6.32	4.49	3.77	4.05	3.74
Fs	3.73	2.81	1.01	2.09	1.00
Mt	3.49	3.05	3.52	2.80	4.06
Hm					
Il	1.39	1.12	0.81	0.87	0.80
Ap	0.40	0.33	0.38	0.48	0.50
Fr					
Cc	0.32		0.05	0.18	0.05
Total	99.02	99.24	99.31	99.39	99.22
D.I.	59	67	74	69	67
Analyst	B. Chappell	L. Shapiro and others	N. Skinner Z. Hamlin	F. Brown	L. Artis

* n.d. = not determined + x-ray fluorescene analysis

Table IV. Continued

Map Unit	Kpgr	Kpgr	Kpgr	Kpgr	Kpg
Sample	IVP+	M881-1	KS	M1298-2	M1293-1
Plot symbol	H	I	J	K	L
SiO_2	65.04	66.40	66.90	67.90	68.40
Al_2O_3	15.98	15.30	15.10	15.00	15.10
Fe_2O_3	2.23	1.80	2.30	2.00	1.60
FeO	2.16	1.60	2.20	1.70	1.90
MgO	1.80	1.30	1.60	1.50	1.40
CaO	4.53	3.70	3.90	3.80	3.50
Na_2O	3.34	3.60	3.10	3.30	3.50
K_2O	3.03	3.40	3.80	3.30	3.20
H_2O	0.78	0.79	0.28	0.84	0.77
TiO_2	0.47	0.36	0.56	0.44	0.40
P_2O_5	0.16	0.12	0.12	0.13	0.11
MnO	0.09	0.09	0.08	0.07	0.08
ZrO_2	0.02	n.d.	n.d.	n.d.	n.d.
CO_2	0.12	0.04	0.06	0.03	0.06
BaO	0.12	n.d.	n.d.	n.d.	n.d.
F	n.d.	n.d.	n.d.	0.04	0.04
Total	99.87	98.50	100.00	100.03	100.04
normative minerals					
Q	21.90	23.30	23.92	26.10	26.01
C					
Z	0.03				
Or	17.93	20.40	22.46	19.49	18.92
Ab	28.30	30.93	26.23	27.91	29.60
An	19.69	15.78	16.06	16.36	16.03
Wo	0.51	0.75	0.88	0.52	0
En	4.49	3.29	3.98	3.74	3.48
Fs	1.52	1.04	1.36	0.87	1.66
Mt	3.24	2.65	3.34	2.90	2.32
Hm					
Il	0.89	0.69	1.06	0.84	0.76
Ap		0.29	0.28	0.31	0.26
Fr				0.06	0.06
Cc		0.09	0.14	0.07	0.14
Total	98.50	99.21	99.71	99.17	99.24
D.I.	68	75	73	74	75
Analyst	B. Chappell	N. Skinner Z. Hamlin	H. Smith	C. Jones R. Somers	C. Jones R. Somers

* n.d. = not determined + x-ray fluorescene analysis

Table IV. Continued

Map Unit	Kpg	Kpgr	Kpgr	Kpg	Tpg
Sample	M1228-1	M1272-2	BC	M1293-2	M1162-1
Plot symbol	M	N	O	P	Q
SiO_2	68.50	68.90	69.50	69.80	70.70
Al_2O_3	14.90	15.10	16.20	14.60	14.80
Fe_2O_3	2.10	1.90	1.60	1.50	1.80
FeO	1.50	1.60	1.30	1.70	1.20
MgO	1.30	1.20	0.62	1.30	0.90
CaO	3.50	3.50	3.70	3.30	2.80
Na_2O	3.40	3.40	3.80	3.30	3.30
K_2O	3.20	3.20	2.70	3.10	3.60
H_2O	0.72	0.67	0.79	0.86	1.00
TiO_2	0.41	0.38	0.26	0.40	0.35
P_2O_5	0.12	0.12	0.16	0.12	0.12
MnO	0.06	0.07	0.08	0.09	0.08
ZrO_2	n.d.	n.d.	n.d.	n.d.	n.d.
CO_2	0.30	0.01	0.04	0.01	0.01
BaO	n.d.	n.d.	n.d.	n.d.	n.d.
F	0.04	0.04	n.d.	0.04	0.05
Total	100.03	100.07	100.75	100.10	100.69
normative minerals					
Q	28.07	27.63	28.20	29.53	30.54
C	0.54	0.07	0.77	0.20	0.79
Z					
Or	18.90	18.90	15.84	18.30	21.13
Ab	28.76	28.75	31.92	27.90	27.73
An	14.46	16.29	16.93	15.29	12.67
Wo					
En	3.24	2.99	1.53	3.23	2.23
Fs	0.45	0.87	0.78	1.39	0.28
Mt	3.04	2.75	2.30	2.17	2.59
Hm					
Il	0.78	0.72	0.49	0.76	0.66
Ap	0.28	0.28	0.38	0.28	0.28
Fr	0.06	0.06		0.06	0.08
Cc	0.68	0.02	0.09	0.02	0.02
Total	99.26	99.33	99.23	99.13	99.00
D.I.	76	75	76	76	79
Analyst	C. Jones R. Somers	C. Jones R. Somers	L. Artis	C. Jones R. Somers	C. Jones R. Somers

Table IV. Continued

Map Unit	Kpg	Kpg	Tda	Tpg	Tpg
Sample	M516-1	M744-2	M347-3	M500	M500+
Plot symbol	R	S	T	U	U
SiO_2	70.90	71.90	72.00	73.00	72.34
Al_2O_3	15.70	14.10	13.00	14.30	14.46
Fe_2O_3	0.74	1.70	1.30	0.59	0.58
FeO	0.58	1.10	1.20	0.92	0.88
MgO	0.37	0.98	0.52	0.41	0.51
CaO	2.10	2.70	1.60	2.50	1.57
Na_2O	5.00	3.10	3.10	3.80	3.87
K_2O	3.10	3.60	5.00	3.90	3.97
H_2O	0.56	0.22	0.63	0.37	0.70
TiO_2	0.23	0.29	0.27	0.21	0.20
P_2O_5	0.07	0.08	0.10	0.13	0.08
MnO	0.03	0.06	0.05	0.06	0.05
ZrO_2	n.d.	n.d.	n.d.	n.d.	0.01
CO_2	0.02	0.07	0.23	0.07	0.17
BaO	n.d.	n.d.	n.d.	n.d.	0.13
F	0.06	n.d.	0.08	0.05	n.d.
Total	99.43	99.90	99.05	100.29	99.52
normative minerals					
Q	25.41	33.18	31.71	30.24	30.83
C	0.66	0.55	0.55		1.45
Z					0.02
Or	18.43	21.30	29.83	22.98	23.57
Ab	42.55	26.26	26.48	32.06	32.90
An	9.49	12.44	5.36	10.41	6.46
Wo				0.16	
En	0.93	2.44	1.31	1.02	1.28
Fs	0.13	0.25	0.78	0.96	0.90
Mt	1.08	2.47	1.90	0.85	0.84
Hm					
Il	0.44	0.55	0.52	0.40	0.38
Ap	0.17	0.19	0.24	0.31	0.19
Fr	0.11		0.15	0.08	
Cc	0.05	0.16	0.53	0.16	0.39
Total	99.44	99.79	99.36	99.63	99.21
D.I.	86	81	88	85	87
Analyst	C. Jones	H. Smith R. Somers	Z. Hamlin	Z. Hamlin N. Skinner	B. Chappell

* n.d. = not determined + x-ray fluorescene analysis

Table IV. Continued

Map Unit	Kpg	Tda	Tpg	Tpg
Sample	BHS	M315-1	M32-1	M1044-1
Plot symbol	V	W	X	Y
SiO_2	72.80	74.30	74.70	75.60
Al_2O_3	15.10	12.80	13.40	12.60
Fe_2O_3	0.86	0.78	0.41	0.71
FeO	0.76	0.94	0.16	0.48
MgO	0.43	0.54	0.26	0.29
CaO	2.20	1.10	0.76	1.20
Na_2O	3.10	2.70	4.50	3.10
K_2O	3.50	4.60	4.60	4.30
H_2O	0.96	0.90	0.49	0.45
TiO_2	0.20	0.24	0.07	0.14
P_2O_5	0.18	0.10	0.05	0.05
MnO	0.08	0.01	0.03	0.08
ZrO_2	n.d.	n.d.	n.d.	n.d.
CO_2	0.02	0.08	0.02	0.03
BaO	n.d.	n.d.	n.d.	n.d.
F	n.d.	0.06	n.d.	0.02
Total	00.19	99.12	99.45	99.04
normative minerals				
Q	36.28	38.51	29.38	38.66
C	2.68	1.96		0.90
Z				
Or	20.64	27.42	27.33	25.66
Ab	26.18	23.05	38.29	26.48
An	9.59	3.96	2.79	5.38
Wo			0.23	
En	1.07	1.36	0.65	0.73
Fs	0.50	0.71		0.22
Mt	1.24	1.14	0.41	1.04
Hm				
Il	0.38	0.46	0.13	0.27
Ap	0.43	0.23	0.12	0.12
Fr		0.11		0.03
Cc	0.05	0.18	0.05	0.07
Total	99.04	99.09	99.83	99.56
D.I.	83	89	95	91
Analyst	L. Artis	C. Jones R. Somers	N. Skinner Z. Hamlin	Z. Hamlin

these plots is the smooth trend observed for all elements. Al_2O_3, FeO, TiO_2, CaO, MgO, and P_2O_5 all decrease with increasing silica content while Na_2O and K_2O increase. Corundum-normative samples are not distinct from the main trends for Al_2O_3 or K_2O, as might be expected if rock chemistry reflected extensive alteration.

Tilling (1973) used binary and ternary plots to study chemical variation in the rocks of the Boulder Batholith. He found that a plot of K_2O/K_2O+Na_2O vs. SiO_2 best illustrated two different groups of rocks believed to represent two contemporaneous magmas. Data from the Pioneer Batholith is shown in Fig. 12. The boundaries defined by Tilling for the Main Series and Sodic Series rocks of the Boulder Batholith are outlined. The Pioneer rocks are more like the Sodic Series rocks in composition. The southernmost plutons of the Boulder Batholith which belong to the Sodic Series are the closest Boulder plutons to the Pioneer Batholith. Other features (higher initial strontium, age span) distinguish the Pioneer from the Boulder.

A molar AFM plot for the Pioneer Batholith, Fig. 13, shows a smooth trend towards the alkali corner. Little overlap occurs between map units and the muscovite-bearing rocks are the most alkali-rich. Within the granodiorite, the samples closest to the Cretaceous granite contact plot closest to the granite in composition.

The sum of the oxides represented in the AFM diagram accounts for less than 50% of the total oxides in the rocks. Wright (1974) and others have criticized the use of AFM diagrams as a basis for drawing petrogenetic conclusions. As Wright pointed out, related rocks will show a trend on an AFM plot, but unrelated rocks may also show smooth

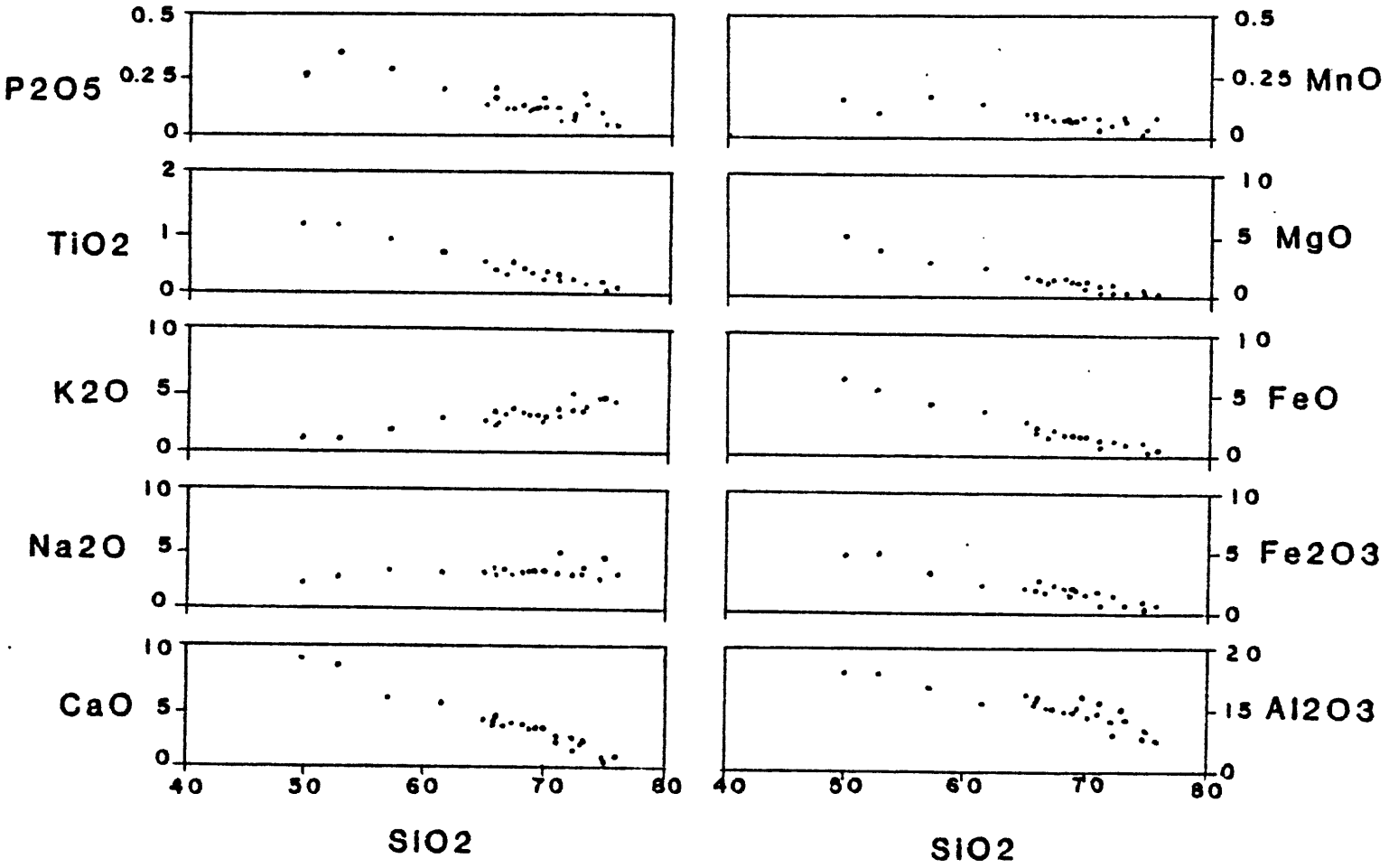

Figure 11. Harker diagrams for major elements in Pioneer rocks. Data given in Table IV.

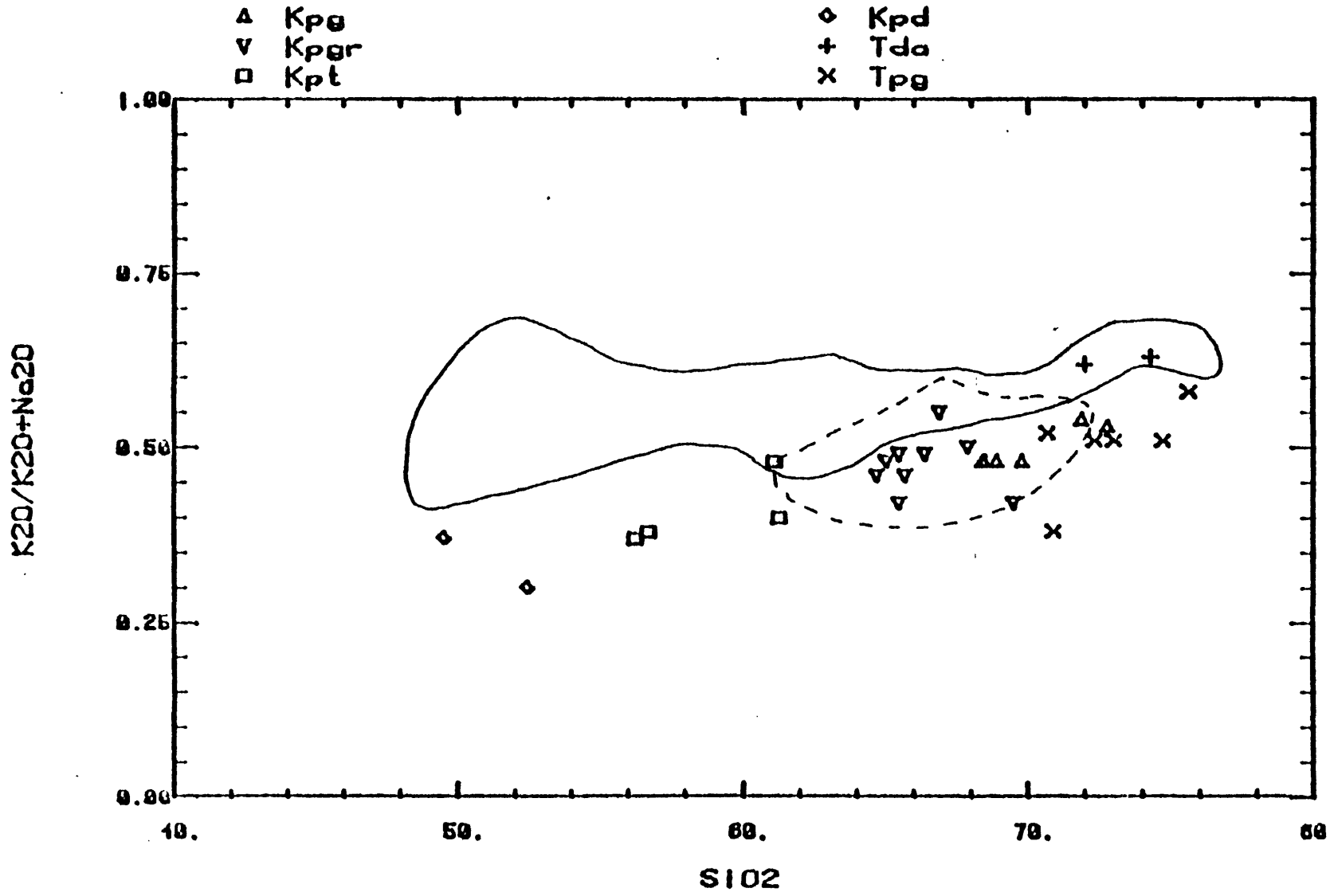

Figure 12. $K_2O/K_2O + Na_2O$ vs. SiO_2 plot Pioneer rocks. Solid (main series) and dashed (sodic series) lines define fields for the rocks of the Boulder Batholith (Tilling, 1973).

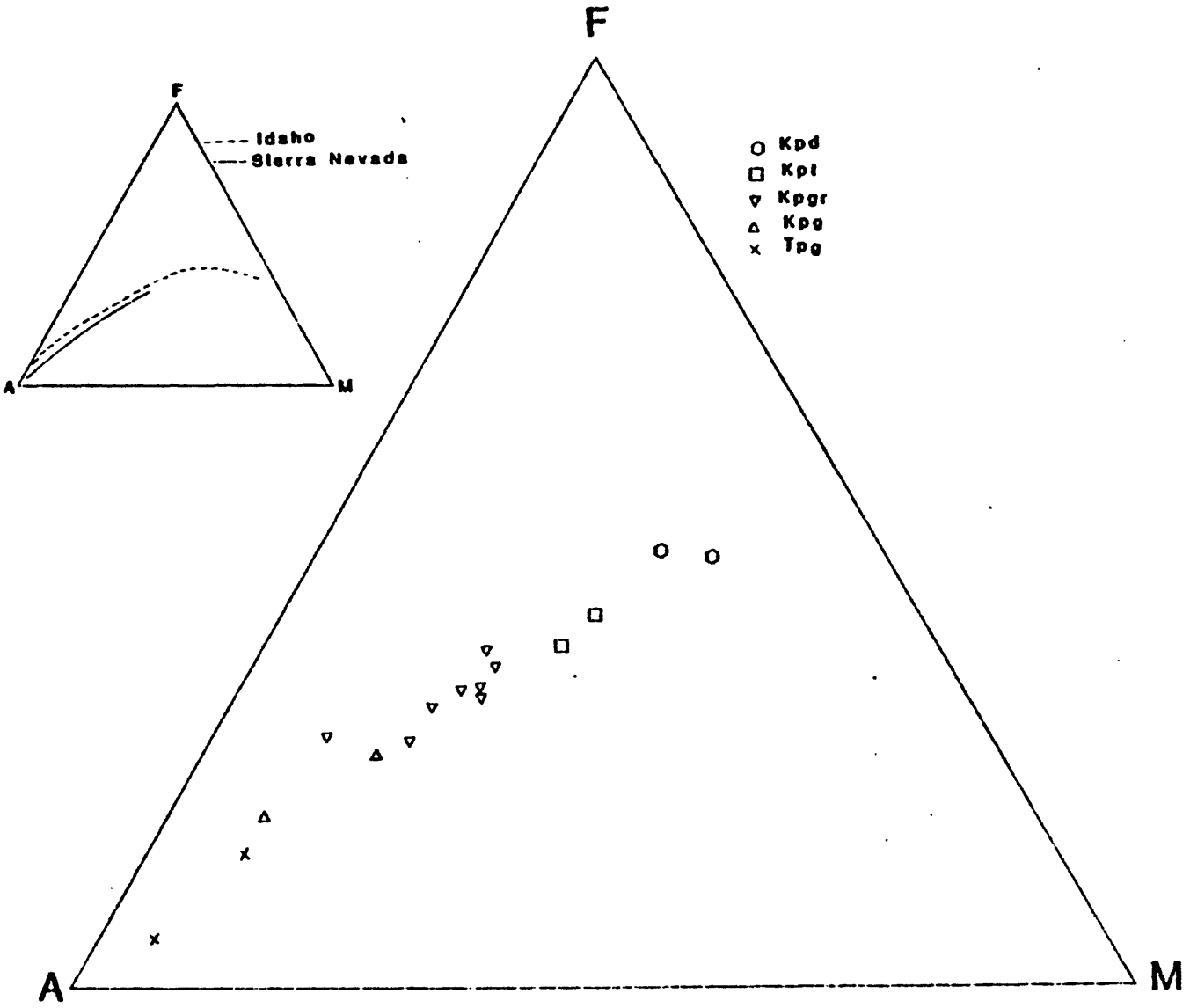

Figure 13. Molar $K_2O + Na_2O$, FeO, MgO (AFM) plot for rocks of the Pioneer Batholith. Inset shows fractionation trends for the Sierra Nevada and southern California and Idaho batholiths (Mueller and Saxena, 1977).

trends, due to the number of factors (other constitutents) ignored. Perhaps the most useful aspect of such chemical plots is as a basis for comparisons between suites of rocks which are thought to represent similar processes. The Pioneer trend is similar to trends observed for other calc-alkalic batholith complexes, such as the Sierra Nevada and the Boulder, as shown in Fig. 13.

Minor element chemistry

Multi-element instrumental neutron activation analyses were performed on most of the samples to determine rare earth and trace element abundances.

Chondrite-normalized rare-earth patterns based on data in Table V are plotted in Fig. 14. Rare earth trends for all the rocks show relative enrichment in the light REE. Such patterns are consistent with melts derived from a pyroxene or hornblende rich parent rock (Zen, written communication). Both pyroxene and hornblende as residual phases affect melt REE patterns by depleting the middle and heavy REE (Haskin, 1978).

Selected trace elements and ratios are plotted against silica in Fig. 15. Rubidium, which exhibits similar chemical behavior to potassium and is masked by potassium, should show a positive correlation with K. Due to a larger cation radius (1.49 for Rb^+ vs 1.33 for K^+), Rb should preferentially concentrate in residual melt phases during fractional crystallization. In suites of rocks related by differentiation, the typical trend is for K/Rb to decrease from mafic to acid compositions. Fig. 16 illustrates such a trend for the Pioneer rocks. The K/Rb ratio for the Pioneer rocks is nearly constant at 300, near the high end of

Table V. Trace element abundances (ppm)*

Map unit	Kpd	Kpgr				
Sample	M313-1	IVP	FG	BC	M121-1	M881-1
Cr	<8.4	5.8	7.0	6.6	6.3	7.0
Co	26.5	7.1	7.5	3.6	7.2	7.0
Zn	96	62	49	52	54	47
Ba	382	916	799	1390	891	1070
Zr	559	249	280	190	189	101
La	26	42	42	40	32	41
Ce	50	70	71	64	54	55
Nd	28	29	25	25	23	23
Sm	7	6	5	5	4.9	3.9
Eu	1.62	1.24	1.09	0.98	0.93	0.89
Tb	0.95	0.70	0.56	0.47	0.51	0.46
Tm	0.49	0.41		0.34	0.31	0.31
Yb	3.0	2.2	2.3	1.6	2.1	1.8
Lu	0.45	0.38	0.39	0.23	0.34	0.28
Rb	34	89	n.d.	73	112	100
Sr	498	475	n.d.	629	403	409

Map unit	Kpp	Kpg		Tpg	
Sample	BH9850'	BHS	M744-2	M500	M32-1
Cr	13.3	4.0	n.d.	5.6	5.1
Co	10.8	2.2	4.7	2.0	0.3
Zn	72	29	34	36	17
Ba	993	1393	709	1283	518
Zr	289	156	95	130	55
La	51	39	28	35	11
Ce	86	64	48	58	19
Nd	37	23	19	23	8
Sm	6.9	4.2	4.6	4.5	2.0
Eu	1.52	0.97	0.89	0.79	0.32
Tb	0.82	0.52	0.60	0.47	1.2
Tm	0.35	0.29	n.d.	<0.20	<0.23
Yb	2.5	1.4	1.2	1.1	2.0
Lu	0.39	0.24	n.d.	0.16	0.29
Rb	88	98	102	106	123
Sr	428	262	272	240	213

*elements Cr through Lu determined by multielement instrumental neutron activation analysis in U.S.G.S. Laboratories (P. Baedecker, L. Schwarz, analysts)
Reported values represent averages of 1-3 determinations per sample.
Rb and Sr determined by J. Arth, U.S.G.S. n.d.=not determined

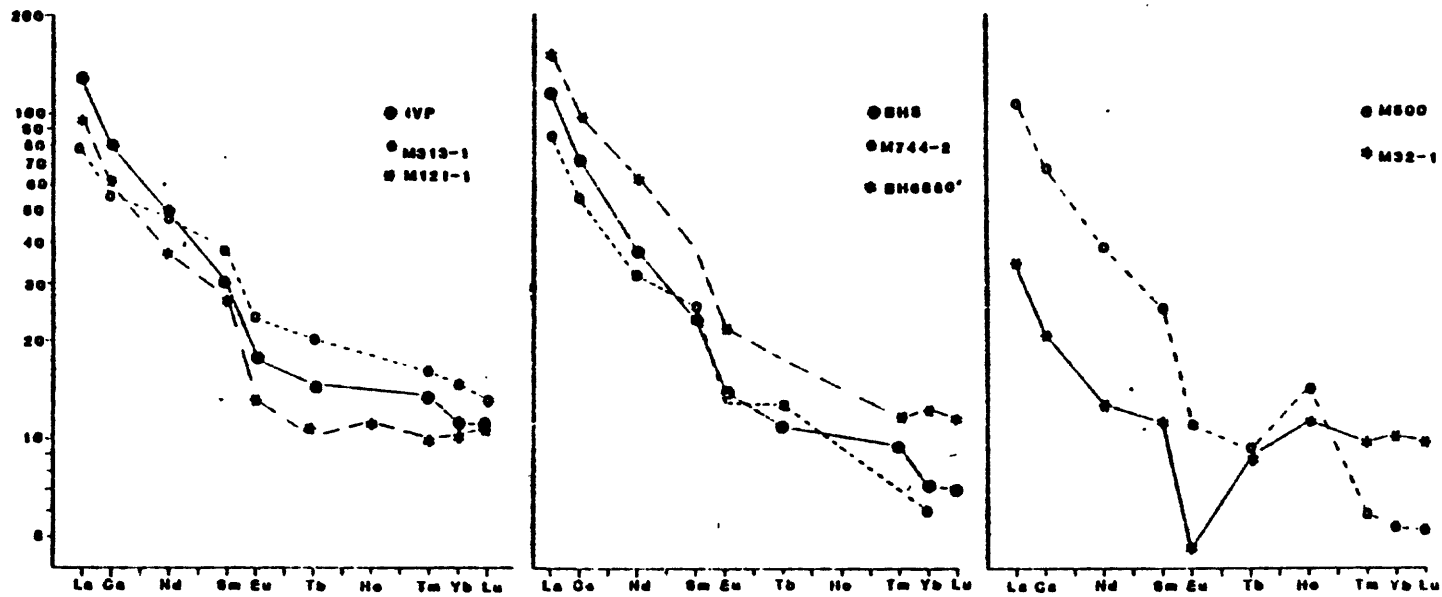

Figure 14. Chondrite-normalized rare earth element patterns for Pioneer rocks. Data are given in Table V. Plots are grouped in terms of age (Cretaceous vs. Paleocene) and initial strontium ratios.

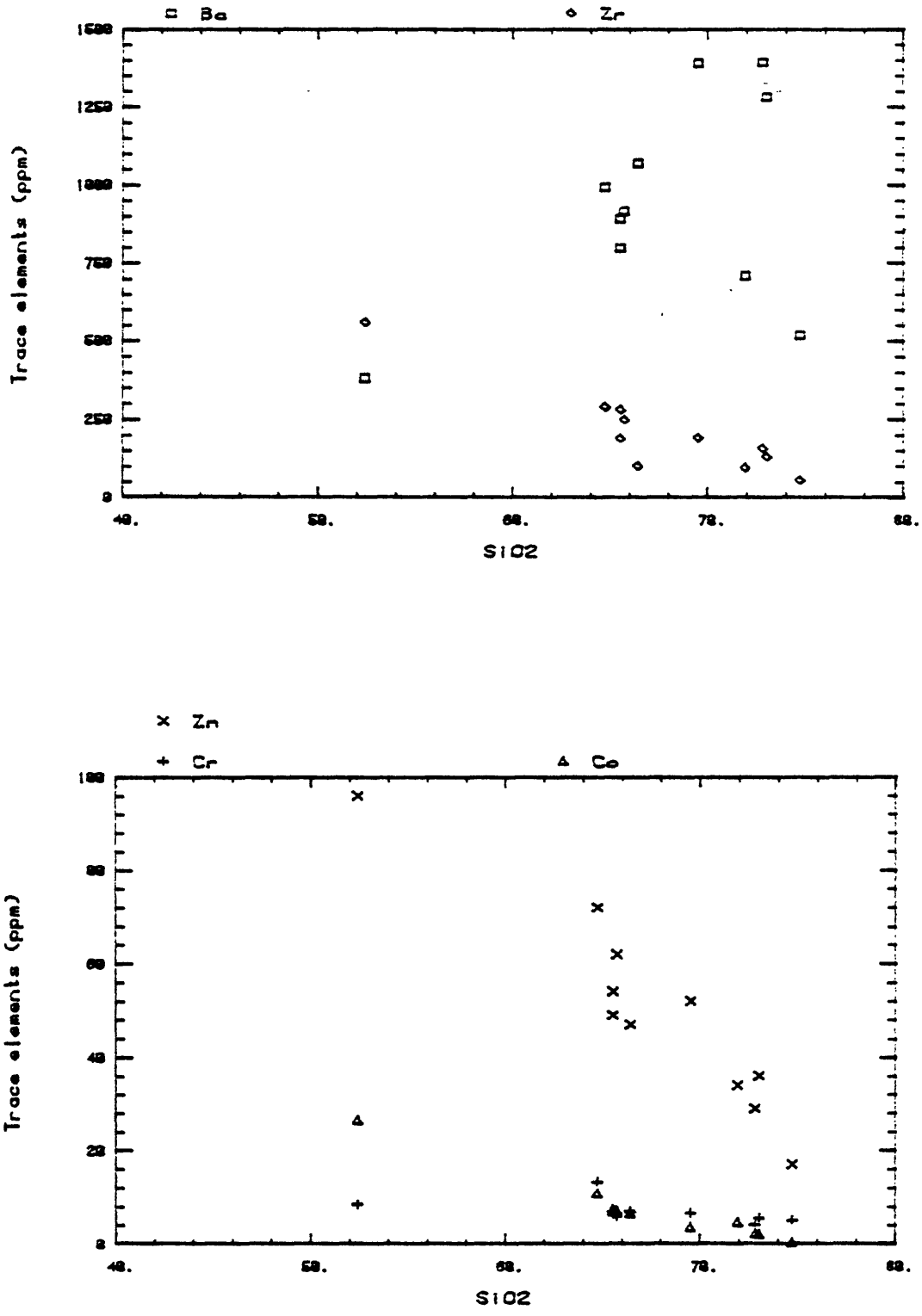

Figure 15. Trace element concentrations (ppm) vs. SiO_2 for Pioneer rocks. Data are given in Table V.

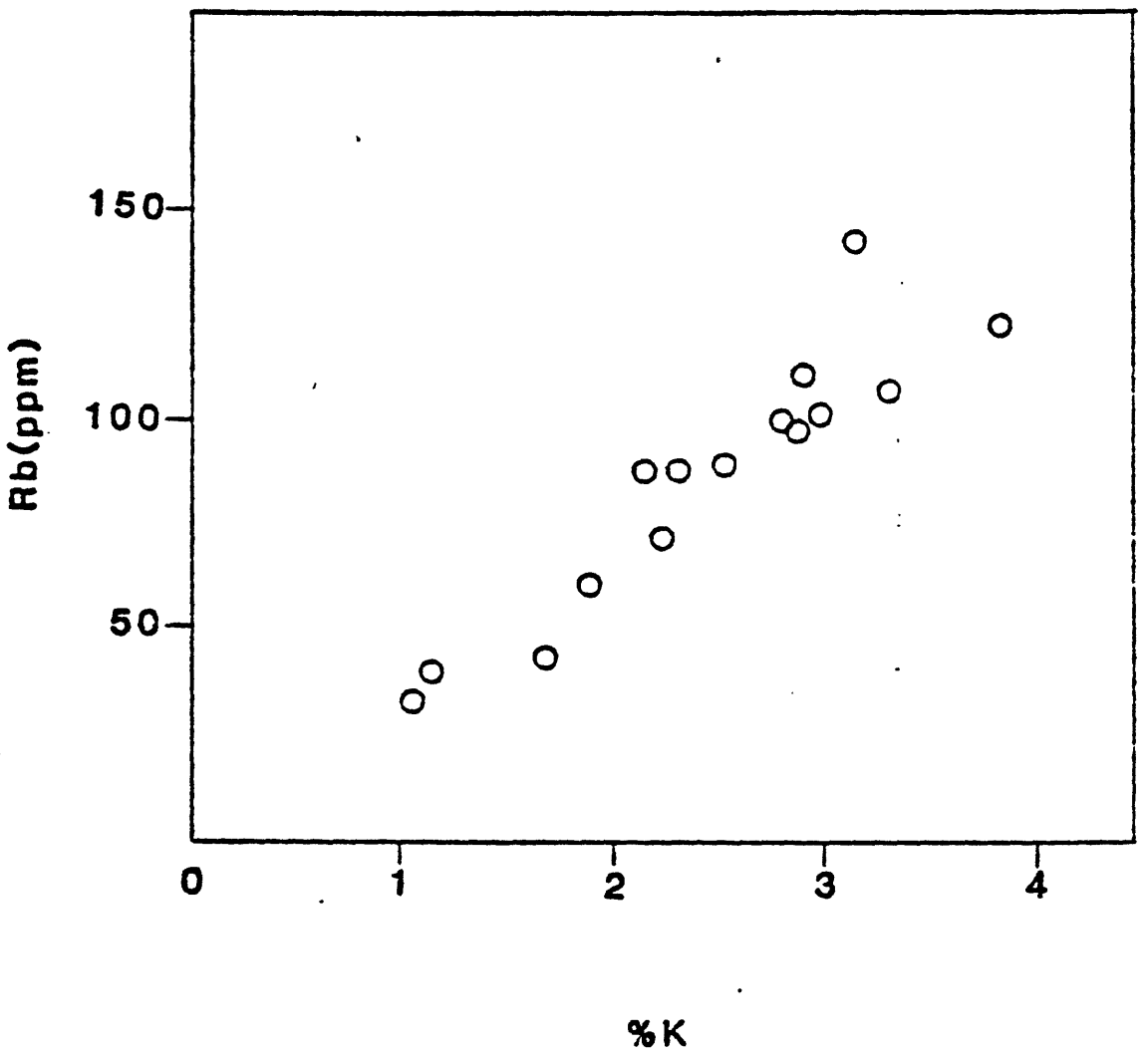

Figure 16. Rb (ppm) vs. %K diagram for Pioneer rocks.

the range (160-300) usually observed for granitic rocks. The lowest K/Rb ratio,220, is for a contaminated quartz diorite and the highest, 378, is for a tonalite which may actually be part of another group of intrusive rocks (probably Cretaceous, but exact age uncertain). High K/Rb ratios are consistent with crystallization of biotite from the melt, i.e., removal of a low K/Rb mineral from the melt. The effect of potassium feldspar removal, a high K/Rb mineral, should be to decrease the K/Rb ratio in progressively more felsic rocks, as observed in the Sierra Nevada by Bateman and Chappell (1980). All of the Pioneer rocks contain biotite, and all but the quartz diorite contain potassium feldspar, which appears to be a phase that begins crystallizing late in the stages of magma solidification on textural grounds relative to plagioclase, quartz and mafic minerals.

Rb and Rb/Sr tend to increase with increasing silica content; Ba is erratic and Zr tends to decrease.

Mineral chemistry

Analytical technique

Major element compositions of amphiboles, micas, feldspars and accessory minerals in polished thin sections were determined by microprobe analyses. Collection sites and distribution of samples among the various plutons of the batholith are indicated on the sample location map in Fig. 3. ARL microprobes at the U.S. Geological Survey in Reston, Virginia (3 channel) and at V.P.I. & S.U. (9 channel) were used in this study. Both probes were operated at 15 KV with beam current 0.05 - 0.10 microamps. Natural mineral standards were used for most elements and data reduction was accomplished by using automated Bence-Albee correction schemes (1968) incorporating Albee & Ray's (1970) alpha factors. Standard deviations on replicate analyses indicate that values obtained are reliable to ± 3% of the amount present for major elements in a mineral (>20 weight %) and to ± 10% of the amount present for minor elements (<20 weight %). Complete tables of analyses for hornblende, biotite and muscovite from representative samples are given in Appendices I-III. Mineral separations of hornblende, biotite, muscovite and potassium feldspar were obtained for some samples in conjunction with age and isotope studies and separates were available for selected chemical and x-ray studies.

In order to estimate ferrous/ferric iron ratios in biotites, ferrous iron was analysed by decomposing biotite separates by HF digestion in a dry nitrogen atmosphere followed by titration with a standard dichromate solution using diphenylamine sulfonate as an indicator. This is a modification of the procedure outlined by Shapiro (1975). Average

total iron as FeO for a given sample was taken from microprobe data and the difference between FeO by microprobe and FeO by titration was computed as Fe_2O_3. The ferrous iron value determined by this method is a minimum. Apart from analytical error, two major sources of error exist: 1) oxidation during handling of the sample and 2) erroneous total iron determination by microprobe. Samples were ground by hand in an agate mortar in air, handling times were kept as short as possible, and acid decompositions and titrations were done in an atmosphere of flowing dry nitrogen to reduce the risk of oxidation. Standards were analysed along with the samples to check accuracy and replicate analyses were done, sample permitting. Points for microprobe analysis were chosen to include variations in grain size and rim to core relations in grains. Total iron was checked by atomic absorption analysis for two samples; results are within the standard deviations determined by microprobe. Results of Fe analyses are shown in Table VI.

Three biotite separates and two muscovite separates were analysed for lithium by flame emission spectrophotometry.Samples were put into solution by digestion with HF, HNO_3 and HCl (Maxwell, 1968). Standards were made up from crystalline Li_2CO_3 and corrected for silica. A standard rock (U.S.G.S. GSP-1) was prepared as an unknown and run with the micas. All five micas are low in lithium. Results are given in Table VIb.

Structural states of potassium feldspars were determined by the 3-peak method of Wright (1968). Separates were obtained from ground whole rock splits by using heavy liquids and magnetic separation or megacrysts were drilled out of hand specimens. Peaks were determined by averaging triplicate scans (1/2°/minute) of smear mounts with CaF_2 as an internal

Table VIa. Results of iron analyses on biotites.

		FeO (weight percent)		
Method of analysis		microprobe *1	atomic absorption *2	titration *3
Map unit	Sample			
Kpd	M313-1	19.34 ± 0.48		16.78
Kpgr	FG	17.21 ± 0.23		14.17
	M881-1	17.86 ± 0.05		13.76
	M121-1	17.54 ± 0.19	17.92	14.28
Kpg	BHS	17.48 ± 0.27	17.96	15.22
Kpp	BH9850	19.53 ± 0.58		16.25
Tpg	M500	21.43 ± 0.47		17.43

*1 average values for total iron as FeO ± 1 standard deviation

*2 total iron as FeO

*3 average values for ferrous iron determined by titration with standard dichromate solution using diphenylamine sulfonate indicator

Table VIb. Results of lithium analyses on micas.

Sample	% Li
USGS Standard GSP-1	0.003*
M500 Muscovite	0.004
BHS Biotite	0.036
FG Biotite	0.023
M121-1 Biotite	0.036

*Reported values for Li range from 0.0026% to 0.0053%

standard. A diffractometer equipped with a curved graphite monochrometer was used for all x-ray work.

Hornblende

Representative analyses of hornblendes are cited in Table VII. Formulae were calculated on the anhydrous basis of 23 oxygens (Borg, 1967). F and Cl for some points were determined by microprobe; $Fe^{+3}/Fe^{+3}+Fe^{+2}$ was defined as 27% for all analyses based on ferric and ferrous iron values in three chemical analyses on separates from different plutons. Average probe analyses are in good agreement with the chemical analyses (Table VIII). A theoretical water content was calculated as a check on oxide sums. Site occupancy assignment for cations follows the scheme described by Czamanske and Wones (1973).

All of the amphiboles analysed are "magnesio-hornblendes" as defined by Leake (1978);i.e., Si=6.50-7.25, $Mg/Mg+Fe^{+2}>0.50$, $(Ca+Na)>1.34$, $Na<0.67$, $(Na+K)<0.50$ and $Ti<0.50$. In the Pioneer hornblendes, most Al enters the tetrahedral site, virtually all Na enters the A site and Ca is constant at 1.8-1.9 cations per 23 O. Where core-rim differences are noted, the cores are higher in total Al and Ti and lower in Si relative to the rims, reflecting dropping temperatures and increasing silica activity as crystallization proceeds. Fig. 17 illustrates the relative differences in hornblende composition and variation in composition within a single grain for a) a quartz diorite, sample M107-1, where a brownish core and distinct greenish rim are observed and b) a granodiorite, sample WC, which exhibits patchy coloration but no distinct core and rim.

Table VII. Hornblende analyses.

Map Unit	Kptl		Kpgr		
Sampl	M984-2	M984-2	FG	IVP	M704-1
SiO_2	42.02	45.96	50.08	46.91	44.64
Al_2O_3	10.64	7.02	4.74	8.13	8.88
Fe_2O_3*	4.59	5.20	3.76	4.52	4.87
FeO	11.16	12.66	9.14	11.00	12.61
MgO	11.60	11.81	15.83	12.91	11.36
CaO	11.02	10.52	11.74	12.30	11.75
Na_2O	2.09	1.33	0.90	1.25	1.39
K_2O	0.94	0.49	0.42	0.68	1.01
TiO_2	3.40	1.25	0.80	1.22	1.19
MnO	0.42	0.45	0.84	0.73	1.00
F	n.d.	n.d.	n.d.	0.27	n.d.
Cl	n.d.	n.d.	n.d.	0.09	n.d.
Sum	97.88	96.70	98.22	100.01	98.70
F=O				0.11	
Cl=O				0.02	
H_2O calc	2.01	2.00	2.09	1.92	2.03
Sum	99.89	98.70	100.31	101.80	100.73
Cations on the basis of 23 oxygens					
Si	6.25	6.89	7.22	6.78	6.60
Al^{iv}	1.75	1.11	0.78	1.22	1.40
T	8.00	8.00	8.00	8.00	8.00
Al^{vi}	0.12	0.13	0.03	0.17	0.14
Fe^{+3}	0.51	0.59	0.41	0.49	0.58
Fe^{+2}	1.38	1.50	1.08	1.33	1.56
Mg	2.57	2.64	3.40	2.78	2.50
Ti	0.38	0.14	0.09	0.13	0.14
Mn	0.04		0	0.09	0.08
M_1-M_3	5.00	5.00	5.01	4.99	5.00
Mn	0.02	0.06	0.10		0.05
Fe^{+2}		0.08	0.02		
Mg					
Ca	1.76	1.69	1.81	1.91	1.86
Na	0.22	0.17	0.07	0.09	0.09
M_4	2.00	2.00	2.00	2.00	2.00
Na	0.39	0.22	0.18	0.26	0.31
K	0.18	0.09	0.08	0.12	0.18
Ca					
A	0.57	0.31	0.26	0.38	0.49
F					
Cl					
Fe/Fe+Mg	0.42	0.44	0.30	0.40	0.46
#Points	3	3	2	2	2
Comment	brown core	green rim			core

*all Fe_2O_3 calculated for 27% Fe^{+3}

Table VII. Continued

Map Unit	Kpgr		Kpp	Kpg	
Sample	M704-1	M121-1	BH9850	M1293-1	M1119-1
SiO_2	46.20	44.42	43.79	46.78	44.70
Al_2O_3	7.80	9.39	8.41	7.72	8.43
Fe_2O_3*	4.90	4.84	5.09	4.59	4.87
FeO	11.93	11.77	12.38	11.10	11.86
MgO	12.72	11.94	11.40	11.92	11.36
CaO	12.04	12.40	12.09	11.94	12.56
Na_2O	1.19	1.35	1.24	1.18	1.20
K_2O	0.77	1.00	0.84	0.92	0.81
TiO_2	0.95	1.22	1.24	1.08	1.13
MnO	0.99	0.78	0.68	0.77	0.87
F	n.d.	0.30	0.21	0.21	n.d.
Cl	n.d.	n.d.	0.09	n.d.	n.d.
Sum	99.49	99.41	97.46	98.27	97.80
F=0		0.13	0.09	0.09	
Cl=0			0.02		
H_2O calc	2.05	1.89	1.87	1.94	2.01
Sum	101.54	101.18	99.22	100.12	99.81
Cations on the basis of 23 oxygens					
Si	6.75	6.54	6.60	6.88	6.67
Al^{iv}	1.25	1.46	1.40	1.12	1.33
T	8.00	8.00	8.00	8.00	8.00
Al^{vi}	0.09	0.17	0.09	0.22	0.15
Fe^{+3}	0.54	0.54	0.58	0.51	0.55
Fe^{+2}	1.46	1.45	1.56	1.38	1.48
Mg	2.77	2.62	2.56	2.61	2.53
Ti	0.10	0.14	0.14	0.12	0.13
Mn	0.04	0.08	0.07	0.10	0.11
M_1-M_3	5.00	5.00	5.00	4.94	4.95
Mn	0.08	0.02	0.01	0	
Fe^{+2}					
Mg					
Ca	1.88	1.96	1.95	1.88	2.00
Na	0.04	0.02	0.04	0.12	0
M_4	2.00	2.00	2.00	2.00	2.00
Na	0.29	0.37	0.32	0.22	0.35
K	0.14	0.19	0.16	0.17	0.15
Ca					0.01
A	0.43	0.56	0.48	0.39	0.51
F		0.14	0.10	0.10	
Cl			0.02		
Fe/Fe+Mg	0.42	0.43	0.45	0.42	0.45
#Points	2	3	2	4	3
Comment	rim				core

*all Fe_2O_3 calculated for 27% Fe^{+3}

Table VIII. Comparison of wet chemical analyses with average microprobe analyses for 3 hornblendes.

	M313-I (9)			BH9850' (12)			IVP (10)		
	Chemistry	Probe	S.D.	Chemistry	Probe	S.D.	Chemistry	Probe	S.D.
SiO_2	44.36	44.35	± 1.50	44.76	45.56	± 1.09	47.56	47.67	± 1.44
Al_2O_3	10.30	9.90	± 1.20	8.99	8.62	± 0.25	7.21	7.22	± 0.83
FeO	15.43+	14.13	± 1.13	17.04+	17.81	± 0.32	13.78+	14.43	± 0.54
MgO	11.53	12.63	± 0.62	10.88	11.28	± 0.15	13.39	13.24	± 0.62
CaO	11.44	11.62	± 0.19	11.91	12.06	± 0.21	11.88	12.20	± 0.14
Na_2O	1.20	1.55	± 0.33	1.09	1.16	± 0.06	0.97	1.11	± 0.15
K_2O	0.86	0.59	± 0.11	0.92	1.02	± 0.07	0.61	0.53	± 0.09
H_2O+	1.69			1.59			1.75		
TiO_2	1.92	1.86	± 0.45	1.22	1.31	± 0.11	1.07	1.03	± 0.21
P_2O_5	0.04			0.23			0.17		
MnO	0.40	0.36	± 0.11	0.57	0.71	± 0.06	0.75	0.83	± 0.07
* Σ	97.44	96.99		97.38	99.53		97.22	98.26	
$+Fe_2O_3$	4.59			5.34			4.14		
FeO	11.30			12.24			10.06		

* Σ = Σ for all Fe=FeO
H_2O=0, P_2O_5=0

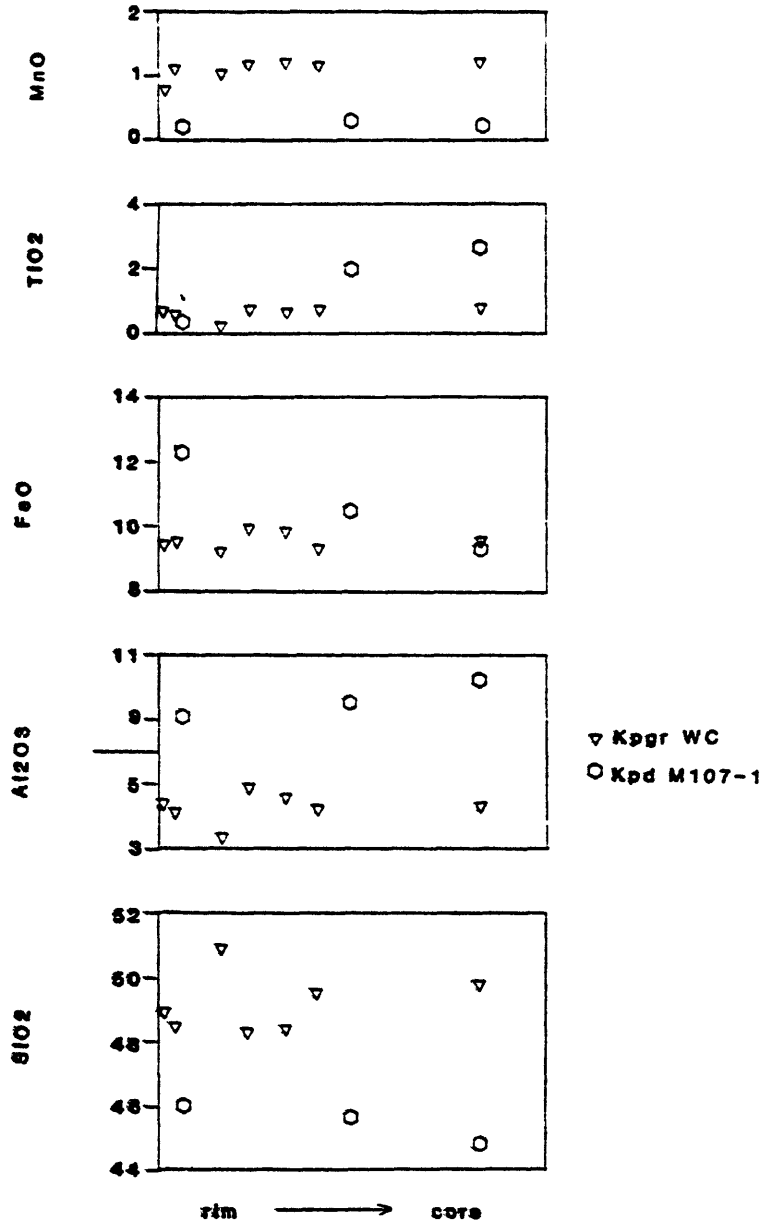

Figure. 17. Results of microprobe analyses across individual hornblende grains from rim to core for a) a hornblende from Kpd sample M107-1, which has a brown core and a distinct greenish rim and b) a hornblende from Kpgr sample WC, which is green and has a "patchy" coloration rather than a distinctly colored core and rim.

Compositional variations within amphibole grains and between rock types may be studied in terms of simple and coupled substitutions. Amphiboles deviate from the simplest amphibole formula, tremolite, $\circ\ Ca_2\ Mg_5\ Si_8\ O_{22}\ (OH)_2$ where $\circ$ stands for a vacancy in the A-site, Ca fills the M_4 site, Mg fills the M_1-M_3 sites and Si is the only tetrahedral cation present, by a variety of coupled substitutions which may be broken down into 4 main types (Doolan and others, 1978) depending on which sites are involved. Czamanske and Wones (1973) also described in detail the coupled substitutions which maintain charge balance and give rise to end-member amphibole compositions. Table IX gives examples of possible substitutions.

Fig. 18 shows the range of composition within each map unit in terms of tetrahedral Al and total A-site occupancy variation with Ti.

Robinson and others (1971) noted that the relationship $Al^{iv} = \Sigma$ A-site + $(Al^{vi} + Fe^{+3} + 2Ti^{+4})$ is obeyed for the edenite and tschermakite substitutions. Fig. 19 shows that although some analyses fall along the $1Al^{iv}:1(A+Al^{vi}+Fe^{+3}+2Ti^{+4})$ line, most lie below the line, suggesting that substitutions involving the M_4 site are operative. Plots of Na_{M4} vs A-site and Na_{M4} vs $(Al^{vi}+Fe^{+3})$, which test for the richterite and riebeckite-glaucophane substitutions, respectively, were largely uninformative. Doolan and others (1978) presented a plot of $(Al^{vi}+Fe^{+3}+2Ti^{+4})-Na_{m4}$ vs $Al^{iv}+Na_{M4}$ for 840 amphibole analyses from the literature. Such a plot best separates the effects of various substitutions. As this study pointed out, the quantity $(Al^{vi}+Fe^{+3}+2Ti^{+4})$, which they define as y*, sums glaucophane and tschermakite substitutions and y^*-Na_{M4} removes the effect of the glaucophane substitution. They

TABLE IX. Some types of possible coupled substitutions in amphiboles

SITE				AMPHIBOLE
A	M_4	M_1-M_3	T	
	Ca_2	Mg_5	Si_8	ideal tremolite
Na,K			Al	edenite
Na	Na			richterite
	Na	Al		glaucophane
	Na	Fe^{+3}		riebeckite
	2 Na	Ti		
		Al	Al	tschermakite
		Fe^{+3}	Al	
		Ti	2 Al	

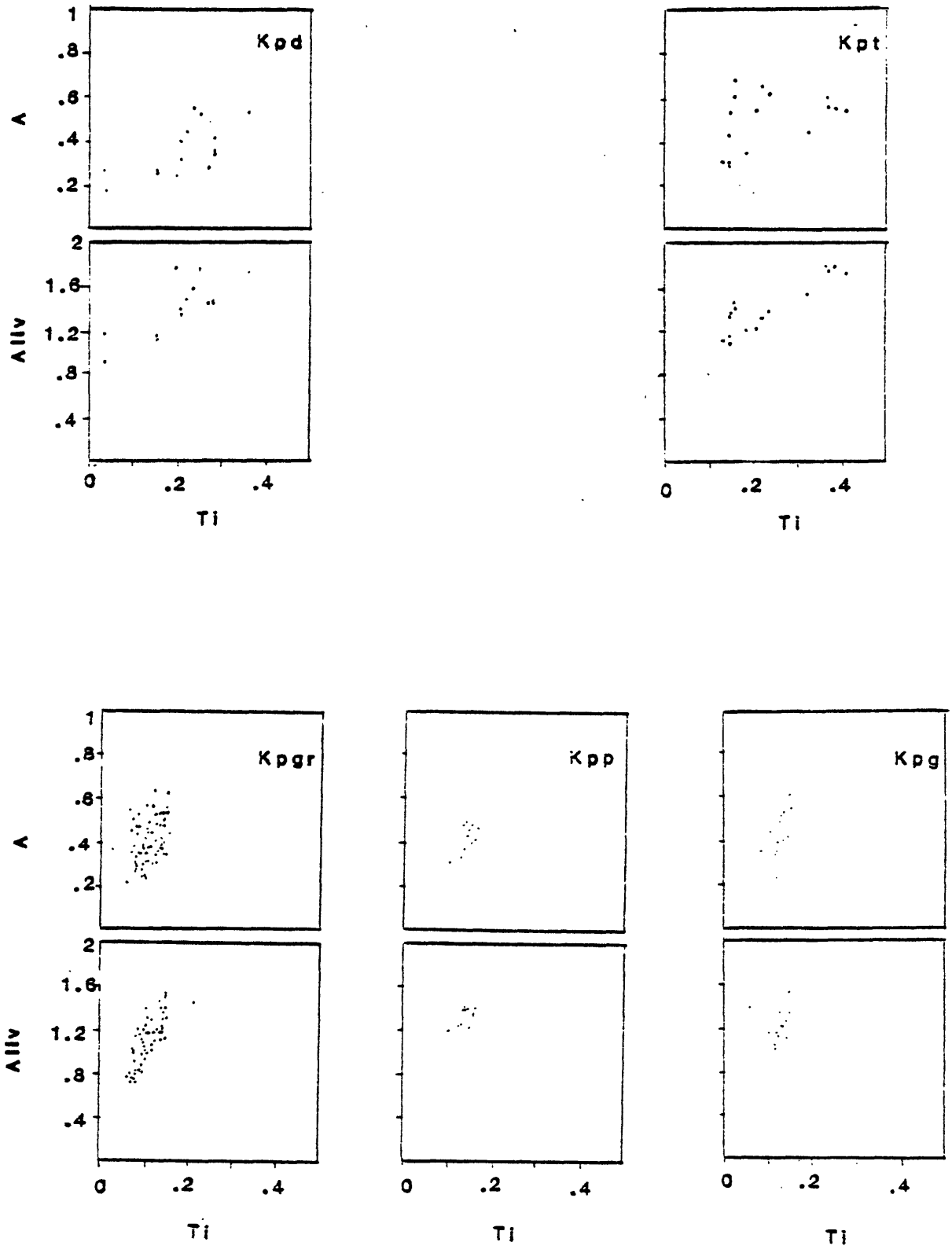

Figure 18. Variation of Al^{vi} and total A-site occupancy as a function of Ti per formula unit for hornblende, from major plutons of the Pioneer Batholith.

found that all analyses fell below a line defined by the equation $y^*-Na_{M4}=0.82\ (Al^{iv}+Na_{M4})$ and that most fell along a line with a slope of 0.65. Fig. 20 shows the trend observed for Pioneer amphiboles on such a plot. Changes in Ti content within grains and between rocks suggest that Ti is involved in coupled substitutions. Ti in M_1-M_3 may be coupled with an M_4 occupant in a glaucophane (2Na+Ti)-type substitution or with tetrahedral occupants in a tschermakite ($Ti+2Al^{iv}$)-type substitution. Figure 18 illustrates a positive correlation between Al^{iv} and Ti. Several aspects of these plots are noteworthy. First, there is a poor linear fit through the data, closer to a 1:3 slope than the 1:2 slope expected for a Ti:2Al substitution. Zen (1980, written communication) noted the abundance of Fe^{+3} cations (Fe^{+3}:Ti ~ 3:1) and suggested that a 1:3 slope may arise from a combination of a Ti-tschermakite (Ti+2Al) and a tschermakite (Fe^{+3}+Al) substitution. Second, the most Al^{iv} and Ti rich compositions correspond to cores in hornblendes from quartz diorite and tonalite. Rim compositions fall in the middle of the range of compositions, where most granite and granodiorite analyses lie. The least Al- and Ti- rich compositions correspond to granodiorite samples from the southernmost parts of the batholith.

Discussion

Substitutions in hornblendes have been investigated by field and experimental studies and attempts have been made to correlate trends observed with changes in T, f_{O2} and bulk composition. Dodge, Papike and Mays (1968) reported on hornblendes in the Sierra Nevada Batholith and cited studies which propose that Al substitution for Si increases with increasing temperature of crystallization. Relative stabilities

of amphiboles investigated experimentally - pargasite is thermally more stable than tremolite (Ernst, 1968) - and the observation of increasingly more pargasitic hornblende (relative to tremolitic) with increasing metamorphic grade agree with this proposal. Helz (1973) reported on hornblende compositions encountered in experimental runs on basalts and found the the total A-site occupancy and tetrahedral Al increased with increasing temperature for a given bulk composition and oxygen fugacity. She proposed that linear trends observed for plots of Al^{iv} vs. A-site (slopes +2, +3 depending on bulk composition) result from crystal-chemical constraints required to maintain charge balance when Ti (+4) and Al(+3) substitute for +2 cations in the M_1-M_3 sites; i.e., a change in edenite-type substitution is counterbalanced by a change in tschermakite-type substitution. Furthermore, Helz confirmed a temperature dependence for the Ti-tschermakite substitution suggested by the observation of increasing TiO_2 in amphiboles at higher metamorphic grades and the occurrence of kaersutitic hornblendes in high temperature rocks. Helz demonstrated that the extent of the Ti-tschermakite substitution depends on oxygen fugacity as well as temperature. Decreasing f_{O2} at constant temperature and bulk composition resulted in 1) an increase in TiO_2 content in Helz's hornblendes (hematite-magnetite to quartz-fayalite-magnetite buffer ranges for f_{O2}), and 2) higher Fe/Mg ratios. Helz also found that at constant f_{O2} Fe/Fe+Mg generally decreased and TiO_2 increased with increasing temperature. Fig. 21 shows the trends in Fe/Fe+Mg and TiO_2 in hornblende observed in three of Helz's experiments--the 1921 Kilauea olvine tholeiite on the quartz-fayalite-magnetite (QFM) and hematite-magnetite (HM) buffers and the

1801 Hualalai alkali basalt on the quartz-fayalite-magnetite buffer. Despite the fact that these bulk compositions are not directly applicable to the Pioneer study, Helz's experiments (PH_2O = 5 kbar, T = 680-1000°C) do show the relative effects of varying intensive parameters on hornblende compositions which span the range of hornblende compositions encountered in the Pioneer and other calc-alkalic batholiths. In all three experiments Helz reported reaction of hornblende + sphene in the temperature range 850° to 1000°C to produce a more Ti- and Mg-rich hornblende (QFM conditions) or Mg-rich hornblende and titanohematite (HM conditions).

Hornblende data for the Sierra Nevada Batholith (Dodge and others 1968), the Southern California Batholith (Larsen and Draisin, 1950), the Finnmarka Complex (Czamanske and Wones, 1973) and the Pioneer Batholith are also shown. A normal, or "reducing" trend of crystallization, where f_{O2} decreases as temperature drops resulting in crystallization of more iron-rich mafic silicates as differentiation proceeds was proposed by Dodge et al. for the Sierra Nevada rocks. At Finnmarka, a trend of oxidation with differentiation has been established by field study and examination of mineral chemistry (Czamanske and Mihalik, 1973; Czamanske and Wones, 1973). The range of compositions of Pioneer amphiboles is similar to the Sierra Nevada and markedly different from the Finnmarka trend. High Ti contents for hornblende cores in quartz diorite and tonalite indicate that they formed at higher temperatures than rims and granodiorite and granite hornblendes. Bulk composition as well as the drastic effects of relatively high oxygen fugacities on limiting Ti may account for the limited TiO_2 in Pioneer and Sierra amphiboles (i.e., f_{O2} was higher than QFM buffer conditions throughout).

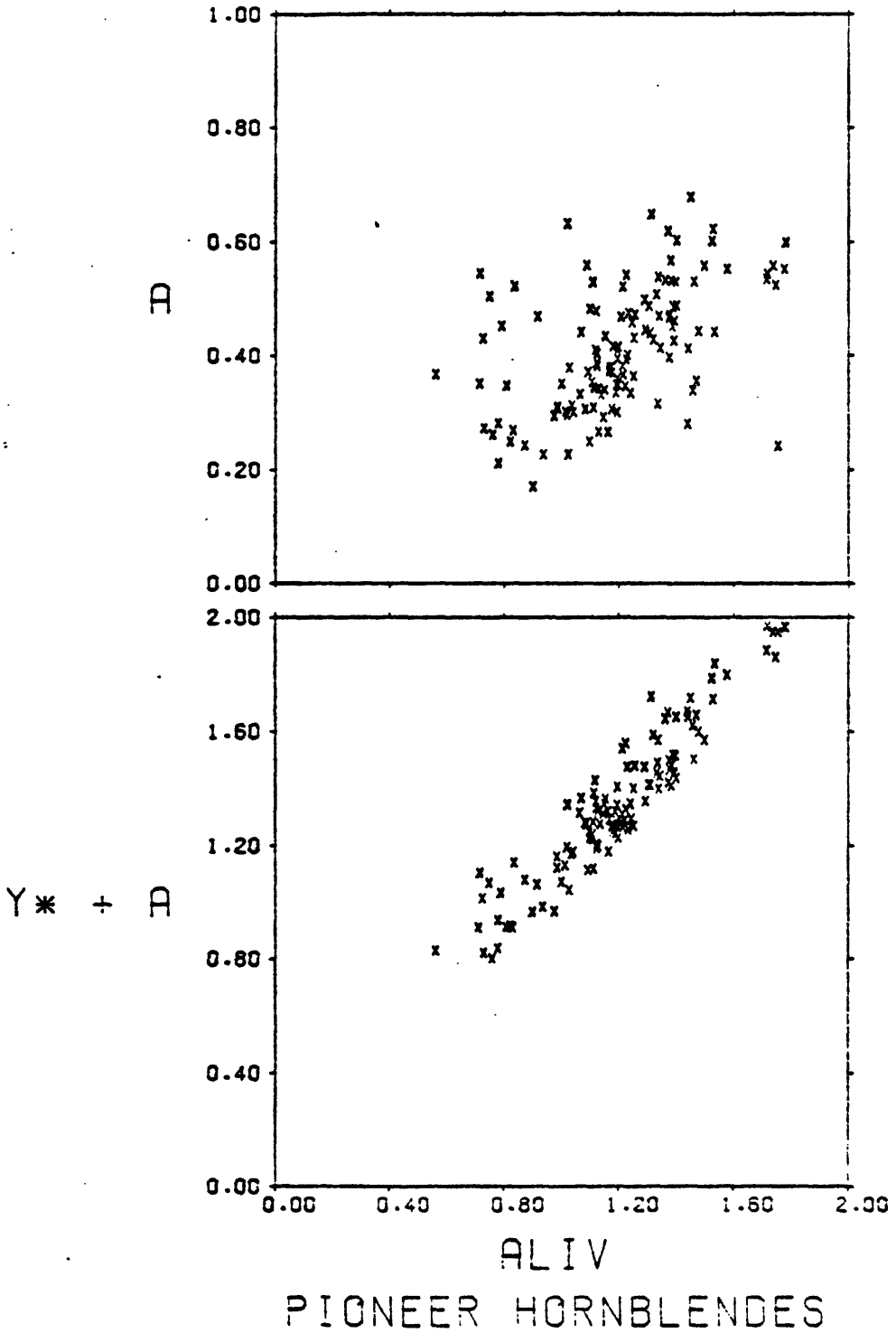

Figure 19. Plots of total A-site occupancy and y^*+A versus Al^{IV} for all Pioneer hornblendes. $y^* = Al^{VI} + Fe^{+3} + 2Ti^{+4}$

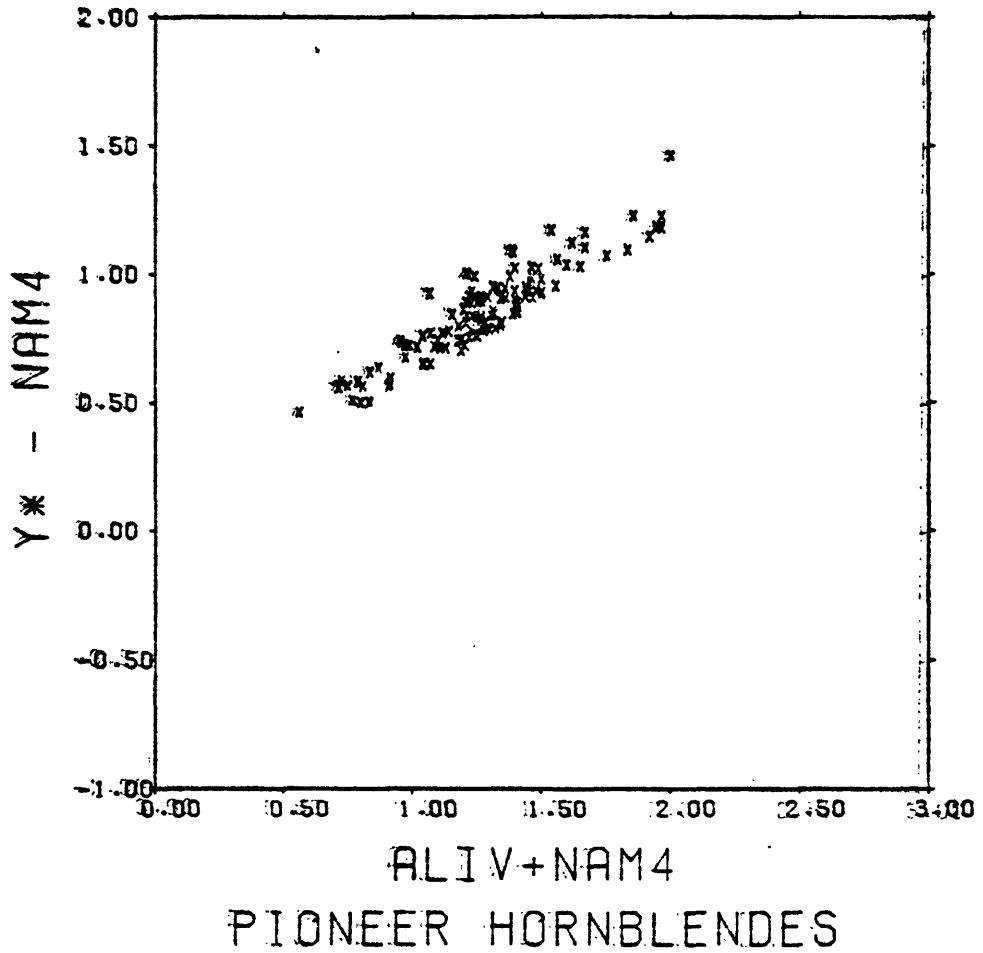

Figure 20. Plot showing y^*-Na_{M4} vs. $Al^{IV} + Na_{M4}$ for all Pioneer hornblendes. $y^* = Al^{VI} + Fe^{+3} + 2Ti^{+4}$; Na_{M4} = cations Na per M4 site based on hornblende site-partitioning scheme outlined by Czamanske and Wones (1973).

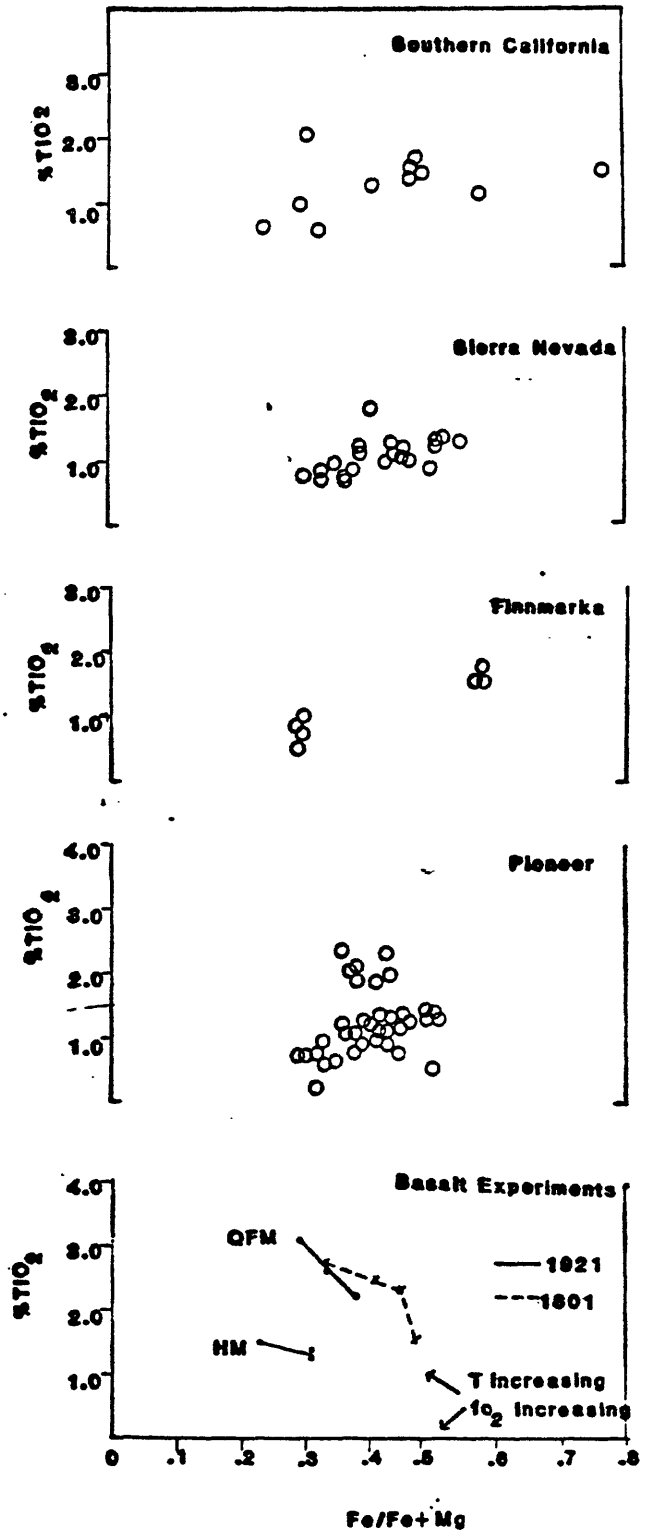

Figure 21. Ranges of TiO_2 and Fe/Fe+Mg for hornblendes from calc-alkalic granitic complexes compared with hornblende compositions encountered in experimental work on basalts. Data are from the following sources: Southern California batholith, Larsen and Draisin, 1948; Sierra Nevada batholith, Dodge, Papike and Mays, 1968; Finnmarka complex, Czamanske and Wones, 1973; Pioneer batholith, this study; experimental, Helz, 1973.

Biotite

Brown biotite occurs in all of the rocks of the batholith. In terms of end-member biotite compositions, the Pioneer biotites are intermediate, falling along a trend between phlogopite and siderophyllite, as shown in Fig. 22. Table X gives representative microprobe analyses. Ferric/ferrous ratios were determined for at least one sample per map unit, and resulting ratios were applied to all samples from a given unit. As previously discussed, FeO values are a minimum, but it was believed that minimum FeO values were preferable to calculation of all iron as FeO.

Silicon and aluminum fill the tetrahedral site and in most cases, aluminum also enters the octahedral site. M-site occupancies ($Al^{vi}+Fe^{+3}+Fe^{+2}+Mg+Mn+Ti$) range from 2.79 to 2.90 out of an ideal 3.00 based on 11 oxygens per formula unit. A-site occupancies (K+Ca+Na) range from 0.91 to 1.01. Fluorine and chlorine were analysed by microprobe for some samples; fluorine atoms per formula unit always occupy less than 10% of the available 2 anions per OH-site. No significant amounts of chlorine were detected. Lithium, which may substitute for Al, commonly increases with differentiation (Deer, Howie & Zussman, 1963). Li analyses for three biotite separates (Table VIb) ranged from 0.023% and 0.036% Li for Cretaceous granodiorite to 0.036 for typical Cretaceous granite. All three values are lower than reported values for biotites from calc-alkalic igneous rocks (Nockolds, 1947; Deer and others,1963), which are around 0.1-0.3% Li_2O.

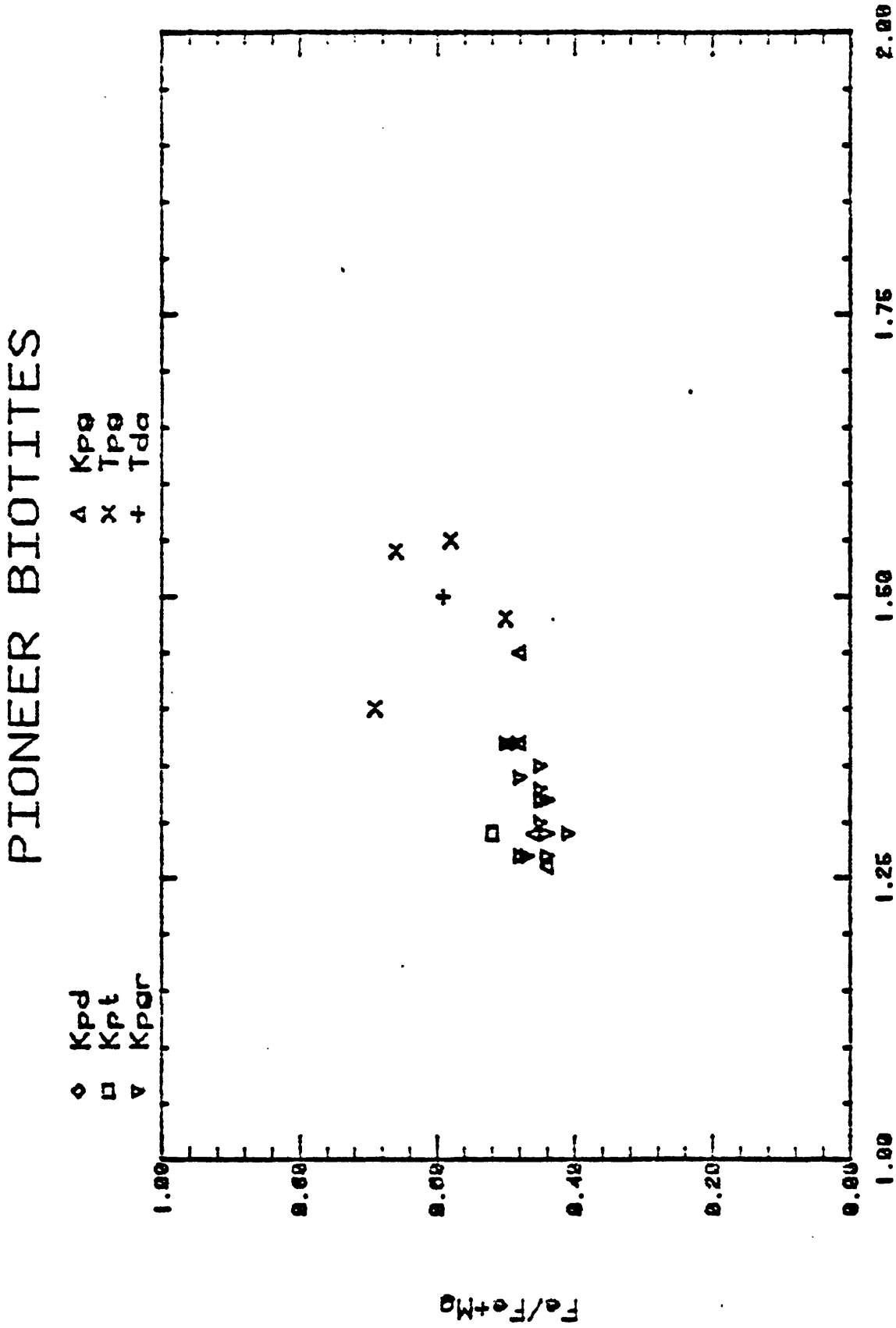

Figure 22. Pioneer biotite compositions in terms of end-member biotite compositions defined by Fe/Fe+Mg and Al for biotite formulae based on 11 oxygens per formula unit.

Nockolds (1947) compiled data on variations in igneous biotite compositions with rock type For calc-alkalic intrusive rocks, Nockolds found that in the progression of mineral assemblages from biotite + hornblende to biotite along to biotite + muscovite, Si^{iv} in biotite decreases while Al^{iv}, Al^{vi} and FeO/MgO usually increase. Such trends are observed for Pioneer biotites. Biotites coexisting with muscovite are the most Al-, Fe-, and Mn-rich. This suggests that biotite is of appropriate composition for coexistence with magmatic muscovite. As Nockolds pointed out, the association of muscovite with Al-poor biotite would support a secondary origin for muscovite, provided biotite did not reequilibriate during muscovite formation.

Simple and coupled substitutions similar to those observed in amphiboles may also apply to biotites, although assignment of cations to particular sites is less constrained. Mg decreases as Fe (total iron) increases. Consistent with observed trends in amphiboles, biotite from quartz diorite and tonalite fall in the middle of the range of compositions.

As in the amphiboles, Al^{vi} decreases with increasing Ti (Fig. 23), suggesting a $3Ti \rightarrow 4Al^{vi}$ substitution. Anderson (1980) cited numerous recent studies of metamorphic assemblages which indicate that the limits for Ti saturation in biotites and hornblendes decrease with decreasing temperature. Robert (1976) and Abrecht and Hewitt (1980) investigated Ti solubility in phlogopite and biotite experimentally and substantiated Ti dependence on temperature. Average weight% TiO_2 in biotite varies from a high of 4.7% in the northernmost tonalite pluton to a low of 2.6% in Paleocene muscovite granite.

Na_2O is low (<0.20 weight per cent) for all biotites. Wones (1980) interpreted low Na_2O contents of Lucerne biotites as a result of subsolidus reequilibration on the basis of Rutherford's (1969) experimental work on iron biotite-alkali feldspar equilibria which indicated higher Na_2O contents for iron biotites coexisting with intermediate alkali feldspar.

Several lines of evidence indicate that biotite in the small quartz diorite pluton has been affected by intrusion of the nearby Cretaceous granite pluton, as suggested by Zen, Marvin and Mehnert (1975). First, biotite from the quartz diorite gives a disturbed Ar spectrum (Snee, informal communication) and is in disagreement with the hornblende age. Second, Fe/Fe+Mg ratios, Fe^{+2}/Fe^{+3} ratios and TiO_2 contents are similar to those observed for nearby granite. Third, some of the biotite exhibits sweeping extinction suggesting a metamorphic texture.

Table X. Biotite analyses.
(averages ± 1 standard deviation)

Map unit	Kpd		Kpt_1		Kpgr		Kpgr	
Sample	M313-1		M984-1		FG		BC	
SiO_2	35.57	.77	36.59	.70	36.98	1.02	36.26	.78
Al_2O_3	15.02	.40	14.55	.44	14.82	.20	14.37	.32
FeO_T	19.34	.48	21.09	.58	17.21	.23	17.52	.56
MgO	11.25	.20	10.84	.23	13.87	.42	12.23	.51
CaO	0.09	.04	0.06	.02	0.06	.02	0.08	.04
Na_2O	0.08	.01	0.15	.04	0.14	.03	0.12	.02
K_2O	9.38	.24	9.49	.16	9.92	.17	9.65	.24
TiO_2	3.25	.60	4.74	.37	4.44	.32	3.90	.37
MnO	0.30	.05	0.45	.04	0.58	.02	0.98	.11
F	0.05		ND					
Cl	0.28		ND					
Sum	94.53		97.96		98.02		95.11	
FeO*	16.78				14.17			
Fe_2O_3	2.85				3.38			
H_2O(calc)	3.77		3.99		4.06		3.92	
Sum	98.30		101.95		102.08		99.03	
Cations on the basis of 11 oxygens								
Si	2.76		2.75		2.73		2.77	
Al^{iv}	1.24		1.25		1.27		1.23	
Al^{vi}	0.13		0.04		0.02		0.07	
Fe^{+2}	1.25		1.32		1.06		1.12	
Mg	1.30		1.21		1.53		1.39	
Ti	0.19		0.27		0.25		0.22	
Mn	0.02		0.03		0.04		0.06	
Ca	0.01		0.0		-		-	
Na	0.01		0.02		0.02		0.02	
K	0.93		0.91		0.94		0.94	
F	0.01		-		-		-	
Cl	0.04		-		-		-	
M	2.76		2.83		2.85			
A	0.95		0.93					
Fe/Fe+Mg	0.49		0.52		0.41		0.45	
#points	4		8		5		13	

*based on FeO titration

Table X. continued

Map Unit	Kpgr		Kpgr		Kpgr		Kpgr	
Sample	WC		MC		IP		M708-1	
SiO_2	36.09	.41	36.27	.30	36.61	.68	36.08	.52
Al_2O_3	14.05	.27	14.05	.22	14.63	.36	14.08	.28
FeO_T	18.55	.56	18.83	.27	17.79	.54	17.64	.34
MgO	11.96	.44	12.01	.14	12.42	.59	12.55	.30
CaO	0.03	.05	ND		0.08	.05	ND	
Na_2O	0.04	.07	ND		0.14	.07	ND	
K_2O	9.95	.15	9.57	.10	9.13	.19	9.56	.39
TiO_2	4.42	.28	4.04	.17	3.50	.27	4.28	.43
MnO	1.03	.17	0.52	.18	0.57	.10	0.71	.09
F					0.27	.09		
Cl					0.02	.02		
Sum	95.22		95.29		95.04		94.90	
FeO								
Fe_2O_3								
H_2O(calc)	3.90		3.92		3.80		3.92	
Sum	99.12		99.21		98.84		98.82	
Cations on the basis of 11 Oxygens								
Si	2.78		2.78		2.79		2.76	
Al^{iv}	1.22		1.22		1.21		1.24	
Al^{vi}	0.05		0.05		0.11		0.03	
Fe^{+2}	1.19		1.21		1.13		1.13	
Mg	1.27		1.37		1.41		1.43	
Ti	0.26		0.23		0.20		0.25	
Mn	0.07		0.03		0.04		0.05	
Ca	-		-		0.01		-	
Na	0.01		-		0.02		-	
K	0.98		0.94		0.89		0.93	
F	-		-		0.07		-	
Cl	-		-		-		-	
OH(calc)	2.00		2.00		1.93		2.00	
M	2.84		2.89		2.89		2.89	
A	0.99		0.94		0.93		0.93	
Fe/Fe+Mg	0.48		0.47		0.45		0.44	
#points	16		4		9		8	

Table X. Continued.

Map Unit	Kpgr		Kpgr		Kpgr		Kpgr	
Sample	M881-1		M342-1		M121-1		M697-1	
SiO_2	36.59	.54	37.78	.85	36.76	.63	33.73	.58
Al_2O_3	14.78	.04	14.70	.48	14.78	.45	14.40	.23
FeO	17.86	.05	18.02	.70	17.54	.19	19.14	.36
MgO	12.48	.14	12.85	.65	12.66	.23	11.58	.06
CaO	0.03	.02	0.04	.03	0.05	.07	0.02	.02
Na_2O	0.10	.01	0.11	.03	0.14	.05	ND	
K_2O	9.66	.36	10.05	.58	9.93	.17	10.17	.16
TiO_2	3.23	.02	3.29	.46	3.27	.16	4.22	.30
MnO	0.70	.03	0.69	.16	0.68	.05	0.60	.18
F			0.28	.11	0.40		0.29	.06
Cl					ND		ND	
Sum	95.43		97.69		96.04		94.03	
FeO	13.76				14.28			
Fe_2O_3	4.56				3.62			
H_2O(calc)	3.94		3.90		3.77		3.67	
Sum	99.37		101.59		99.81		97.69	
Cations on the basis of 11 Oxygens								
Si	2.78		2.81		2.78		2.66	
Al^{iv}	1.22		1.19		1.22		1.34	
Al^{vi}	0.11		0.10		0.10		0.0	
Fe^{+2}	1.14		1.12		1.11		1.26	
Mg	1.42		1.42		1.43		1.36	
Ti	0.18		0.18		0.19		0.25	
Mn	0.04		0.04		0.04		0.04	
Ca	-		-		-		-	
Na	0.02		0.02		0.02		-	
K	0.94		0.95		0.96		1.02	
F	-		0.07		0.10		0.09	
Cl	-		-		-		-	
OH(calc)	2.00		1.93		1.90		1.93	
M	2.89		2.86		2.88		2.91	
A	0.96		0.97		0.98		1.02	
Fe/Fe+Mg	0.45		0.44		0.44		0.48	
#points	2		7		5		3	

Table X. Continued.

Map Unit	Kpgr		Kpp		Kpg		Kpg	
Sample	M704-1		BH9850		M744-2		M1293-1	
SiO_2	36.63	1.05	39.94	0.76	34.81	0.25	37.28	0.17
Al_2O_3	15.10	0.36	15.17	0.86	13.58	0.49	14.33	0.30
FeO	18.31	0.36	19.53	0.58	17.76	0.33	17.97	0.92
MgO	12.65	0.10	10.98	0.40	12.86	0.16	11.87	0.73
CaO	0.07	0.01	0.08	0.06	0.16	0.13	0.03	0.03
Na_2O	0.11	0.01	0.09	0.03	ND		0.12	0.07
K_2O	9.66	0.30	9.68	0.35	9.95	0.43	9.81	0.24
TiO_2	3.05	0.20	2.60	0.47	3.52	0.24	3.42	0.49
MnO	0.76	0.05	0.48	0.07	0.69	0.09	0.62	0.09
F			0.28	0.18	0.61	0.06	0.30	0.08
Cl			0.01	0.01				
Sum	96.34		95.72		93.68		95.63	
FeO			16.25					
Fe_2O_3			3.65					
H_2O(calc)	3.97		3.79		3.53		3.80	
Sum	100.31		99.58		99.51		99.44	
Cations on the basis of 11 Oxygens								
Si	2.76		2.82		2.73		2.83	
Al^{iv}	1.24		1.18		1.26		1.17	
Al^{vi}	0.11		0.19		0		0.12	
Fe^{+2}	1.16		1.25		1.17		1.14	
Mg	1.42		1.25		1.50		1.34	
Ti	0.17		0.15		0.21		0.20	
Mn	0.05		0.03		0.05		0.04	
Ca	0.01		0.01		0.01		0	
Na	0.02		0.01				0.02	
K	0.93		0.94		1.00		0.95	
F			0.07		0.15		0.07	
Cl			0					
OH(calc)	2.00		1.93		1.85		1.93	
M	2.91		2.86		2.93		2.84	
A	0.95		0.96		1.01		0.97	
Fe/Fe+Mg	0.45		0.50		0.44		0.46	
#points	7		12		5		5	

Table X. Continued

Map Unit	Kpg		Kpg		Tpg		Tpg	
Sample	M1119-1		BHS		M500-1		BLM9800'	
SiO_2	36.02	0.47	36.01	0.93	35.34	0.47	34.32	0.63
Al_2O_3	14.95	0.21	15.87	0.42	17.23	0.42	16.70	0.50
FeO	18.63	0.22	17.48	0.27	21.43	0.47	24.04	0.33
MgO	11.28	0.22	10.69	0.57	8.88	0.47	6.94	0.28
CaO	0.02	0.04	0.03	0.04	0.04	0.02	0.07	0.08
Na_2O	0.16	0.11	0.10	0.04	0.09	0.05	0.08	0.13
K_2O	9.05	0.14	9.55	0.44	10.02	0.43	9.92	0.35
TiO_2	2.97	0.26	2.74	0.37	2.65	0.22	2.98	0.24
MnO	0.43	0.03	0.81	0.08	0.93	0.09	1.17	0.15
F			0.54	0.16	0.92	0.10	0.82	0.14
Cl			0.01	0.03	0.03	0.01		
Sum	93.51		93.60		97.17		96.69	
FeO			15.22		17.43			
Fe_2O_3			2.51		4.45			
H_2O(calc)	3.86		3.60		3.47		3.44	
Sum	97.37		92.20		100.64		100.14	
Cations on a basis of 11 Oxygens								
Si	2.80		2.80		2.71		2.69	
Al^{iv}	1.20		1.20		1.29		1.31	
Al^{vi}	0.17		0.25		0.26		0.23	
Fe^{+2}	1.21		1.14		1.37		1.57	
Mg	1.30		1.24		1.01		0.81	
Ti	0.17		0.16		0.15		0.18	
Mn	0.03		0.05		0.06		0.08	
Ca	0		0		0		0.01	
Na	0.02		0.02		0.01		0.01	
K	0.90		0.95		0.98		0.99	
F			0.13		0.22		0.20	
Cl			0		0		0	
OH(calc)	2.00		1.87		1.80			
M	2.88		2.83		2.85		2.86	
A	0.92		0.97		0.99		1.01	
Fe/Fe+Mg	0.48		0.48		0.58		0.66	
#points	3		17		8		16	

Table X continued.

Map Unit	Tpg		Tpg		Tda	
Sample	M32-1		M1162-1		M315-1	
SiO_2	36.30	0.95	34.65	0.65	35.67	0.35
Al_2O_3	16.61	0.27	15.15	0.22	16.44	0.28
FeO	18.54	0.89	22.48	0.45	21.61	0.95
MgO	10.41	0.62	8.75	0.44	8.49	0.38
CaO	0.06	0.03	0.15	0.12	0.04	0.07
Na_2O	0.20	0.07	ND		0.07	0.02
K_2O	9.67	0.49	9.97	0.24	10.11	0.21
TiO_2	3.68	0.45	4.04	0.46	2.72	0.31
MnO	0.82	0.13	0.48	0.09	0.50	0.12
F			0.51	0.07	0.56	0.12
Cl						
Sum	96.29		96.07		95.97	
FeO						
Fe_2O_3						
H_2O(calc)	3.97		3.60		3.61	
Sum	100.26		99.67		99.58	
Cations on a basis of 11 Oxygens						
Si	2.74		2.70		2.76	
Al^{iv}	1.26		1.30		1.24	
Al^{vi}	0.22		1.47		0.26	
Fe^{+2}	1.17		1.10		1.40	
Mg	0.21		1.47		0.98	
Ti	0.05		0.02		0.16	
Mn	0		0.04		0.03	
Ca	0		0.01		0	
Na	0.03				0.01	
K	0.93		0.99		1.00	
F					0.14	
Cl						
OH(calc)	2.00		2.00		1.86	
M	2.82		2.86		2.83	
A	0.96		1.00		1.01	
Fe/Fe+Mg	0.50		0.59		0.59	
#points	9		6		6	

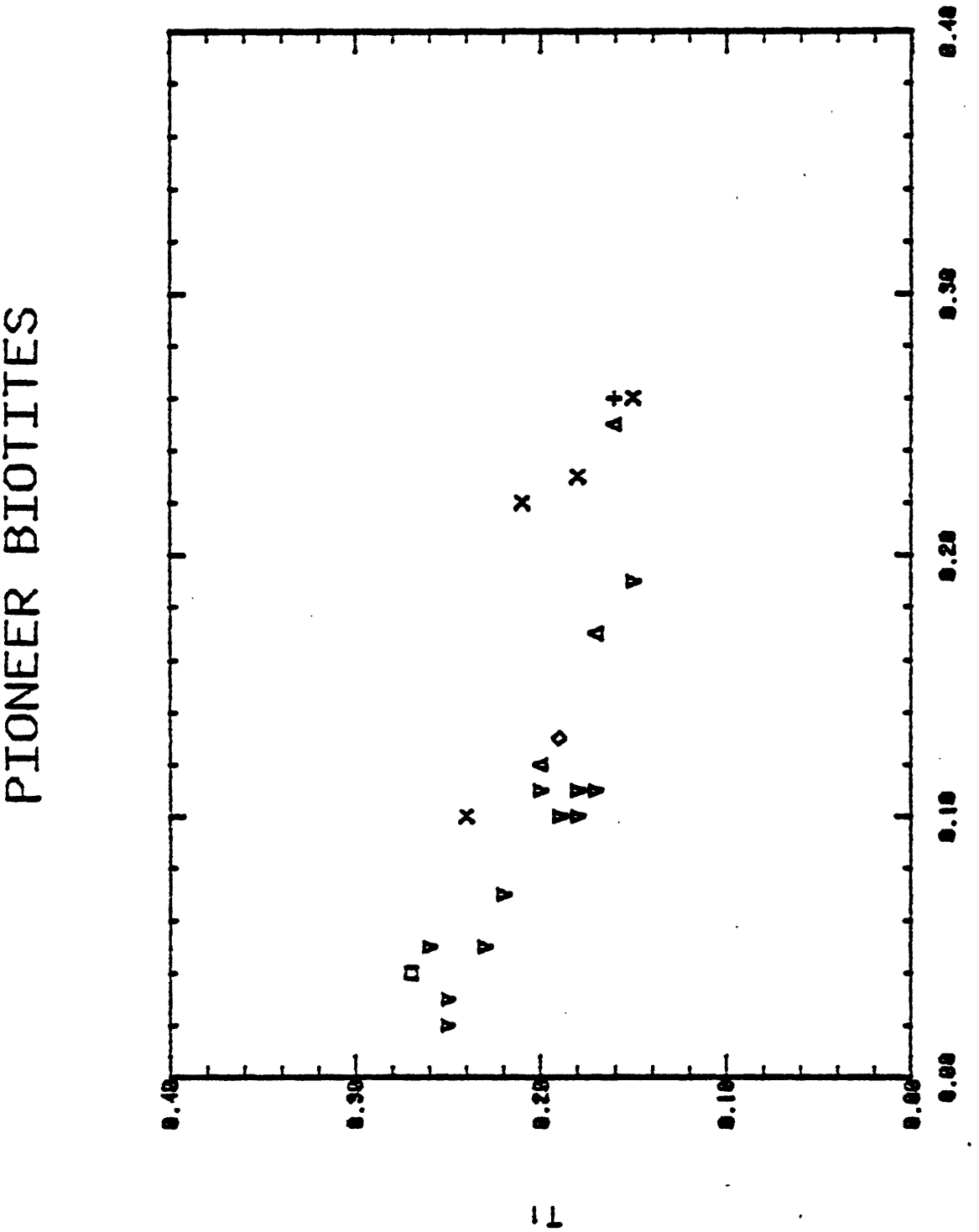

Figure 23. Pioneer biotites in terms of numbers of cations of octahedral Al and Ti per formula unit.

Muscovite

A limited number of muscovite analyses were obtained from representative samples of three Tertiary muscovite granite plutons (Tpg) as well as from a muscovite-bearing dike (Tda) and from Cretaceous granite (Kpg). While all of the muscovite in Kpg is interpreted as alteration mica on the basis of texture, muscovites in the other rocks appear both "primary" and "secondary" in origin, in the sense used by Miller and others (1980). They studied compositions of plutonic muscovites from 16 plutons and found that plutonic muscovites deviate from "ideal" muscovite, $KAl_2AlSi_3O_{10}(OH)_2$, by substitutions of Na for K; Fe, Mg and Ti for octahedral Al; and presence of excess Si and deficient Al compared to stoichiometric muscovite. Although both textural varieties were found to be similar in the way they deviate from ideal compositions, primary muscovites were generally more Ti,Na and Al-rich than secondary muscovites, which were richer in Mg and Si.

All Pioneer muscovites deviate from ideal muscovite in a manner similar to the plutonic muscovites described by Miller et al. Representative analyses are cited in Table XI. Compositions are plotted in terms of Si, Σ octahedral Fe^{+2} + Mg + Ti + Mn and Al in Fig. 24, and in terms of the major octahedral substituents, Ti, Mg and Na in Fig. 25. Iron is shown as FeO and treated as the Fe^{+2} cation due to lack of data on ferrous/ferric ratios. Miller's study included Mossbauer work on 9 muscovites which yielded high Fe^{+3}/Fe ratios (most were over 70%, but ranged from 27-89%). Octahedral cation sums for Pioneer muscovites calculated on the basic of 11 oxygens with all iron in the ferrous state are always in excess of the sum of 2.00 cations, generally by

Table XI. Muscovite compositions.

Map Unit	Kpg	Tpg					T?da		
Sample	BHS	BLM	9800[1]	M32-1	M500		M315-1		
SiO_2	45.84	45.76	46.11	47.80	45.42	46.66	46.71	47.30	46.53
Al_2O_3	28.69	32.88	32.79	30.66	33.84	32.99	31.37	30.33	32.56
FeO	4.92	4.03	4.03	4.66	3.61	3.25	4.03	4.74	3.84
MgO	1.85	0.84	0.78	1.63	0.99	1.59	0.84	1.23	0.58
CaO	0.02	0.10	0.05	0.05	0.20	0.33	0.03	0	0.01
Na_2O	0.15	0.49	0.36	0.36	0.51	0.43	0.30	0.16	0.22
K_2O	9.99	9.93	10.40	10.58	9.78	9.68	10.41	10.63	10.69
TiO_2	0.26	0.87	0.36	0.70	0.62	0.22	1.00	0.91	0.59
MnO	0.08	0.13	0	0.12	0	0.06	0.04	0.07	0.04
F	0.18	0.25	0.36	n.d.*	0.23	0.40	0.29	0.30	0.09
Sum	91.98	95.28	95.24	96.56	95.20	95.61	95.02	95.67	95.15
F=0	0.08	0.11	0.15	-	0.10	0.17	0.12	0.12	0.04
Sum	91.90	95.17	95.09	96.56	95.10	95.44	94.90	95.54	95.11
H_2O (calc)	4.17	4.31	4.25	4.48	4.34	4.29	4.28	4.28	4.39
Sum	96.07	99.48	99.34	101.04	99.44	99.73	99.18	99.82	99.50
Cations on the basis of 11 oxygens									
Si	3.23	3.10	3.13	3.20	3.06	3.13	3.17	3.20	3.15
Al^{iv}	0.77	0.90	0.87	0.80	0.94	0.87	0.83	0.80	0.85
T	4.00	4.00	4.00	4.00	4.00	4.00	4.00	4.00	4.00
Al^{vi}	1.61	1.72	1.75	1.62	1.76	1.73	1.68	1.63	1.74
Fe^{+2}	0.29	0.23	0.23	0.26	0.20	0.18	0.23	0.27	0.22
Mg	0.19	0.08	0.08	0.16	0.10	0.16	0.09	0.12	0.06
Ti	0.01	0.04	0.02	0.04	0.03	0.01	0.05	0.05	0.03
Mn	0	0.01	0	0.01	0	0	0	0	0
M	2.10	2.08	2.08	2.09	2.09	2.08	2.05	2.07	2.05
Ca	0	0.01	0	0	0.01	0.02	0	0	0
Na	0.02	0.06	0.04	0.05	0.07	0.06	0.04	0.02	0.03
K	0.90	0.86	0.90	0.90	0.84	0.83	0.90	0.92	0.92
A	0.92	0.93	0.94	0.95	0.93	0.91	0.94	0.94	0.95
F	0.04	0.05	0.08	-	0.05	0.08	0.06	0.06	0.02
OH (calc)	1.96	1.95	1.92	2.00	1.95	1.92	1.94	1.94	1.98
Na/K	0.02	0.07	0.04	0.06	0.08	0.07	0.04	0.02	0.03
#points	2	2	2	2	3	4	5	2	3
Texture	secondary with chlorite	primary	secondary in plagioclase	primary	primary	secondary in plagioclase	primary	secondary rim an opaque	secondary in plagioclase

+0.05. Assumption of ferric iron reduces the octahedral sum to a value closer to the ideal 2.00 expected for octahedral occupancy involving trivalent cations.

Ti ranges from <0.01 to 0.06 cations per 11 oxygens. Miller and others (1980) proposed the following 2 substitution mechanisms for Ti in octahedral sites:

1) $Mg^{vi} + Ti = 2Al^{vi}$ 2) $Ti^{vi} + Al^{iv} = Al^{vi} + Si^{iv}$

Na/K ratios for Pioneer muscovites are variable (0.02-0.09). Thompson (1974) demonstrated that Na increases in metamorphic muscovites from low to moderate grade and then decreases at near magmatic temperatures. Although the spread in Na/K for "primary" muscovites spans the observed range, "secondary" muscovite compositions are confined to lower Na/K values (<0.05) (Fig. 26). Bradfish (1979) carefully documented muscovite compositions as a function of texture for the Tea Cup Granodiorite in Arizona. Bradfish found all compositions to be phengitic and concluded that all muscovites were subsolidus in origin. When plotted in terms of Na/K and Ti, Bradfish's data are similar to the data for Pioneer muscovites; i.e., his textures that we would classify as "primary" (discrete flakes and muscovite intergrown with biotite) have higher Ti contents than textures such as muscovite rimming magnetite, in feldspars and filling fractures and veins. As in the Pioneers, the Tea Cup muscovites are variable in Na/K, but lowest Na/K ratios are observed for "secondary"-type textures.

These compositional trends do not imply a rigorous chemical basis for distinguishing primary versus secondary muscovite, but indicate the presence of two compositional populations of muscovite in the same rock.

Differences may reflect a) magmatic versus subsolidus origin or b) subsolidus origin involving different mineral reactions and/or conditions during formation.

Fluorine contents are generally low.

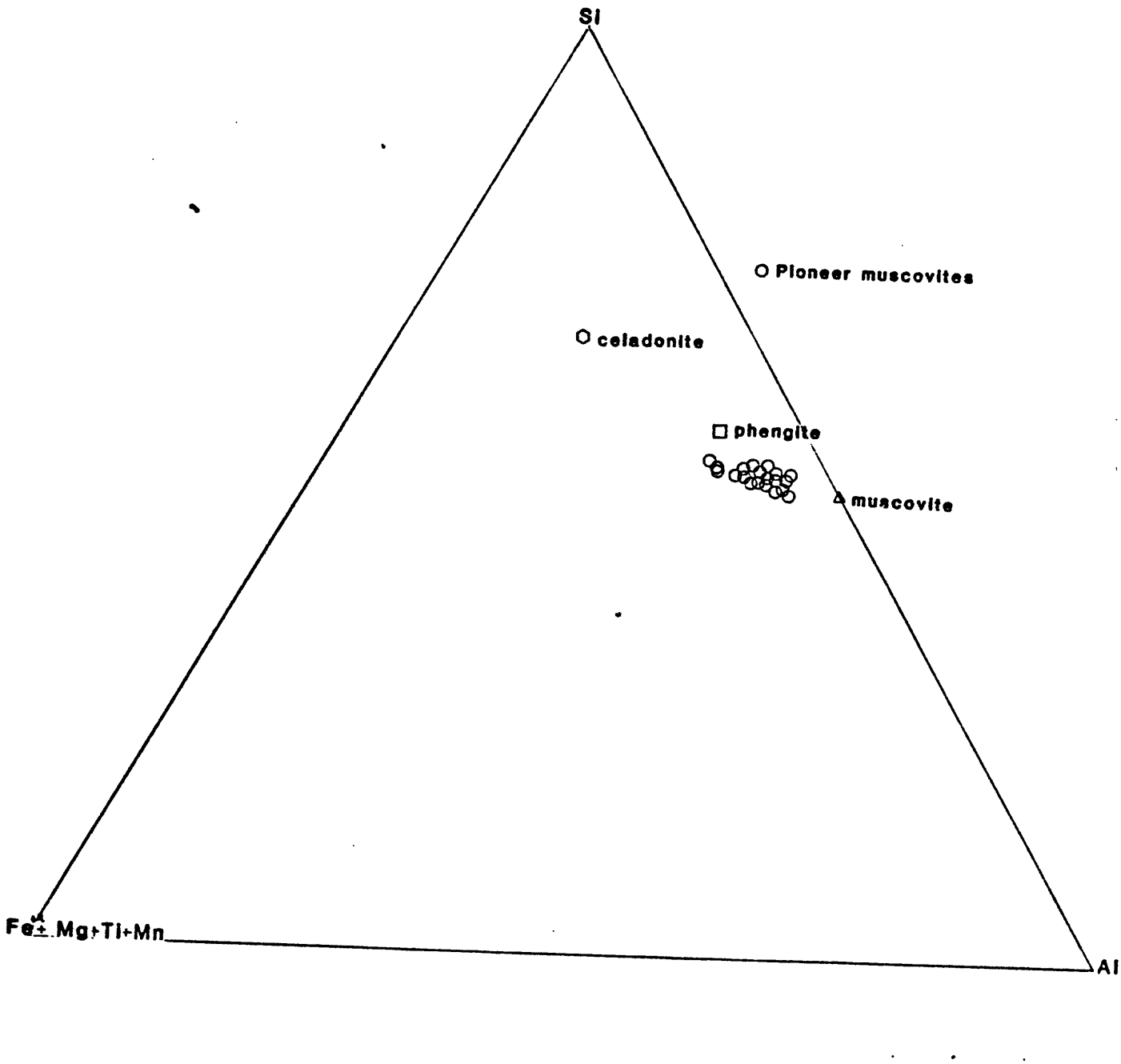

Figure 24. Pioneer muscovite compositions in terms of Si, octahedral Fe^{+2} + Mg + Ti + Mn and total Al.

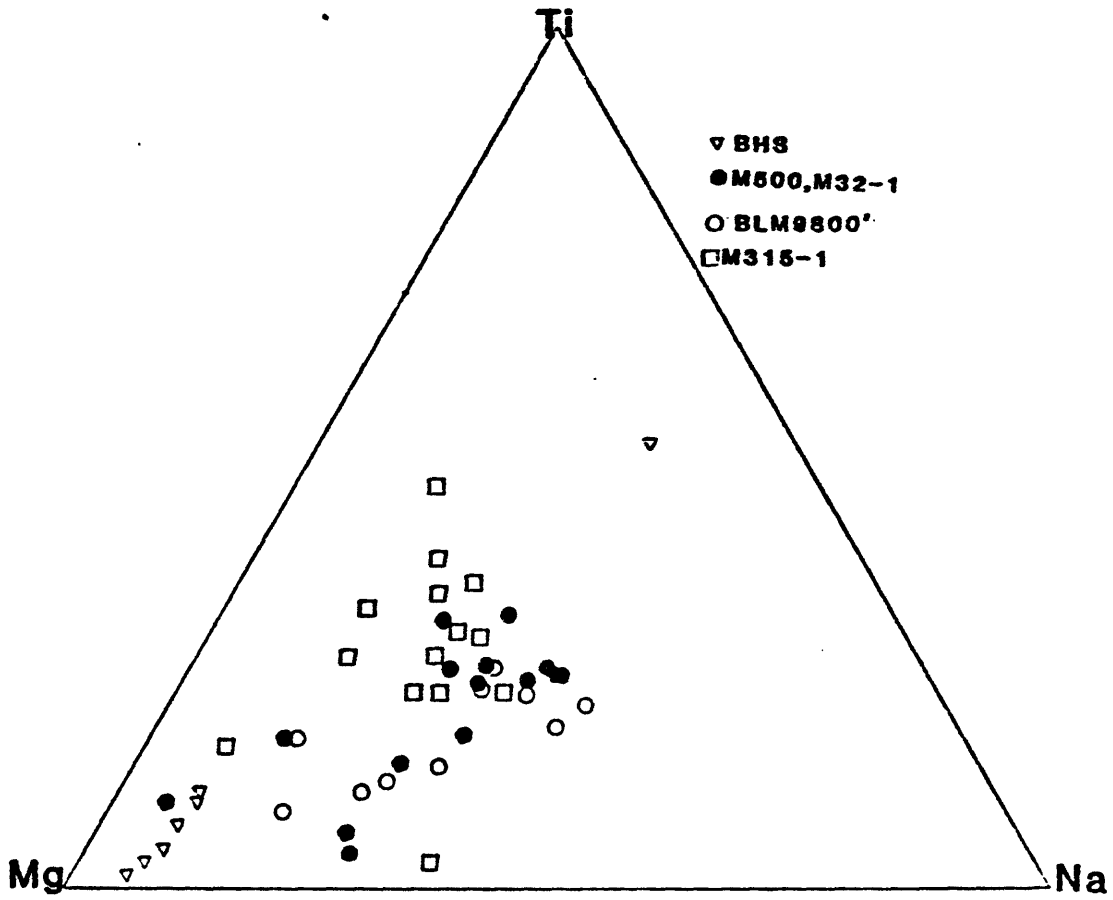

Figure 25. Ternary plot (Ti, Mg, Na) of cations substituting for octahedral Al and for K in Pioneer muscovites.

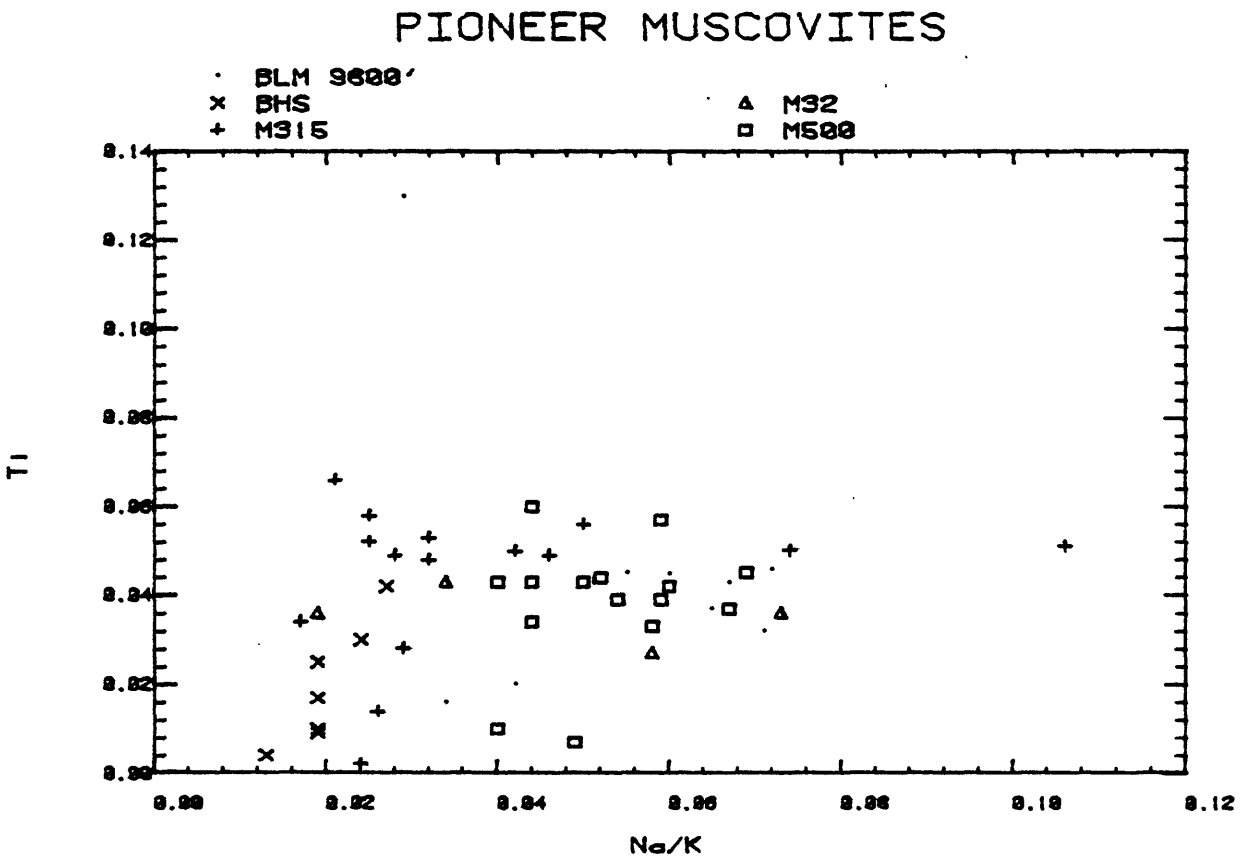

Figure 26. Ti vs. Na/K for Pioneer muscovites. "Secondary" textures are restricted to relatively low Ti and Na/K compositions. "Primary" muscovites are variable in terms of Na/K, but are generally restricted to >0.03 Ti per formula unit.

Feldspars

Feldspar compositions were determined by microprobe analyses of points in thin sections for the following elements: Si,Al,Ca,Na,K, Ba, ± Fe, ± Mg.Cations were calculated on the basis of 8 oxygens. Zoning patterns were established by traversing across individual crystals for a given element in small steps (5-25 microns). Quality of analyses was maintained by accepting only those points which met the following criteria: 1) sum of all oxides = 98-102%, 2) Si + Al = 4.00 ± 0.02, 3) Ca + Na + K + Ba + Fe + Mg = 1.00 ± 0.04 and 4) Al-Σ (cations other than Si, Al x charge) = 0.0 ± 0.07 (Zen, 1981).

Plagioclase

Plagioclase crystallized early in all the rocks of the batholith. Textural variants include 1) large zoned and twinned phenocrysts which often occur in synneusis relations 2) large crystals with prominent oval, mottled cores separated from rims by a band of sericitic alteration 3) small inclusions in biotite and 4) crystals of varying size and degree of resorption in potassium feldspar megacrysts.

Representative analyses are shown in Table XII and the range of compositions for the entire batholith is shown on a plot of An-Ab-Or in Fig 27.

Quartz diorite (sample 313) hosts the most calcic plagioclase (An 79) and exhibits the largest range in composition within individual grains (An 25 -79). Fig. 28 illustrates the range of compositions within each rockand from rock to rock. The most calcic plagioclase for a rock containing potassium feldspar is An 64 (Kpt sample M547-1).

Zoning patterns, such as the one illustrated in Fig. 29, are

Table XII. Representative feldspar compositons.
(P = plagioclase, K = potassium feldspar)

Map Unit	Kpd		Kpt					Kpgr
Sample	M313-1		M547					FG
Feldspar	P	P	P	P	P	P	P	P
SiO_2	49.93	58.68	56.07	53.96	53.24	58.19	66.07	55.67
Al_2O_3	31.17	26.46	27.57	29.87	29.58	25.00	18.38	27.85
CaO	13.00	7.52	8.96	11.35	10.49	6.78	0	9.65
Na_2O	4.09	7.05	6.47	5.47	5.91	7.50	0.82	5.84
K_2O	0.01	0.13	0.23	0.14	0.08	0.20	14.81	0.23
BaO	0	0	0.10	0.05	0.06	0	0.54	0
FeO	0.17	0.15	0.28	0.26	0.25	0.27	n.d.	n.d.
MgO	0.09	0.07	0.05	0.03	0.02	0.05	n.d.	n.d.
Sum	98.46	100.05	99.72	101.12	99.64	97.98	100.62	99.24
Si	2.31	2.62	2.53	2.42	2.42	2.65	3.02	2.52
Al	1.70	1.39	1.47	1.58	1.58	1.34	0.99	1.48
Ca	0.64	0.36	0.43	0.54	0.51	0.33	0	0.47
Na	0.37	0.61	0.56	0.47	0.52	0.66	0.07	0.51
K	0	0.01	0.01	0.01	0	0.01	0.86	0.01
Ba	0	0	0	0	0	0	0.01	0
Fe	0.01	0.01	0.01	0.01	0.01	0.01	-	-
Mg	0.01	0	0	0	0	0	-	-
Sum	5.04	5.00	5.01	5.03	5.04	5.00	4.95	4.99
X	1.02	0.99	1.01	1.03	1.04	1.01	0.94	0.99
Y	0.03	0.03	0.02	0	0.03	0.01	0.04	0.03
Z	4.01	4.01	4.00	4.00	4.00	3.99	4.01	4.00
Comment	core	rim	core	outer rim	inner rim	outer rim		core

Map Unit			Kpg			Tpg		
Sample	Kpgr		BHS			M32-1		
Feldspar	P	P	P	P	K	P	P	K
SiO_2	57.94	64.49	57.55	61.95	64.76	59.02	63.04	65.19
Al_2O_3	26.49	18.30	27.40	24.68	18.64	24.80	21.36	18.19
CaO	8.28	0.07	8.45	5.48	0.03	6.43	4.09	0
Na_2O	6.64	1.62	6.76	8.46	1.38	7.67	8.80	0.47
K_2O	0.19	13.97	0.17	0.22	14.19	0.32	0.65	15.24
BaO	0	0	0.02	0	0.77	0.05	0.15	0.02
FeO	n.d.	n.d.	n.d.	n.d.	n.d.	n.d.	n.d.	n.d.
MgO	n.d.	n.d.	n.d.	n.d.	n.d.	n.d.	n.d.	n.d.
Sum	99.54	98.46	100.34	100.78	99.76	98.29	98.09	99.11
Si	2.60	3.00	2.57	2.73	2.99	2.68	2.85	3.02
Al	1.40	1.00	1.44	1.28	1.01	1.32	1.14	0.99
Ca	0.40	0	0.40	0.26	0	0.31	0.20	0
Na	0.58	0.15	0.58	0.72	0.12	0.67	0.77	0.04
K	0.10	0.83	0.10	0.01	0.84	0.02	0.04	0.90
Ba	0	0	0	0	0.01	0	0	0
Fe	-	-	-	-	-	-	-	-
Mg	-	-	-	-	-	-	-	-
Sum	4.99	4.98	4.99	5.00	4.97	5.00	5.00	4.95
X	0.98	0.98	1.00	0.99	0.97	1.00	1.01	0.94
Y	0.02	0.02	0.04	0.03	0.03	0.01	0.07	0.05
Z	4.00	4.00	4.01	4.01	4.00	4.00	3.99	4.01
Comment	rim		core	rim		core	mid core-rim	

typical. The core of the grain is An-rich realtive to the rim, but the maximum An content is found in the outer core area, which may or may not be separated from the more sodic rim by a band of sericitic alteration. Plagioclases enclosed within potassium feldspars exhibit similar zoning patterns (Fig.30), and often have a very thin albite rim developed at the plagioclase-potassium feldspar contact. A limited number of analyses of plagioclases in biotites reflect the same range of compositions as other plagioclases in the same rock.

Reverse zoning (An increasing outward relative to Ab) in cores followed by normal zoning in rims may be interpreted in terms of changing water pressure in the magma. The effect of an increase in water pressure on the plagioclase liquidus is (at constant temperature) to depress the liquidus and could permit crystallization of a more calcic plagioclase. When the increase in P_{H2O} ceases (saturation), crystallization of increasingly more sodic compositions could continue resulting in a normally zoned rim. Thus, plagioclase cores may have crystallized at depth during a period of conditions of water pressure build-up and rims may represent "normal" zoning with decreasing temperature after the magma was emplaced at higher levels in the crust.

Alternatively, plagioclase cores could represent relict phases inherited from a parent rock or the increase in An from core outwards could represent conditions of superheating at relatively constant pressure.

Microprobe traverses on Pioneer plagioclase show fine-scale oscillatory zoning for Ca and Na with the more dramatic reversely zoned core - normally zoned rim pattern superimposed. This could result from local pressure or diffusion gradients or convection in the magma.

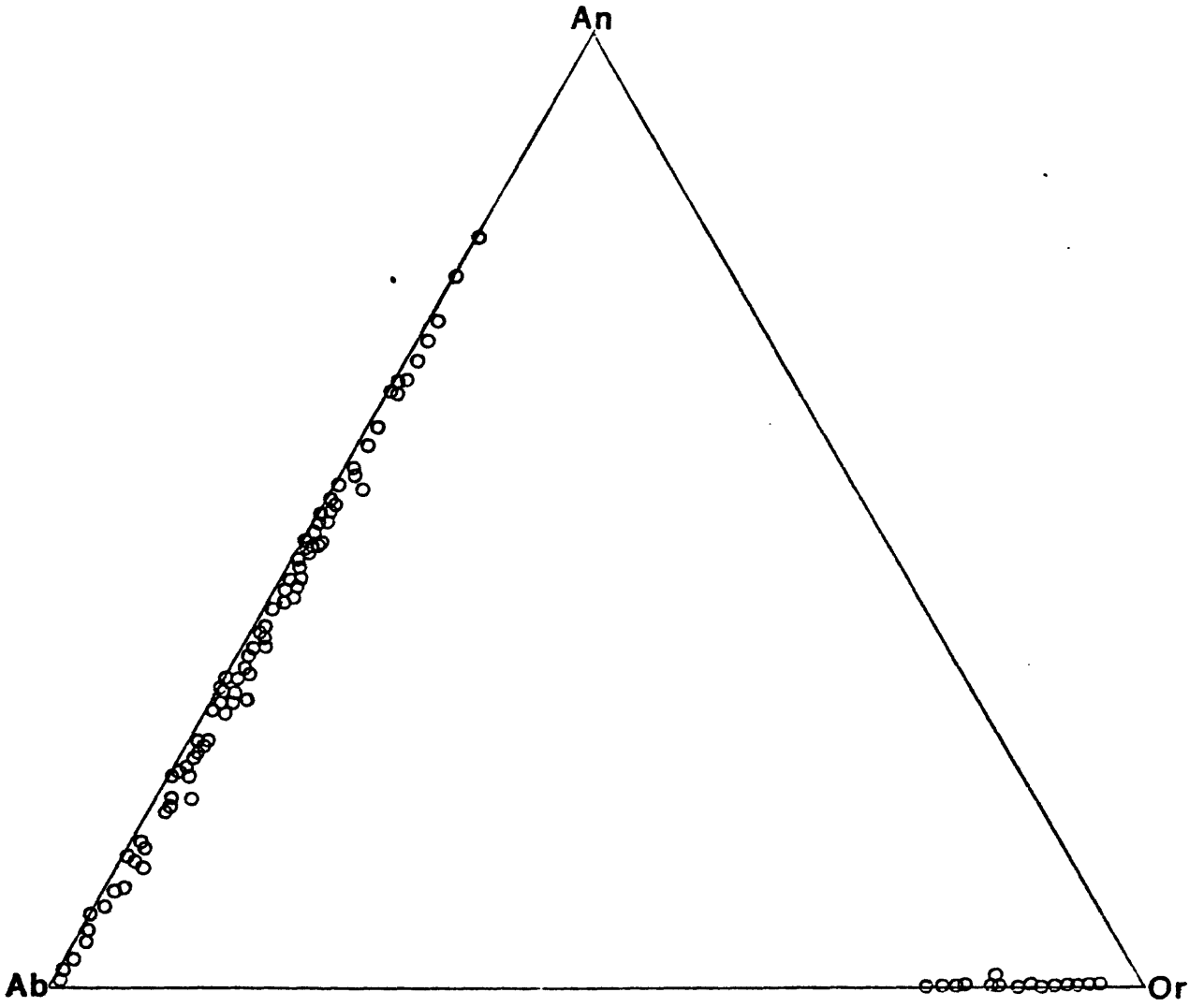

Figure 27. Range of feldspar composition for Pioneer plutonic rocks in terms of albite (Ab), anorthite (An), and orthoclase (Or). Celsian component is included with Or.

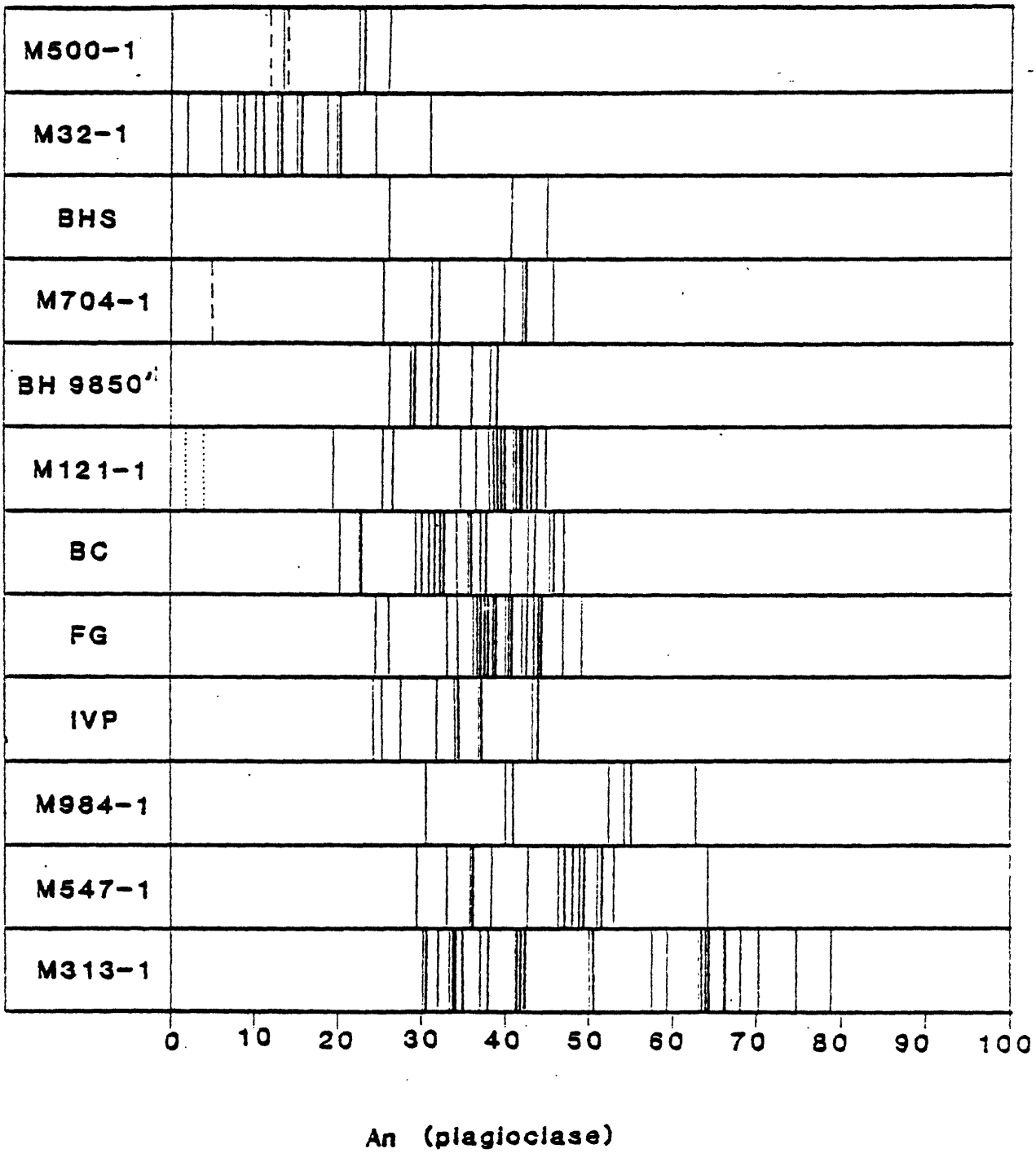

Figure 28. Plagioclase compositions in terms of % An for representative samples of Pioneer rocks. Each line represents a single analysis. Dashed lines refer to exsolved phases in perthitic potassium feldspars.

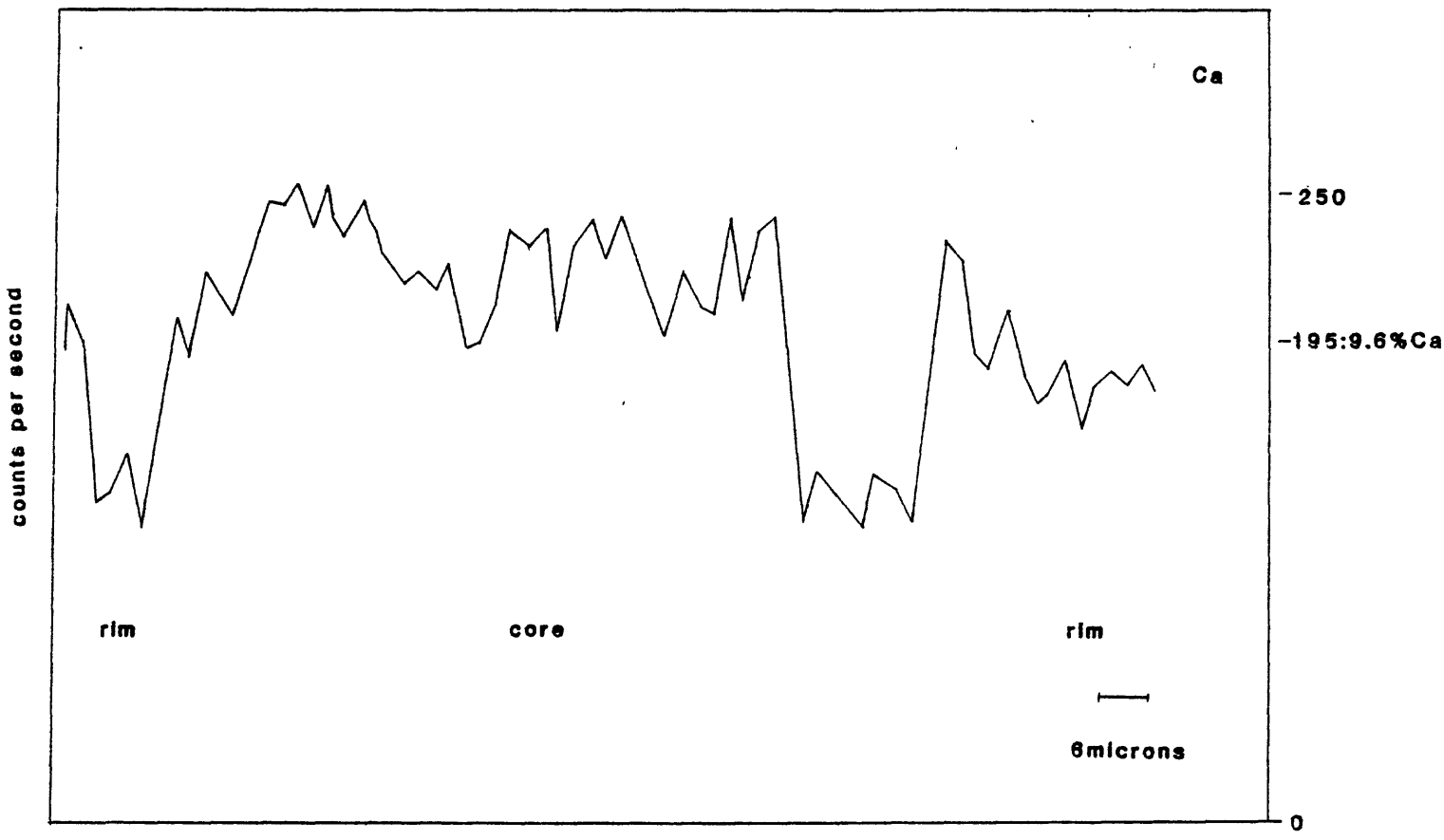

Figure 29. Results of microprobe traverse across a plagioclase crystal in Kpgr sample FG. Ca and Na were counted for 1 second at 5 micron intervals across a crystal from rim through core to opposite rim.

Potassium feldspar

Potassium feldspar occurs as large white phenocrysts in muscovite granite, as pink megacrysts in Cretaceous granite, as large anhedral crystals enclosing all other minerals and filling interstices between grains in granodiorite, and as phenocrysts and small, rounded groundmass constituents in porphyritic granodiorite.

The range of potassium feldspar composition within a given rock and throughout the various plutons of the batholith is illustrated by Fig. 30. Point analyses by microprobe reveal a composition range of Or79 to Or97. BaO varies from 0 to 1.5 weight %, and is generally concentrated in cores. Barium zoning is shown in Fig. 31 for a large anhedral grain in granodiorite near the granite contact. Perthite is not extensively developed in the batholith; coarsest perthites are from the muscovite granites. Petrographic observation of the lack of well-developed perthite is supported by microprobe analyses. Both normal beam (beam diameter approximately 5 microns) and expanded beam (beam diameter 25-30 microns) analyses give comparable results. Traverses across crystals at closely spaced intervals for K,Ba and Na ($\pm$ Ca) reveal 1) extent of perthite development and 2) zoning patterns. Count rates were compared with count rates obtained for the K standard, Benson orthoclase (Stewart and Wright, 1974) and the Na standard, Tiburon albite (Crawford, 1966) during the same session.

Variations in degree of perthite development in three plutons are illustrated by Fig. 32. K and Na were counted for 1 second at 5-micron step intervals across potassium feldspar grains for a distance of 500 microns. In the sample from the tonalite (Kpt_1), decreases in counts

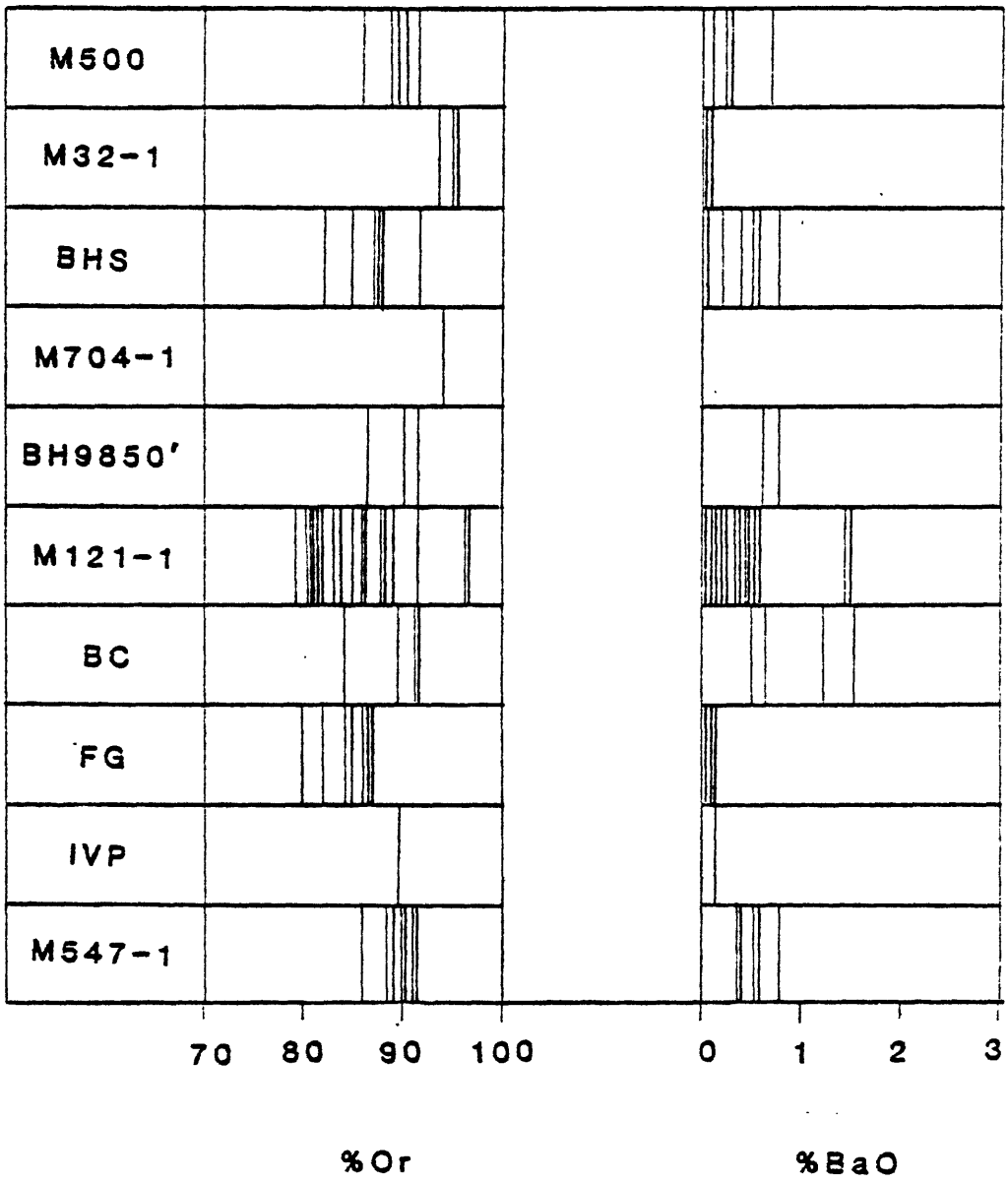

Figure 30. Potassium feldspar compositions in terms of %orthoclase (Or) and weight % BaO. Each line represents a single analysis.

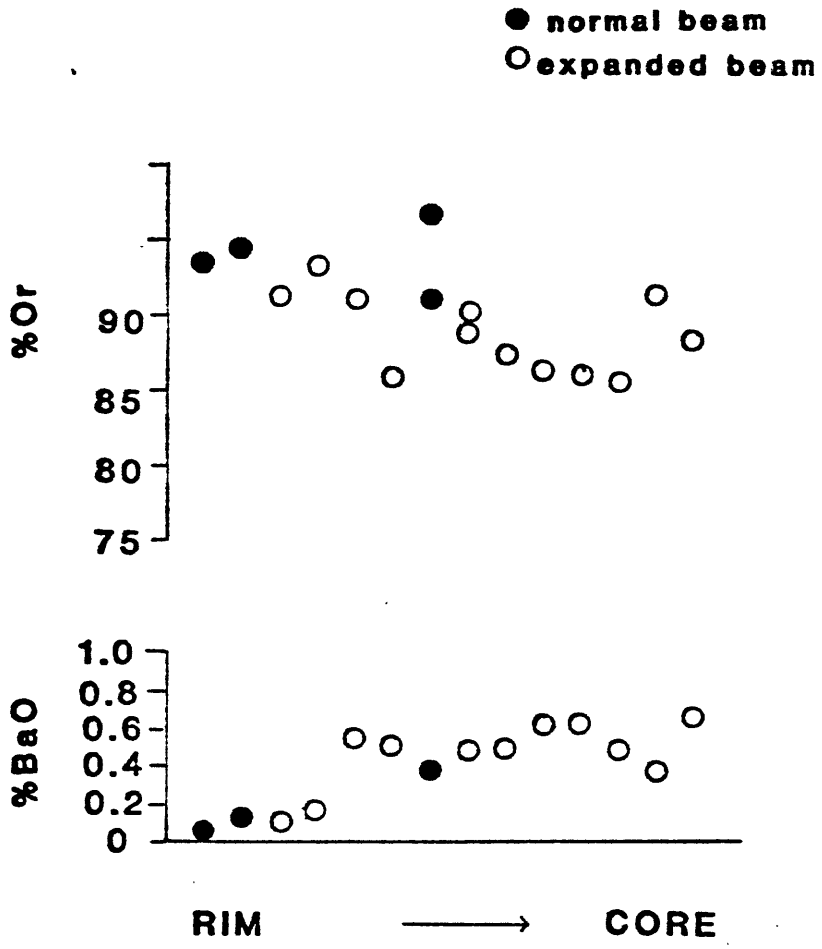

Figure 31. Zoning in potassium feldspar megacryst in granodiorite sample M121-1. Most points were analysed with an expanded beam (about 25-30 microns in diameter). Four points were analysed with a normal beam (5-10 microns in diameter).

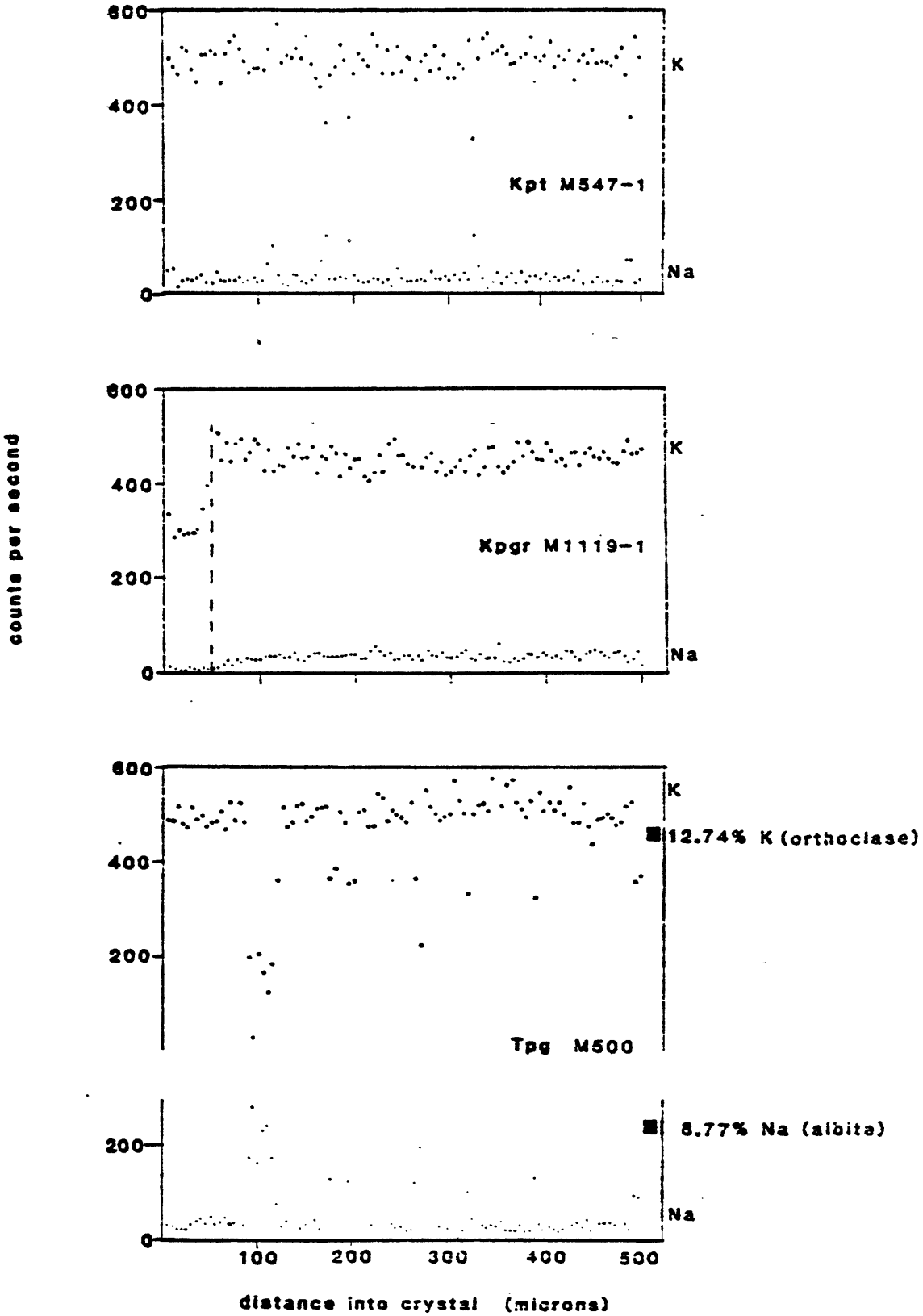

Figure 32. Microprobe traverses across potassium feldspar grains. K and Na were counted for 1 second in 100 5-micron steps across each crystal. Reference count rates are given for standard albite and orthoclase.

for K correspond to increases in Na counts. Exsolved lamellae are narrow (<20 microns across) and are considerably less sodic than pure albite. No evidence of two discrete phases is obvious in the traverse from Cretaceous granite. The muscovite granite traverse shows patches of as wide as 40 microns of distinctly albitic compositions.

For two perpendicular 500-micron long traverses across a perthitic potassium feldspar in sample M500-1 (muscovite granite), distinctly potassic (>Or 50) compositions were observed for 82 and 63% of the spots analysed.

Determination of bulk composition of perthitic potassium feldspar is a problem. Various techniques are cited in the literature, such as atomic absorption analysis of single crystals for Na, Ca and K , x-ray fluorescence analysis of powders, sanidinization, and expanded beam microprobe analysis.

Spectrophotometric techniques were deemed unsuitable for analysis of bulk potassium feldspar compositions in Pioneer rocks because the potassium feldspars contain inclusions of other minerals, notably plagioclase, which would be included in the analysis. Ca-rich areas can be avoided in microprobe analysis by observing analysed areas optically and by monitoring Ca count rates. Whitney and Stormer (1976) successfully used a defocused electron beam (diameter ~ 30 microns) to obtain bulk compositions of microperthite. Wones (1980) described a technique for homogenizing perthites from the Lucerne pluton by heating samples which had been crushed and pelletized at 950°C for several days. X-ray diffraction techniques described by Wright and Stewart (1968) were then used to obtain composition of the sanidinized material.

Wones pointed out that plagioclase was not homogenized into the alkali feldspar at 950°C.

Alkali feldspar separates were obtained for two of the most perthitic rocks, typical muscovite granite and typical Cretaceous granite. The feldspar was lightly ground, placed in silver-palladium foil envelopes, and heated in air at 930°C for 114 hours. X-ray patterns were taken before and immediately after heating. For both samples, the 22° peak disappeared and the 28° peak diminished greatly as a result of heating. This suggests that these peaks represent an albite phase homogenized into the potassium-rich feldspar as a result of heating; a calcic feldspar would not be expected to homogenize at such a low temperature.

Wright and Stewart (1968) defined "anomalous" feldspars and Stewart and Wright (1974) elaborated on the concept and established criteria for identifying anomalous feldspars on the basis of x-ray data. The term "anomalous" refers to cell dimensions. Anomalous feldspars are common in nature and indicate strain associated with incipient exsolution in perthites. The 201 peak, which is roughly linearly proportional to the a cell dimension cannot be used to estimate composition for anomalous feldspars because it is largely a function of the Na content of the feldspar, and for strained feldspars gives impossible compositions. An indication of the degree to which a given feldspar is strained can be ascertained by comparing the 201 peak position read off a plot of 060 and $\bar{2}04$ (Wright, 1968) with the actual measured value of $\bar{2}01$. If the difference between the measured and observed value exceeds 0.12 °2 θ the feldspar is termed "anomalous".

The feldspar from the Cretaceous granite appeared anomalous both before and after heating. The feldspar from the muscovite granite was slightly anomalous, but within the limit of +0.12°2θ. Fig. 33 shows the effects of heating. Peak shifts on heating indicate that the composition changed from Or87 to Or82. The feldspar also moved towards a more disordered structural state. Agreement between the potassium feldspar composition determined by x-ray before heating (Or 87) and the composition determined by microprobe on a thin section of the same rock (Or 86-92) is good. The change of only 5% Or produced by heating may reflect 1) the reequilibrated composition of the feldspar or 2) lack of homogenization on heating. It was concluded that microprobe data provides an estimate of the bulk composition of the alkali feldspars.

X-ray diffraction patterns were obtained for Pioneer feldspars following the procedures outlined by Wright and Stewart (1968) to a) check structural state and b) compare compositions obtained by x-ray data against microprobe data.

Wright (1968) showed that the $\bar{2}01$, 060 and $\bar{2}04$ peaks for natural and synthetic alkali feldspars can by linearly related to the a, b and c cell parameters. Peaks were indexed according to tables found in Wright and Stewart (1968) and checked for the following points:

1) presence of $\bar{2}01$ for an albite phase
2) shape and peak position of $\bar{2}01$ for a potassic phase
3) splitting of 131 indicative of a triclinic versus a monoclinc phase
4) peak positions of $\bar{2}01$, 060 and $\bar{2}04$ for a potassic phase

Data for Pioneer feldspars are summarized in Fig. 34, which is a

plot of 060 versus $\bar{2}04$ peak positions in terms of 2 θ Cu K α after Wright (1968, p.92). Comparison with Or-rich feldspars of known structural state indicates that Pioneer feldspars fall between the orthoclase and maximum microcline series. Although the $\bar{2}01$ and 060 are generally sharp, indexing of the 204 peak is often ambiguous due to the presence of more than one peak (often 2 or 3) in the range 2 θ =50.6 to 50.9° 2- θ . Wright stated that ambiguous $\bar{2}04$ reflections are commonly observed for orthoclases with anomalous cell dimensions (see below) and presented a plot of two other peaks, 113 and 002, which can be used as aids in determining which of several peaks is actually $\bar{2}04$. In some cases, the 113 region showed multiple peaks and the $\bar{2}04$ could not be identified with any certainty. No cell refinements were obtained to resolve this problem.

In all but one case the 131 reflection occurs as a single, usually sharp peak indicating the presence of a monoclinic feldspar. One sample, a megacryst plucked from a sample of muscovite granite showed the 131-$1\bar{3}1$ split characteristic of a triclinic feldspar and on the 060-$\bar{2}04$ plot, this feldspar falls quite close to the maximum microcline series.

In most patterns, weak peaks were observed at about 22° and 28° 2 θ, suggesting the presence of either exsolved albite or plagioclase impurity in the sample.

Tilling (1968) was able to map areas of the Rader Creek pluton on the basis of variations in the structural state of alkali feldspar. Parsons and Boyd (1971) investigated the distribution of microcline and orthoclase in a variety of intrusive sequences and found that the frequency of occurrence of microcline increases relative to orthoclase as fractional crystallization proceeds in many cases. They proposed

that features present at the time of crystallization dictate the course of ordering in alkali feldspar with cooling and can affect the metastable preservation of the orthoclase at low temperatures. Water and peralkalinity, both of which concentrate with increasing degree of fractional crystallization, were cited as factors which tend to promote transition to microcline, whereas peraluminous composition was cited as a factor which can inhibit the orthoclase-microcline transition. The peraluminous nature of the Cretaceous and Tertiary granites in the Pioneer rocks may be a contributing factor in the persistence of the orthoclase structural state.

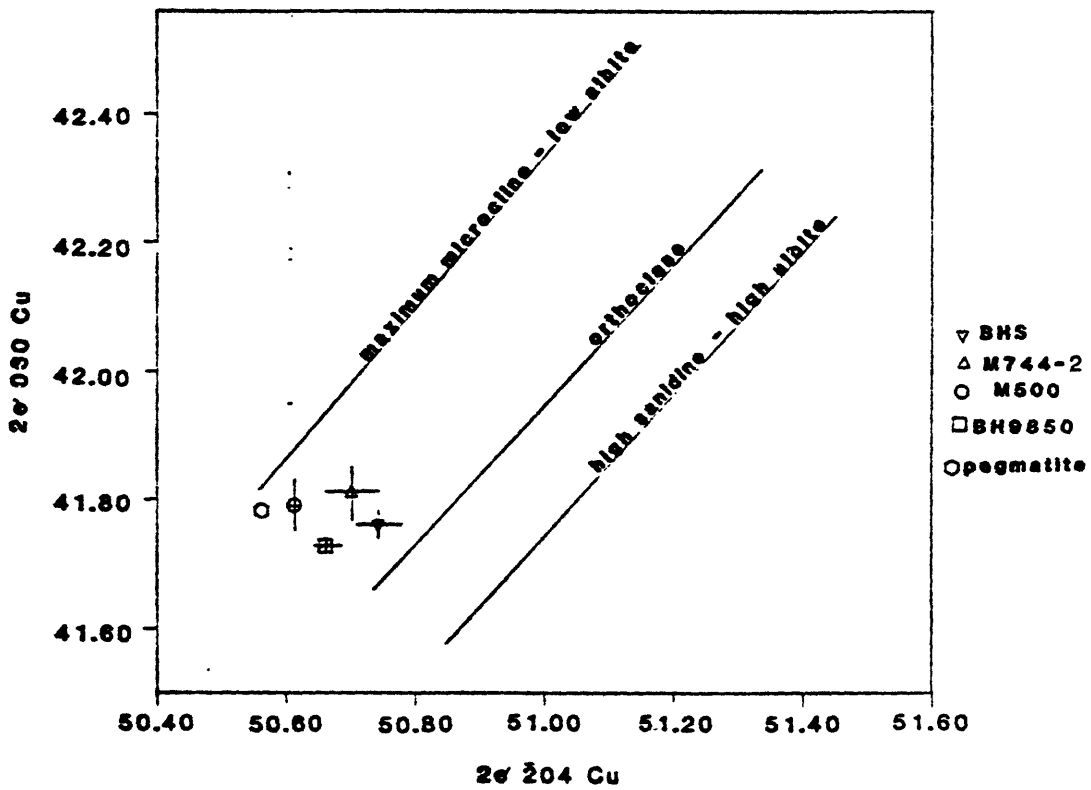

Figure 33. Structural state of potassium feldspars in Pioneer rocks as determined by x-ray diffraction using Wright's (1968) 3-peak method.

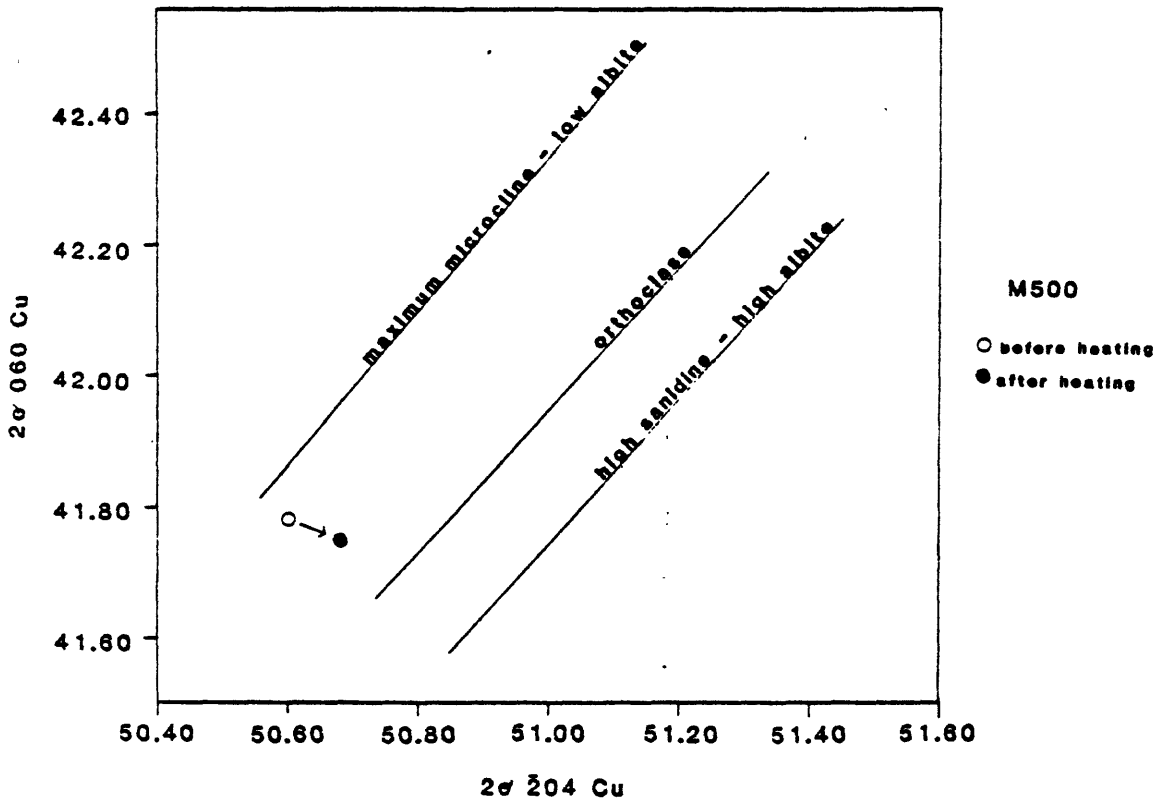

Figure 34. Effect of heating a potassium feldspar separate from Tpg sample M500-2 for 114 hours at 930 C.

Sphene

Euhedral rhombs, small granular anhedra of sphene in mafic silicates, and narrow rims of sphene between biotite and magnetite are ubiquitous in the Cretaceous plutons, rare in Paleocene rocks. Sphenes in seven rocks were analysed to ascertain range of composition and to look for compositional differences between the different textural varieties of sphene. Representative sphene analyses are cited in Table XIII.

Most sphenes are uniform in composition with Fe and Al substituting for about 10% of the Ti. Ribbe (1980) stated that the most common coupled substitution observed for natural sphenes involves Al or Fe^{+3} + Ti and OH or F for O_1^{2-}, where O_1 refers to the underbonded apical oxygen atom in the sphene structure; the substituents Al + Fe^{+3} may account for as much as 30% of the octahedral site. Fluorine is low (0.6 wt% maximum). Oxide sums are generally low, probably resulting from the presence of H_2O, REE. Iron was treated as Fe_2O_3, based on the findings of Higgins and Ribbe (1976), who presented chemical data on a variety of natural sphenes. They found low sums (by microprobe) in some cases and found that by annealing partly metamict sphenes weight per cents for all elements analysed by microprobe increased to give improved sums (95 before heating, closer to 100% after heating). This experiment was not attempted on the Pioneer sphenes, but might improve the low sums although x-ray patterns indicate sharp peaks rather than broadened peaks which would be expected if sphene was metamict.

In the Willow Creek granodiorite sample, a sphene in chlorite had higher Al, Ca, Si and lower Ti than euhedral sphene. Similarly, sphene

in epidote in M1119-1 (Cretaceous granite) showed the same enrichment in Al and Si relative to other sphenes in the rock. These high Al-sphenes are similar to other sphenes in the rock, although Fe^{+3}/Fe^{+2} ratios may be different.

Qualitative observation of sphene spectra by energy dispersive (EDS) analysis suggests that Ce and REE may be significant in euhedral sphenes. Anhedral sphenes in mafic silicates have higher oxide sums, higher Ca contents than euhedral sphenes and EDS spectra do now show peaks in the REE region; REE substitution for Ca in magmatic sphene may prove a useful discriminant, on further, quantitative study.

Table XIII. Sphene analyses

Map Unit	Kpt			Kpgr						
Sample	M547-1			FG					a	
SiO_2	30.67	31.14	30.60	30.78	29.93	30.48	30.13	29.98	31.05	30.11
Al_2O_3	1.48	1.59	1.69	1.11	1.66	1.53	1.32	1.05	1.23	1.51
*Fe_2O_3	1.78	1.26	1.81	1.53	1.83	1.75	1.84	1.85	1.90	1.90
MgO	0	0.01	0	0	0	0	0	0	0	0
CaO	27.54	28.99	27.43	26.92	26.31	26.45	26.76	26.47	28.25	26.85
Na_2O	0.03	0	0.01	0.03	0.03	-	-	-	-	-
K_2O	-	-	-	-	-	-	-	-	-	-
TiO_2	34.94	35.85	34.41	35.69	34.06	33.54	34.26	34.71	35.95	34.09
MnO	0.13	0.12	0.12	0.10	0.10	0.05	0.10	0.09	0.19	0.08
F	0.20	0.30	0.25	0.32	0.20	0.20	0.27	0.06	0	0
Σ	96.77	99.26	96.32	96.48	94.12	94.00	94.68	94.21	98.57	94.54
O=F	0.08	0.13	0.11	0.13	0.08	0.08	0.11	0.03		
Σ	96.69	99.13	96.21	96.35	94.04	93.92	94.57	94.18	98.57	94.54
Si	4.14	4.11	4.15	4.16	4.15	4.22	4.16	4.15	4.11	4.15
Al	0.24	0.25	0.27	0.18	0.27	0.25	0.21	0.17	0.19	0.25
Fe^{+3}	0.18	0.13	0.18	0.16	0.19	0.18	0.19	0.19	0.19	0.20
Ti	3.55	3.56	3.51	3.63	3.55	3.49	3.55	3.61	3.58	3.53
Ca	3.98	4.10	3.99	3.90	3.90	3.92	3.96	3.92	4.01	3.96
Mg	0	0	0	0	0	0	0	0	0	0
Na	0.01	0	0	0.01	0.01	0	0	0	0	0
K	0	0	0	0	0	0	0	0	0	0
Mn	0.01	0.01	0.01	0.01	0.01	0.01	0.01	0.01	0.02	0.01
F	0.09	0.18	0.11	0.14	0.09	0.09	0.12	0.03	0	0
#pts	3	1	2	3	3	3	3	3	3	3

Map Unit	Kpgr					Kpg			
Sample	M881-1			WC		M1293-1		b	c
SiO_2	30.60	30.63	30.97	31.22	29.78	31.82	29.77	29.31	31.79
Al_2O_3	1.50	1.30	1.46	4.23	1.34	1.57	1.57	1.37	2.76
*Fe_2O_3	1.10	1.94	2.59	2.08	1.64	1.24	1.93	1.64	1.11
MgO	0	0.04	0	0.06	0.02	0.04	0	0.14	0.16
CaO	27.51	28.80	28.91	30.88	29.28	26.85	28.04	26.65	27.43
Na_2O	-	-	-	0	0	0.05	0.18	0.03	0.01
K_2O	-	-	-	0.03	0.08	0.20	0.01	0.03	0.11
TiO_2	35.37	36.33	35.59	31.74	34.87	34.51	36.26	35.22	33.48
MnO	0.11	0.17	0.14	0.07	0	0	0.01	0.22	0
F	0.13	0.62	0.45	-	-	0.33	-	-	0.55
Σ	96.32	99.83	100.11	100.31	97.01	96.61	97.77	94.61	97.40
O=F	0.05	0.26	0.19			0.14			0.23
Σ	96.27	99.57	99.92	100.31	97.01	96.47	97.77	94.61	97.17
Si	4.14	4.04	4.07	4.07	4.03	4.28	3.99	4.05	4.24
Al	0.24	0.20	0.23	0.65	0.21	0.25	0.25	0.22	0.43
Fe^{+3}	0.11	0.19	0.26	0.20	0.17	0.13	0.19	0.17	0.11
Ti	3.60	3.61	3.52	3.11	3.55	3.49	3.65	3.66	3.36
Ca	3.99	4.08	4.07	4.32	4.25	3.87	4.03	3.94	3.92
Mg	0	0.01	0	0.01	0	0.01	0.05	0.03	0.03
Na	0	0	0	0	0	0.01	0	0.01	0
K	0	0	0	0	0.01	0.03	0	0.01	0.02
Mn	0.01	0.02	0.02	0.01	0	0	0	0.03	0
F	0.06	0.26	0.19	0	0	0.14	0	0	0.23
#pts	3	3	3			2		3	

*FeO measured by microprobe x 1.111 = Fe_2O_3
a = rim at biotite-magnetite contact; b = in biotite; c = in epidote

Iron oxide and iron titanium oxide minerals

Magnetite occurs in all of the rocks of the batholith. Cretaceous rocks are characterized by magnetite and sphene, with ilmenite absent. The magnetite is close to end-member magnetite in composition, with < 0.5 wt% MnO, TiO and MgO (Table XIV). Highly reflective bright white lamella were observed in some magnetite grains in granodiorite. This phase appears to be hematite and microprobe analyses indicate about 3% less FeO (total iron as FeO), as compared to host magnetite. Occasionally, tiny grains of pyrite are observed with magnetite.

Paleocene muscovite granites host a more complex oxide mineral assemblage. Within and adjacent to muscovite-biotite clusters, two phases are observed. One phase is a titanohematite (13-17% TiO_2, ~ 2% MnO); the other is an extremely Mn-rich ilmenite. Intergrowths of these two phases were not observed in thin section, but were seen in polished mounts of heavy mineral separates from the same rock. Low sums in microprobe of these phases may result from determination of iron as FeO and/or presence of elements not analyzed, such as Zn or Nb. Recalculation of all iron as Fe_2O_3 yields reasonable iron sums for these phases, suggesting that observed composition reflects an oxidized assemblage. In microprobe analysis on polished thin section, only apparently single phase grains were detected. However, analysis on a few grains obtained by heavy mineral separation (which showed exsolution textures) revealed the presence of both phases in a single grain. Pure magnetite similar to magnetite in the Cretaceous rocks occurs as larger blocky grains not associated with muscovite.

Table XIV. Iron oxide and iron titanium oxide mineral compositions. M = magnetite, H = hematite, I = ilmenite

Map Unit			Kpgr	Kpgr	
Sample	M313-1	M708-1	MC	FG	
	M	M	M	M	H
SiO_2	n.d.	0.17	0.18	n.d.	n.d.
Al_2O_3	0.09	0.23	0.38	0.11	0.37
FeO	91.97	92.58	91.88	91.70	89.67
MgO	0	0.01	0.01	0	0.02
CaO	0.08	0	0.02	0.16	0.17
TiO_2	0	0.06	0.12	0.10	0.20
MnO	0.14	0.48	0.06	0.11	0.10
Cr_2O_3	0.07	0	0.12	0	0
Sum	92.36	93.53		92.18	90.52
FeO	30.35	30.55	30.32		29.99
Fe_2O_3	68.40	68.85	68.3	68.20	99.53
Sum	99.13	100.35	99.54	98.94	100.39

Map Unit	Kpg		Tpg		
Sample	M744-2	M1119-1	M500		
	M	M	I(?)	H	M
SiO_2	n.d.	n.d.	n.d.	n.d.	n.d.
Al_2O_3	0.12	0.17	0.03	0.06	0.40
FeO	90.89	90.78	39.71	76.49	90.28
MgO	0	0.13	0	0.04	0
CaO	0.08	0	0	0	0.14
TiO_2	0	0	43.34	13.10	0.07
MnO	0.51	0.13	11.68	1.50	0.51
Cr_2O_3	0	0.17	0.01	0.01	0.03
Sum	91.61	91.29	94.77	91.20	91.44
FeO	29.99	27.23			29.79
Fe_2O_3	67.59	70.60	44.08	84.98	67.14
Sum	98.29	98.34	99.14	99.69	98.08

Preferential concentration of Mn in the ilmenite phase is consistent with the findings of Czamanske and Mihalik (1972) in their study of the opaque oxides at Finnmarka (1972), where up to 30 wt% MnO in ilmenite was reported.

Estimation of intensive parameters during crystallization

Field evidence

Zen and others (1980) cited three lines of evidence which suggest that Pioneer plutons were emplaced at shallow levels in the upper crust (P<1 kbar). First, miarolitic cavities and pegmatites are associated with Cretaceous granodiorite. Second, stratigraphic reconstruction by Zen suggests 3 km of overburden around the time of emplacement. Third, a narrow cordierite-andalusite (i.e., low pressure, high temperature) contact assemblage occurs. All of these features plus the discordant nature of contacts, absence of regional metamorphism and absence of pervasive lineations (Snee, 1978) are in accord with Buddington's (1959) criteria for epizonal (<6 km) emplacement.

Chemical evidence

Comparison of normative whole rock geochemical trends with experimental work in granite systems to estimate pressure is a common practice in the petrologic literature. As Barker and others (1975) demonstrated, comparison "of a residual melt in equilibrium with an igneous gas phase, quartz and alkali feldspar can be used to estimate pressure and temperature using the data of Tuttle and Bowen(1958)". Tuttle and Bowen investigated the system SiO_2-$NaAlSi_3O_8$-$KAlSi_3O_8$ at 0.5 to 5 kbar for the case where $P_{H2O}=P_{total}$; Luth (1969) studied the system under anhydrous conditions; James and Hamilton (1969) examined the effect of adding an anorthite component on the minimum in the system. Normative Q-Ab-Or contents for Pioneer rocks are plotted together with the ternary minima determined experimentally in Fig. 35. In order to compare the normative geochemical data with the experimental data, one must establish

that the rock composition in fact represents a residual melt and was saturated with a gas phase (for $P_{H2O}=P_{total}$). The presence of two magmas indicated by the initial strontium data complicates the interpretation of any rock as a representative residual melt. Aplites or late quartz porphyries neither of which were analysed in this study are likely candidates. The pink hematite coloring potassium feldspar in Cretaceous granites, incipient alteration of ferromagnesian minerals to chlorite, and sericitization of feldspars as well as the presence of miarolites (implying a probably maximum P_{H2O} <3 kbar) in Cretaceous rocks and pegmatites suggest that a water-rich phase existed at some stage in the history of the more siliceous rocks. Fluid inclusions in plutonic rocks are too small and limited in occurrence to reveal any information on magmatic fluids; quartz in pegmatites may prove more useful.

P_{H2O} and P_{total} are distinct variables; the presence of a hydrous mineral in a rock implies only that H_2O was a magma component, but the magma need not have been H_2O saturated for hydrous minerals to crystallize. The disposition of points for Pioneer rocks on the Q-Ab-Or plot is not readily interpreted in light of experimental data due to 1) paucity of analysed samples, 2) high normative anorthite component, and 3) spread of points within a given map unit.

On Fig. 35, Pioneer rocks with >80% normative Q+Ab+Or are shown as solid circles, those with <80% Q+Ab+Or are shown as open circles. The Pioneer rocks display no clustering by map unit. Both Cretaceous and Paleocene granites plot near the 0.5-1.0 kbar water-saturated minima. Considering only the 4 points representing muscovite-bearing

granites, the two quartz-poor points are from the dated (Paleocene) plutons; the other two Tpg points represent 2 samples from another, as yet undated pluton. The undated pluton carries muscovite, but it is not as likely a candidate for "primary" muscovite on textural grounds as some of the muscovite in the dated plutons.

Quartz is observed within potassium feldspar in the two Kpg rocks which fall within the 80% field, near or slightly above the 500 bar $P_{H2O}=P_T$ contour. The effect of an An component was shown to move the minima towards the Q-Or join (James and Hamilton); none of the Pioneer rocks plot near the appropriate (in terms of An content) experimentally derived 1 kbar minimum.

Czamanske and others (1981) found a similar situation for rocks in a Cretaceous-Paleocene Batholith in southwestern Japan and suggested that combined effects of increasing P_{total} which shifts to minima away from quartz (Luth, 1969) increasing P_{H2O} which moves the minima toward Ab (Luth and others, 1964) and increasing An content which moves the minima away from Ab (James and Hamilton, 1969) obscure relations in the vicinity of the minima at low pressures.

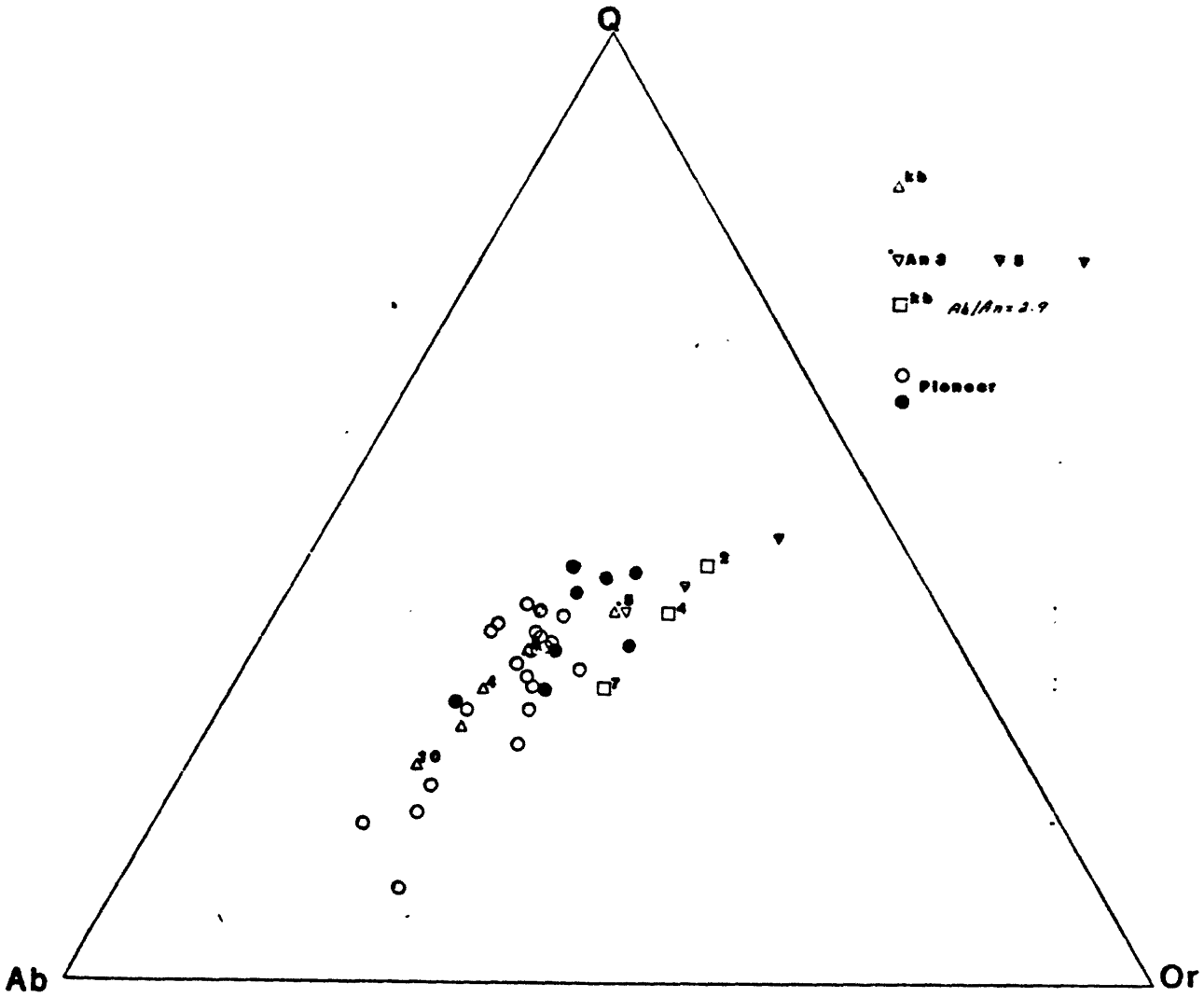

Figure 35. Normative quartz (Q)-albite (Ab)-orthoclase (Or) plot for Pioneer rocks and experimentally determined ternary minima in the granite system.
open circles = Pioneer rocks with <80% normative Q+Ab+Or
closed circles = Pioneer rocks with >80% normative Q+Ab+Or

triangles = ternary minima for 0.5 to 10 kbar P_{H2O} after Tuttle and Bowen, 1958

inverted triangles = projected ternary minima for P_{H2O}=1kbar for compositions with An3, 5, and 7 after James and Hamilton, 1969

squares = projected ternary minima at 2, 4, and 7 kbar for compositions with Ab/An = 2.9 after Luth and others, 1964

Mafic silicates as indicators of T and f_{O2}

Variations in amphibole and biotite compositions reflect bulk composition, mineral assemblage, changes in temperature, pressure, and oxygen fugacity (or other gases) during crystallization and/or subsolidus reequilibration.

Variation in mafic silicate compositions with bulk composition and mineral assemblage is demonstrated in Fig. 36, where molecular Fe/Fe+Mg ratios and weight per cent SiO_2 from whole rock analyses are plotted against average cation ratios from microprobe data on minerals. Correlations between rock and mineral compositions are poor, suggesting that factors other than bulk composition and mineral assemblage control phase chemistry. As previously discussed, biotite compositions do reflect mineral assemblage to the extent that the most Al-rich and Fe-rich biotites occur in the muscovite granites, which have the lowest bulk rock Al_2O_3 contents of the batholith.

Czamanske, Wones and Eichelberger (1977) and Anderson (1980) stressed the importance of establishing the equilibrium relations between mineral pairs as a prerequisite to use of mineral chemistry to estimate intensive parameters during crystallization. Element partitioning between amphibole and biotite is commonly used as a test for phase equilibration (for example, see Moxham, 1965; Greenland and others, 1968; Czamanske and others, 1977; Anderson, 1980). Czamanske and others (1977) proposed that a plot of $Fe/\sum M_1\text{-}M_2$ for biotite versus $Fe/\sum M_1\text{-}M_3$ for hornblende provides a more appropriate test for equilibration between the two minerals than Fe/Mg plots due to crystal-chemical differences between the two minerals. Hewitt and Wones (1972) explained

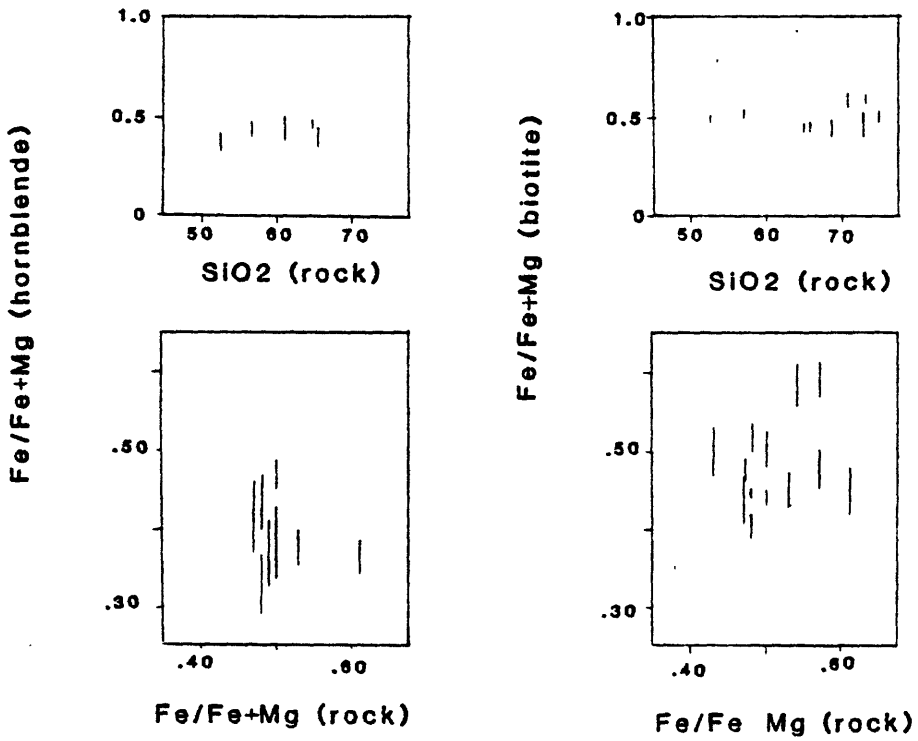

Figure 36. Biotite and hornblende compositional trends in terms of Fe/Fe + Mg as functions of a) whole rock SiO_2 and b) whole rock molecular Fe/Fe+Mg. These plots indicate that mafic silicate compositions are not simply functions of bulk composition.

the positive correlation between Fe and Al^{vi} in biotites in terms of mica crystal chemistry - Fe substitution for Mg in octahedral sites compensates for Al substitution for Si in tetrahedral sites to allow a fit between tetrahedral and octahedal layers. Thus, Fe/Mg is related to Al substitution. Due to the heterogeneity of Pioneer amphiboles, the range of compositions for biotites and hornblendes is plotted (Fig.37) rather than a rock average.

Greenland, Gottfried and Tilling (1968) examined Mn distribution between coexisting biotites and hornblendes in plutonic rocks and found that Kd, defined as $Mn_{hornblende}/Mn_{biotite}$, varied from 1.0 to 2.2. Average microprobe analyses for Pioneer rocks indicate that K_d ranges from 1.02 to 2.08. Greenland et al reported a median K_d of 1.45 for the Boulder and Sierra Nevada Batholiths, 1.75 for the Southern California Batholith and proposed a correlation between Kd and sphene content of the batholith. Both the Sierra Nevada and Boulder batholiths characterized by relatively low K_d's for Mn are sphene-rich whereas the Southern California batholith has a higher K_d for Mn and lacks sphene.

Ti generally decreases in both biotite and amphibole as the Pioneer rocks become increasingly more leucocratic; an exception to this is the biotite in the quartz diorite which has Ti, Fe/Mg typical of the nearby granite and probably represents a reequilibrated composition caused by heating during emplacement of the granite.

Wones and Eugster (1965) studied the stability of biotite and demonstrated that the composition of biotite coexisting with potassium feldspar, magnetite, quartz and magma varies as a function of T, PH_2O, P_{total} and f_{O2}. They proposed that biotite composition provides a

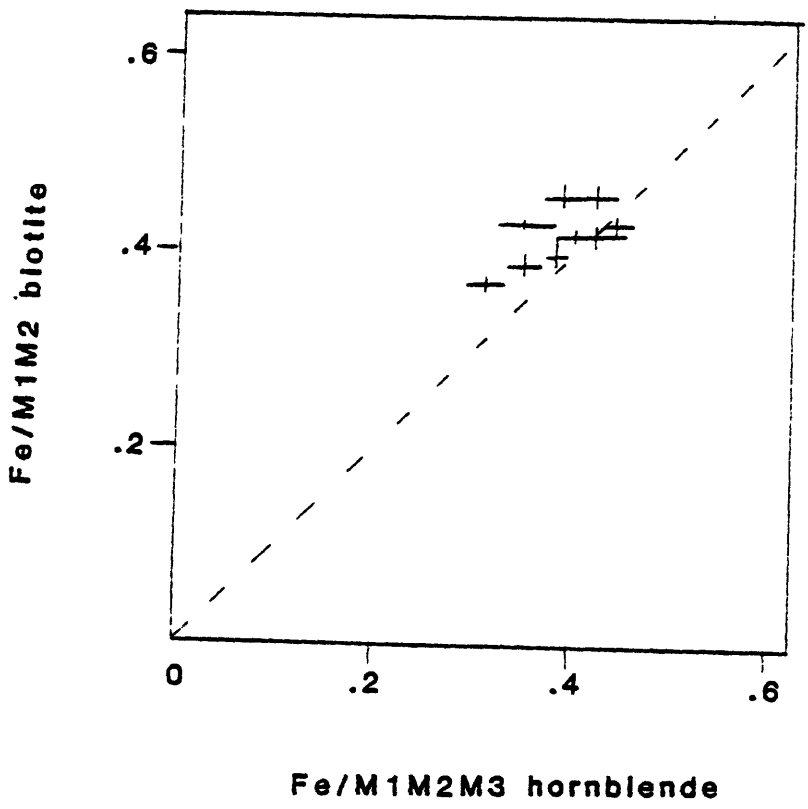

Figure 37. Fe/ΣM sites for biotite and hornblende. Length of crosses represent range of composition for each rock. Distribution of points near the 1:1 slope line suggests that equilibrium is approached.

crude estimate of T and f_{O2} at constant f_{H2O}. Data for the Pioneer biotites where ferrous/ferric ratios were determined are plotted with the experimentally buffered biotite curves of Wones and Eugster (1965) in Fig. 38.

Approximate $Fe^{+3} / Fe^{+2} + Fe^{+3}$ ratios for biotites experimentally buffered on the hematite-magnetite and nickle-bunsenite buffers were 0.25 and 0.10 respectively. Minimum $Fe^{+3}/Fe^{+2}+Fe^{+3}$ estimates for Pioneer biotites range from 0.13 to 0.23. Fe/Fe+Mg for the 16 rocks analysed ranges from 0.41 (southernmost Cretaceous granodiorite sample) to 0.66 (Tertiary muscovite granite).

Compared to other trends for biotites from intrusive complexes, the Pioneer most resemble the trends reported for the Sierra Nevada rocks. A case where biotites from a compositionally zoned granite had uniform major element compositions (Fe/Fe+Mg = 0.45) apparently resulting from late stage equilibration with a constant f_{O2} independent of temperature was reported by Dodge and Moore (1968) for the Cartridge Pass pluton in the Sierra Nevada Batholith. Cases where Fe/Fe+Mg decrease with increasingly fractionated rocks are generally related to oxidation (Finnmarka complex, Czamanske and Wones, 1973; Ploumanach complex, Barriere and Cotton, 1979).

Dodge and Ross (1971) compared relative Fe^{+3}-Fe^{+2}-Mg abundances in coexisting biotites and hornblendes from a variety of calc-alkalic plutonic suites to evaluate the role of oxygen fugacity in mafic silicate paragenesis. Such plots, following Wones and Eugster's (1965) experimental work on biotites, can be useful as an indication of the a) relative effects of oxygen on biotite and hornblende, b) the effec-

tiveness of the mineral assemblage as an oxygen buffer or c)crystallization in an unbuffered system. Dodge and Ross found the Sierra Nevada trend, interpreted as crystallization in a closed system with oxygen fugacities buffered by the mineral assemblage, to be the usual case. Data for the three hornblendes from the Pioneers analysed by wet chemical methods and for the biotites analysed by microprobe and colorimetry are plotted. As in the case for the Sierra Nevada hornblendes, Pioneer hornblendes are more oxidized (higher Fe^{+3}/Fe^{+2}) than coexisting biotites; Fe/Mg values for hornblendes are lower than for biotites.

Fe^{+3}/Fe^{+2} values from bulk analysis of hornblende separates are probably not representative of Fe^{+3}/Fe^{+2} for all compositions observed, especially where brown cores and green rims are noted. Helz (1973) found changes in color in hornblendes encountered in basalt experiments. QFM-buffered hornblendes were green-blue at low temperatures, brown at high temperatures. HM-buffered hornblendes were pale green at all temperatures investigated. Color changes in Pioneer hornblendes may represent a combination of chemical (namely Ti), temperature and oxygen fugacity variations.

Dodge and Ross pointed out that although Fe^{+3} occupies a different structural site in hornblendes, the relative effect of oxygen on Fe^{+3}/Fe^{+2} is probably the same for both minerals. The three Pioneer hornblendes fall along a trend subparallel to Wones' and Eugster's experimentally determined curve for biotites buffered by hematite-magnetite oxygen fugacities. Pioneer biotites however, do not define a smooth trend.

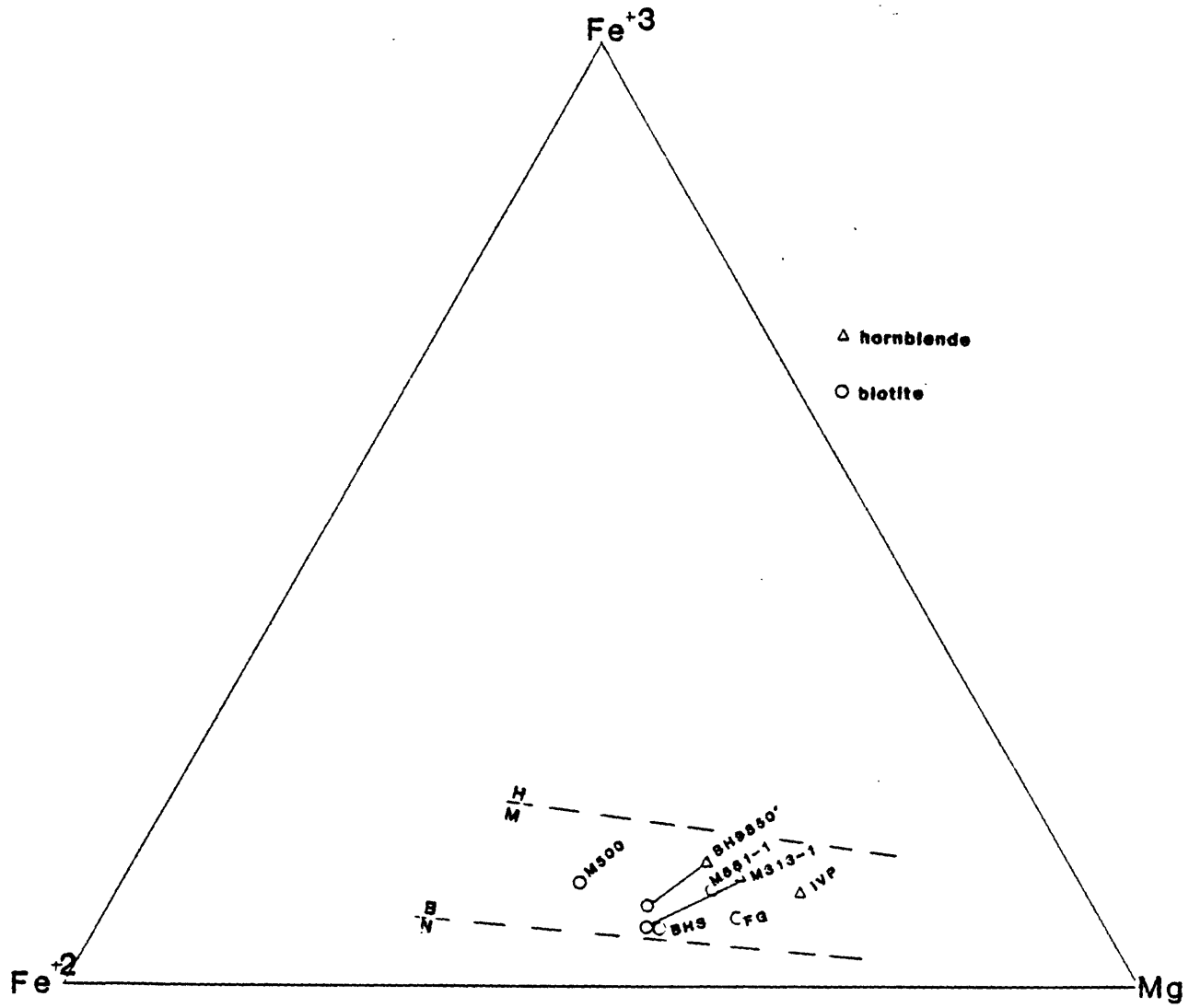

Figure 38. Pioneer biotites and hornblendes in terms of Fe^{+3}, Fe^{+2} and Mg. Only those samples for which Fe^{+3}/Fe^{+2} data are available are shown. Coexisting biotites (circles) and hornblendes (triangles) are connected with a line. Dotted lines represent in trends for experimentally buffered (at fO_2 defined by the nickel-bunsenite buffer) biotites (after Wones and Eugster, 1965).

Wones (1972) described the stability of biotite in equilibrium with potassium feldspar, magnetite and H_2O-bearing melt in terms of temperature, f_{O2} and f_{H2O} as follows:

$$\log f_{H2O} = \frac{7409}{T} + 4.25 + 1/2 \log f_{O2} + 3 \log \alpha^{bt}_{Fe^{+2}} - \log \alpha^{kspar}_{Or} - \log \alpha^{mt},$$

where f = fugacity, a = activity. Hewitt (personal communication, 1981) recently investigated the stability of annite and proposes the following revised expression for biotite-sanidine-magnetite-melt equilibria at oxygen fugacity defined by WM to NB.

$$\log f_{H2O} = \frac{4819}{T} + 6.69 + 1/2 \log f_{O2} + 3 \log X_{annite} - \log a^{MT} - \log a^{KSPAR}_{OR} - \frac{011(P-1)}{T}$$

where $X_{annite} = Fe^{+2}/\Sigma$ octahedral cations. At higher oxygen fugacities (NB to HM buffers), Fe^{+3} increases the stability of biotites of intermediate compositions; thus the revised equation describes the minimum stability curve for oxidized biotites. Stability curves were calculated for three of the Pioneer biotites for which Fe^{+2}/Fe^{+3} data were available. The three samples represent granodiorite, typical Cretaceous granite and muscovite granite. In making these calculations, phase activites were based on microprobe data as follows: mole fraction (x) for Fe^{+2} in biotite was taken from the average value of Fe^{+2}/Σ octahedral cations for each rock; activity of orthoclase in potassium feldspar was taken directly from Or-Ab-An-Cs values computed from microprobe analyses; activity of magnetite was assumed to be 1 because analyses showed magnetite to be pure.

Calculated biotite stability curves in terms of water fugacity and temperature for oxygen fugacities defined by the hematite-magnetite and nickel-bunsenite buffers are shown in Fig. 39A. The observation of hematite lamellae in magnetite and inferred hematite coloring potassium feldspar pink in Cretaceous granite suggest that values defined by the hematite-magnetite are a suitable upper limit on oxygen fugacites; presence of sphene + magnetite in Cretaceous rocks suggests a lower limit on oxygen fugacities near those defined by the nickle-bunsenite buffer, based on the stability of the assemblage sphene + magnetite + hedenbergite + ilmenite + quartz described by Wones (in press). Biotite curves calculated for oxygen fugacity values of the hematite-magnetite buffer do not intersect the granite minimum melting curve. All three biotites intersect the granite curve when lower oxygen fugacity estimates are used in the calculation. The intersection occurs at approximately 500-600 bars water fugacity and temperature around 770-790°C. Although the curves are based on average compositions and are quite similar, the intersection of the curve for biotite from granodiorite occurs at highest temperatures, lowest pressures and that of muscovite granite occurs at lowest temperature. Assuming a water fugacity of 500 bars, these same biotites were plotted as a function of oxygen fugacity and temperature. Czamanske, Wones and Eichelberger (1977) showed that the intersection of biotite stability curves with the nickel-bunsenite buffer curve provides an estimate of the maximum crystallization temperature when the assemblage sphene-magnetite-quartz occurs, implying a lower limit on oxygen fugacities; errors in estimates of water fugacity of 1 kbar result in a shift of only about 0.6 log units for Pioneer

biotite stability curves in terms of temperature and oxygen fugacity are plotted in Fig. 39B. The assemblage sphene + magnetite + quartz does not pertain to the muscovite granite and so actual oxygen fugacities are probably lower than estimated values. Unfortunately, the ilmenite present in these (muscovite granite) rocks is too Mn-rich and altered to reliably estimate a stability curve for ilmenite. The Fe^{+2} values used in calculations are a minimum due to the ease of oxidation of biotite in sample handling and errors in FeO determination. Relative effects of errors in composition and in pressure estimates are indicated by the arrow in Fig. 39B.

Munoz and Ludington (1974) measured F - OH exchange in biotite by fluorine buffering techniques. They demonstrated that F/OH ratios, which are a function of f_{H2O}/f_{HF} in the fluid, Fe/Mg ratios of biotite and temperature, can provide an estimate of the fluid composition and temperature for the last condition of biotite equilibration with a fluorine-bearing fluid. Halogen contents for Pioneer biotites are low (0.4 to 1 wt.% F). Although the data are variable, biotites from muscovite granite tend to be highest in F, biotites from granodiorite tend to be low, and biotites from Cretaceous granite are erratic. For a temperature of 780°C, a maximum, based on the discussion in previous paragraphs, the appropriate Fe/Mg and F/OH ratios for biotites suggest equilibration with a fluid with log f_{H2O}/f_{HF} = 4, which is a value commonly encountered for igneous biotites (Munoz and Ludington, 1974). Biotites in muscovite granite are about twice as rich in fluorine (~ 0.2 atoms F per formula unit) as coexisting muscovite (0.1 or less atoms F per formula unit).

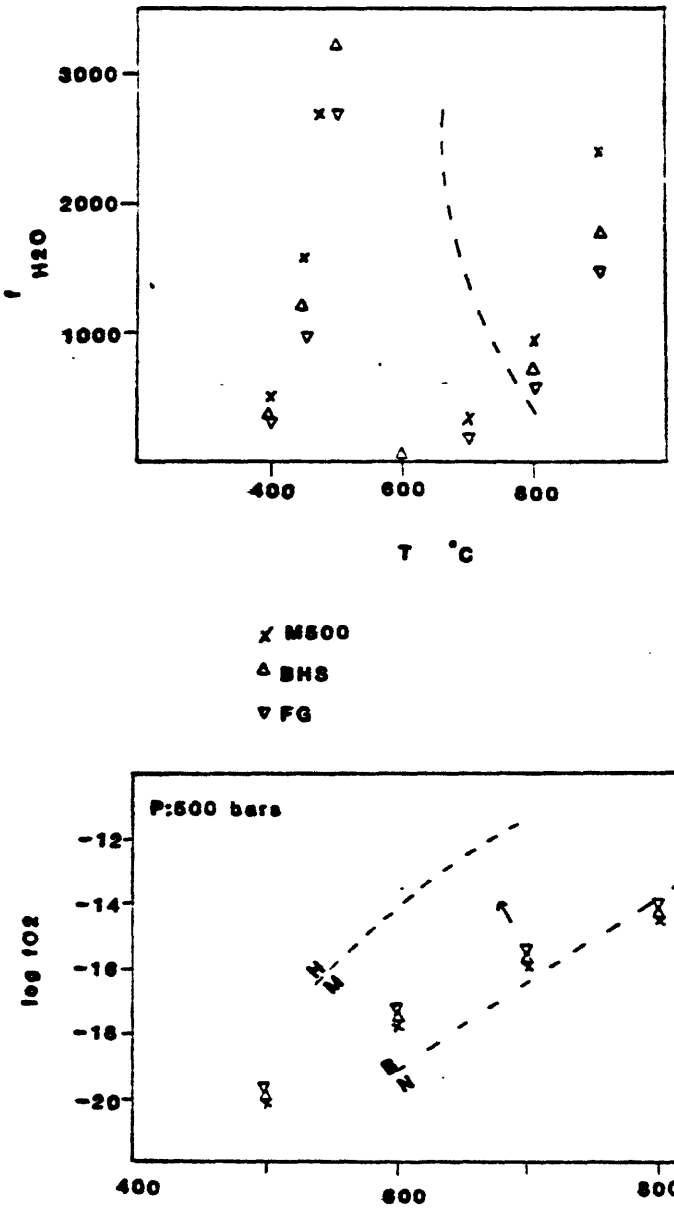

Figure 39. A. Calculated stability curves for 3 Pioneer biotites in terms of f_{H2O} (bars) and T (°C). Dashed line represents the approximate trace of the granite minimum melting curve (Tuttle and Bowen, 1958). Biotite curves calculated for f_{O2} defined by nickel-bunsensite (NB) intersected the granite curve at 760-790°C; biotite curves calculated for hematite-magnetite (HM) f_{O2} conditions do not intersect the granite curve.

B. Same biotite as above in terms of f_{O2} and T. Calculations assume P_{total} = 500 bars, f_{H2O} for P_{H2O} = 500 bars at T taken from Burnham and others (1969).

Although lack of accurate data on halogens OH for micas precludes rigorous assessment of F ⇄ OH exchange, comparison of data on coexisting biotites and muscovites with Munoz and Ludington's (1977) "equilibrometer", which relates log K for biotite and muscovite (log K = Log $(aF/a_{OH})^{bt}$ + log $(a_{OH}/a_F)^{mu}$ to biotite composition (mole fraction Mg in octahedral layer), suggests that some F-loss from biotite may have occurred.

Feldspar geothermometry

Barth (1934) proposed the use of the equilibrium distribution of sodium (albite) between coexisting plagioclase and alkali feldspar as a geothermometer. Stormer (1975) elaborated on the method and published curves relating mole fractions of albite in feldspars to temperature at various pressures, assuming a disordered (sanidine) structural state model for the alkali feldspar. Whitney and Stormer (1976) successfully applied the geothermometer to epizonal plutonic rocks in a study comparing temperatures obtained from Stormer's (1975) curves using expanded beam microprobe data with temperatures obtained from iron titanium oxide mineral geothermometry. The effect of structural state of alkali feldspar on albite distribution was considered by Whitney and Stormer (1977) who presented additional temperature curves for an ordered model (microcline) for alkali feldspar.

Application of the two-feldspar geothermometer requires 1) assessment of textural relations to determine which phases are in equilibrium 2) knowledge of plagioclase composition 3) knowledge of bulk composition and structural state of alkali feldspar and 4) an estimate of total confining pressure.

In the Pioneer rocks, plagioclase is always an early-appearing (liquidus) phase. Textural relations between alkali feldspar and other minerals suggest that it began crystallizing late in the course of magma solidification. Thus it is unlikely that plagioclase cores coexisted in equilibrium with alkali feldspar. Plagioclase-potassium feldspar grain contacts are frequently characterized by myrmekite lobes protruding from the plagioclase into the potassium feldspar. In some cases, a thin rim of albite (An<5) occurs between the two feldspars; this rim probably represents a subsolidus reequilibration event and may represent loss of albite from the potassic phase.

The ranges of feldspar compositions observed for representative samples of Pioneer plutons indicate relatively low (submagmatic) equilibration temperatures when plotted on Whitney and Stormer's (1977) curves for albite distribution between coexisting feldspars at 1 kbar (Fig. 40). Data for albite distribution was taken from microprobe data; the 1 kbar curve were chosen in accord with low pressures for emplacement indicated by field evidence. Increase in estimated pressure displaced the curves towards higher temperatures by about 20°C per kbar (Whitney and Stormer, 1976). Plots are arranged from A to F in order of increasing degree of differentiation (based on differentiation index from rock chemistry). In each case, it is probably reasonable to assume that only the upper portions of each compositional range "box", the plagioclase rim compositions, represent the plagioclase composition in equilibrium with the alkali feldspar. Structural state determinations on alkali feldspar suggest that neither sanidine nor microcline strictly apply, but that some curve intermediate between the two approximates

the true situation. Despite the uniformly low temperatures, there is a hint of a progression from temperatures in the range 500-600°C in the more mafic rocks to temperatures in the range 400-500°C in the muscovite granites. Data did not seem to warrant calculation of specific temperatures for analysed feldspar pairs. Principal causes of error in application of the two-feldspar thermometer which could account for low temperatures are 1) inaccurate determination of the albite component in the alkali feldspar and 2) low estimates of confining pressure.

Extensive reequilibration is not indicated for the batholith as a whole because zoning in both plagioclase and hornblende is preserved as well as zoning of Ba in potassium feldspar. Although the range of Or variation across a given grain of potassium feldpar is limited, highest Or contents are consistently observed near grain margins rather than in cores, suggesting that sodium may have been lost from the feldspar grain.

Muscovites as indicators of pressure

Classical interpretation of pressure of rock crystallization based on the observation of primary (crystallized from a magma) muscovite in a granite is incompatible with a model of crystallization in a low pressure regime. Recent experimental work on stoichiometric muscovite by Chatterjee and Johannes (1974) showed that muscovite is stable as a liquidus phase only at relatively high pressures. The breakdown reaction curve for muscovite + quartz plotted in P-T space intersects the minimum melting curve of granite at ~3.5 kilobars. Muscovite formed below the intersection of these 2 curves must form in the solid state. Translated into rock load pressure, 3.5 kilobars implies more

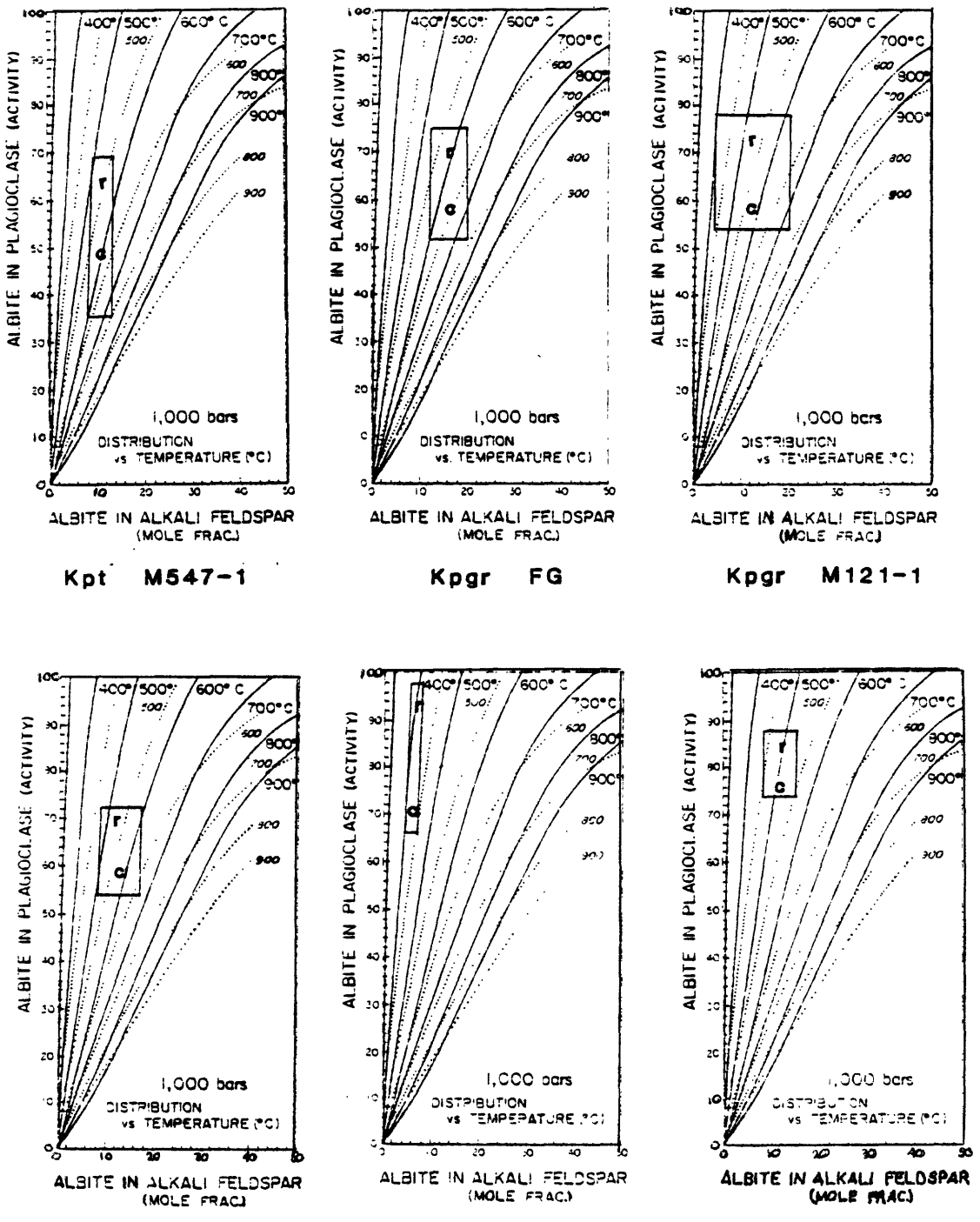

Figure 40. Application of 2 feldspar geothermometry to Pioneer feldspar compositions determined by microprobe analyses. 1 Kbar curves for sanidine (dotted) solid solution model and microcline solid solution model (solid) model are taken from Whitney and Stormer (1977). Boxes show range of compositions for each sample. R = plagioclase rims, C = plagioclase cores. Increasing pressure shifts isotherms to the left, i.e., higher T for a given composition.

than 12 kilometers of overburden above a magma crystallizing muscovite as a liquidus phase. Consequently, many observers of "primary"-looking muscovite in granitic rocks which are interpreted as products of crystallization at shallow depths on the basis of field evidence consider all muscovite in such rocks as a "secondary," subsolidus alteration product rather than a "primary" magmatic phase (see Hyndman, 1972; Benoit, 1971; Bradfish, 1979).

Yoder and Eugster (1955) noted the occurrence of 2 textures of muscovite as interstitial flakes and as sericite in feldspars and suggested that the textures might represent 2 generations of muscovite, one a liquidus phase, one a subsolidus phase. Inherent in the conclusion that primary muscovite + quartz cannot form in a granite magma at pressures less than 3.5 kilobars is the assumption that the experimental work on both granite and muscovite is applicable to the cases under consideration. The P-T curve for granite considered by Yoder and Eugster (1955) was the minimum melting curve for a calcium-free granite (Tuttle and Bowen, 1953, p. 50) and the muscovite used in the experiments was pure, synthetic muscovite. Presence of an An-component raises the granite solidus; other components may have the opposite effect.

The effect of substituents on muscovite stability is not well understood. Miller and others (1981) examined compositional variations in plutonic muscovites and concluded that observed compositions were too non-ideal to use as an indication of pressure. Discussions of the stability of non-ideal muscovite, namely celadonite [$K\ (Mg,Fe^{+2})\ (Fe^{+3}Al)Si_4O_{10}(OH)_2$] relative to the stability of ideal muscovite in recent petrologic literature pose conflicting views (see Bradfish,

1979; Miller and others, 1981; Anderson and Rowley, 1981).

No experimental work bears directly on the problem of magmatic muscovite stability. Velde (1965) experimentally investigated the stability of phengite micas. Velde found that increasing the celadonite component in muscovite at constant pressure decreases the thermal stability of phengite; for constant composition, he found that a pressure increase from 2 to 4.5 kbars slightly expanded the phengite stability field. Velde's work is not directly applicable to the magmatic situation for the following reasons: 1) Ti, an important component in muscovites which are candidates for primary magmatic phases on textural grounds, was not considered in the experiments and 2) the celadonite contents of natural muscovites in plutonic rocks are greater than Velde's phengite stability field would permit at near-magmatic temperatures (Miller and others, 1981). This latter observation, which also applies to the Pioneer muscovites, led Miller and others (1981) to conclude that 1) Velde's data is inapplicable for igneous rocks or 2) that apparent primary muscovite is reequilibrated or secondary in origin.

Wise and Eugster (1964) studied the synthesis and thermal stability of celadonite, $KMgFe^{3+}Si_4O_{10}(OH)_2$, using hydrothermal techniques under conditions of controlled oxygen fugacity with P_{total} = 1000 to 2000 bars. They found that the upper stability limit occurs around 410°C and is only slightly affected by P and f_{O2}. In the P range 1000 to 2000 bars, celadonite broke down to ferriphlogopite + ferrisanidine + quartz + vapor between 400 and 425°C under f_{O2} conditions defined by the nickel-bunsenite buffer.

Bradfish (1979) presented several reactions which could account for subsolidus muscovite. He proposed that the commonly observed association of muscovite with biotite and magnetite may result from a reaction of the type:

$$\underset{(KFe_3AlSi_3O_{10}(OH)_2)}{3\text{biotite}} + 2H^+ + 3/2\ O_2 = \underset{(KAl_3Si_3O_{10}(OH)_2)}{\text{muscovite}} + \underset{(Fe_3O_4)}{3\text{magnetite}} + \underset{(SiO_2)}{6\text{quartz}} + 3H_2O + 2K^+$$

whereas sericite in feldspars may result from reactions of the type:

$$\underset{(NaAlSi_3O_8)}{3\text{albite}} + 2H^+ + K^+ = \underset{(KAl_3Si_3O_{10}(OH)_2)}{\text{muscovite}} + \underset{(SiO_2)}{6\text{quartz}} + Na^+$$

Thus, experimental work on relevant systems lends no support to magmatic muscovite. The effects of Ti and F substitutions, which probably increase the thermal stability of muscovite have not been assessed experimentally.

Bradfish noted that muscovite occurred only in late facies of the intrusive sequence and suggested that the presence of an aqueous phase may have been a key factor in the formation of muscovite.

Zen and others (1980) considered several possible explanations for magmatic muscovite in the apparently high level plutons of the Pioneer rocks, such as lowering the granite solidus temperature by halogens or other components, increasing the load pressure from 1 to 3.5 kilobar in a 10 to 15 million year time span, or crystallizing muscovite at depth in a crystal-liquid mush which was finally emplaced at shallow levels in the crust.

Although no analyses for boron or beryllium have been done on Pioneer rocks, no evidence (accessory tourmaline or beryl, for example) has been observed in support of these elements as major magma components. Chorlton and Martin (1978) showed that addition of 5% B_2O_3 lowers the

solidus of an An-free granite composition by 125°C at PH_2O = 1 kbar. HF and Li_2O are other components which decrease the granite solidus temperature (Wyllie and Tuttle, 1961, 1964). Bailey (1977) reviewed fluorine in granitic rocks and described average F contents of calc-alkalic plutonic series ranging from 0.07 wt.% to 0.11 wt.%, with highest values for biotite and biotite-muscovite granites. This trend reflects the fact that most F in calc-alkalic granites occurs in biotite, with less uptake in hornblende and muscovite. Thirteen whole-rock F analyses for Pioneer rocks indicate a range from 0.02 to 0.08 wt.% F, with all 5 Cretaceous granite samples containing 0.04 wt.% F. No consistent trend is observed in F distribution. As previously described, F and Li contents in micas are not exceptionally high.

Zen, Arth and Marvin (1980) found no field evidence to substantiate the required pressure increase from 1 kbar at 70 Ma when Cretaceous granite was intruded to ~ 4 kbar at 65 Ma, which is the K/Ar date for biotite in the muscovite granite plutons. If the muscovite-bearing plutons represent a deeper level of the same batholith (no miarolites observed in muscovite granite) then considerable structural modification and erosion must have occurred to obliterate the overlying rock load. The only evidence supporting a major erosional event is the absence of volcanics associated with the plutons in the northeastern parts of the batholith (Zen, written communication).

Crystallization of some muscovite at depth and subsequent entrainment in a magma mush emplaced in a lower pressure environment is the most appealing alternative. High Al and Fe contents distinguish biotite in Tertiary granite from biotite in Cretaceous granite. The association

of ilmenite with titanohematite occurs only in Tertiary granite where it is highly oxidized and intimately associated with biotite and muscovite. Ti-free magnetite is observed elsewhere in the same rocks. Sphene is rare in Tertiary granite. Mineral chemistry and mineral assemblage suggest that the micas in Tertiary granite formed in a more reducing environment than the micas in Cretaceous rocks where primary muscovite is absent, biotite iron contents are lower and sphene is ubiquitous. Whether or not this "different" environment is specifically indicative of higher pressure cannot be ascertained.

Opaque Oxide Minerals as Indicators of F_{O2}

The opaque oxide mineral assemblage observed in Pioneer rocks is not amenable to interpretation of intensive parameters such as temperature and oxygen fugacity because a) ilmenite is absent throughout the Cretaceous plutons and b) ilmenite which is present in the Tertiary muscovite granite plutons is extremely Mn-rich and highly oxidized.

Haggerty (1976) discussed the significance of the absence of ilmenite in terms of ilmenite stability with regard to silica activity and oxygen fugacity. Absence of ilmenite with abundance of sphene in Pioneer rocks is consistent the fact that TiO_2 exhibits a greater affinity for CaO than for FeO,MgO and SiO_2. Verhoogan (1962) demonstrated that the association sphene or perovskite + magnetite is more stable than the assemblage ilmenite + diopside at low temperatures and relatively high oxygen fugacities. High oxygen fugacities and high silica activity favor the formation of sphene relative to perovskite.

Wones (1981) reviewed the implications of the assemblage sphene + magnetite with regard to oxygen fugacity and examined thermodynamic data bearing on the reaction

magnetite + sphene + quartz = ilmenite + hedenbergite

$$2Fe_3O_4 + 3CaTiSiO_5 + 3SiO_2 = 3FeTiO_3 + 3CaFeSi_2O_6 + O_2$$

Experimental data place this reaction at oxygen fugacities lying just above those defined by the nickel-bunsenite buffer. Field studies indicate a relatively high prevailing oxidation fugacity for sphene + magnetite assemblages.

Lack of ilmenite and abundance of sphene in Cretaceous rocks suggests that conditions defined by this reaction apply as a lower limit on prevailing oxygen conditions during crystallization of Cretaceous magmas. Presence of hematite in magnetite suggests an upper limit; hematite probably represents a late oxidation event. Haggerty (1976) emphasized the ease with which iron oxide minerals reequilibrate and the difficulty in using them to obtain a record of cryatallization conditions.

Paleocene muscovite granites are characterized by high whole rock FeO/Fe2O3 ratios, high Fe/Mg ratios for biotite, relatively low $Fe^{+3}/Fe^{+2} + Fe^{+3}$ for biotite. Pure magnetite, similar to magnetite found in Cretaceous rocks occurs in Paleocene granite. Sphene is rare to absent. Ilmenite and titanohematite, both Mn-rich, occur as well. One interpretation of the observed mineral assemblage in keeping with a magmatic origin for muscovite, is that muscovite, biotite and Fe-Ti oxide minerals crystallized in an environment characterized by relatively low oxygen fugacities compared to the environment in which Cretaceous rocks crystal-

lized. Final emplacement may have been accompanied by growth of the pure magnetite and oxidation of Fe-Ti minerals at relatively higher oxygen fugacities. Certainly, temperature differences and chemical environment (silica activity, peraluminous character, volatiles) played a complex role in generating the muscovite granites, if in fact, they are related to the Cretaceous rocks at all.

Summary

Mineral compositions for Pioneer rocks preserve some evidence of conditions during magma crystallization and evidence of subsolidus reequilibration. Table XV summarizes primary magmatic vs. reequilibration features.

Hornblendes and biotites record progressive changes from granodiorite to granite to muscovite granite which are consistent with a model of decreasing temperature and oxygen fugacity as crystallization proceeds. Zoning in hornblende and plagioclase is preserved. Plagioclase appears to be a liquidus phase in all rocks and maximum anorthite contents decrease as the rocks become more siliceous. Alkali feldspars do not record magmatic temperatures. Muscovite and iron titanium oxides contain too many impurities to make assumptions about pressure based on experimental work on stoichiometric minerals. Magnetite is observed in plagioclase, biotite and hornblende and is interpreted as a phase which began to crystallize early. Similarly, coarse, euhedral sphene appears to be a primary magmatic phase. Occurrence of magnetite + sphene as primary minerals suggests that the intrinsic oxygen fugacity of the Cretaceous magmas was high (Wones, 1981). Sphene rims on magnetite and granular sphene in mafic silicates

Table XV. Compositional and textural features of Pioneer rocks

Magmatic	Subsolidus reequilibration
zoning in plagioclase (An decreases with increasing rock SiO_2)	thin albite rims at plagioclase-alkalifeldspar contacts
plagioclase synneusis	
myrmekite	
?Ba zoning in alkali feldspar	alkali feldspar bulk compositions
zoning in hornblende (Al, Ti decrease as T decreases, silica activity increases)	Fe/Fe+Mg in hornblende of quartz diorite
decreasing Ti in biotite as rock SiO_2 increases	low Na in biotite
increasing Fe/Fe+Mg in mafic silicates with decreasing f_{O2} from Cretaceous to Paleocene rocks	Fe/Fe+Mg in some Cretaceous biotite
euhedral sphene	granular sphene in mafic silicates
flow banding of biotite (locally observed)	chloritization of biotite
high Ti muscovites cross-cutting biotites or occurring as discrete flakes in Tpg	muscovite (low Ti) in feldspars in all rocks
allanite crystallization	oxidation of opaque oxide minerals

may represent a late magmatic-metamorphic reequilibration.

Biotites from Paleocene granite are distinct from other biotites by virtue of their higher iron content (Fig. 41). Within the Cretaceous rocks, biotites compositions are not a useful discriminant. Hornblendes from the main granodiorite pluton have lower maximum Fe/Mg ratios than hornblendes from the granite pluton. In the problematic zone of contact between the two plutons, hornblende compositions are intermediate. The 4 samples of rocks more mafic than granodiorite (quartz diorite and tonalites) are all from relatively small, border plutons. Sampling of these rocks is too limited to draw any conclusions from mineral compositions other than to say that they are not on the trend of the other rocks. This may indicate 1) that some or all have been affected by later intrusive activity 2) that different conditions (especially oxygen fugacity) prevailed or 3) that they are not genetically related to the granodiorite and granite.

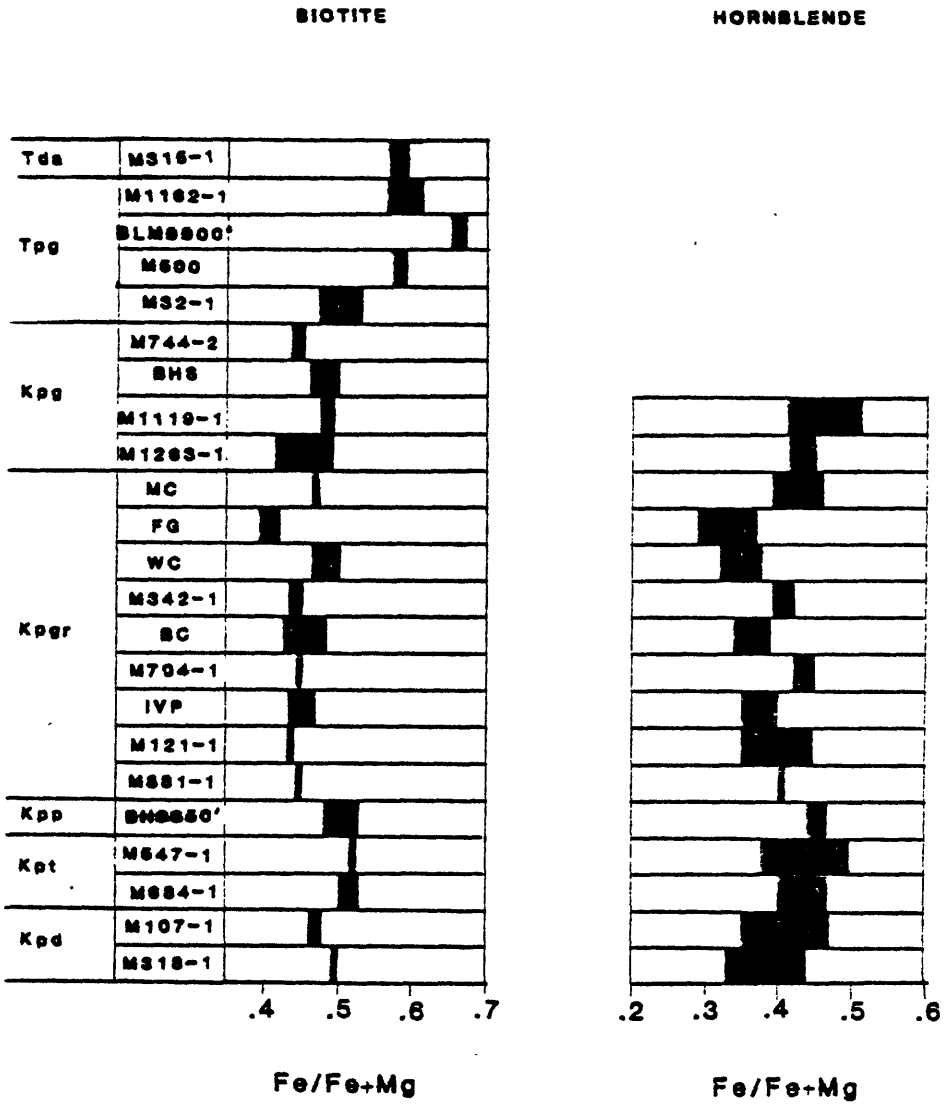

Figure 41. Comparison of observed trends and ranges in composition for Pioneer hornblendes and biotites in terms of Fe/Fe+Mg.

Discussion

The range of rock types observed in the Pioneer batholith (quartz diorite to muscovite granite) and linear major element chemical trends are consistent with a model of magmatic differentiation. High initial strontium ratios for all plutonic rocks suggest that magmas were derived from or heavily contaminated with an upper crustal source (Zen and others, 1980) and variations in initial strontium values suggest that more than one magma and possibly a complex source terrane was involved in the production of Pioneer magmas. Persistence of high initial strontium values from Cretaceous to Paleocene suggest a possible genetic link between plutons of different age. The problem of peraluminous magma generation from a calc-alkalic magma is beyond the scope of this paper. Zen (1980) presented two possible mechanisms consistent with chemical trends in minerals exhibited by the Pioneer rocks. Bradfish (1979) presented a lengthy review of theories of origin of peraluminous magmas cited in current petrologic literature.

Limited data on trace elements and similarities of rare earth patterns are not inconsistent (but do not prove) with magmatic differentiation as the dominant process responsible for variations in Pioneer rocks.

Country rock assimilation does not appear to be a significant factor in accounting for variation in rocks for the following reasons: 1) Sedimentary xenoliths are rare; schlieren and discoid-shaped clots of mafic mineral concentrates are locally abundant but these appear to be cognate (same minerals inside clots as outside, higher concentration of mafic silicates inside clots). 2) Plutons are homogeneous with respect

to mineral assemblage although modal abundances are variable. 3) country rock is carbonate in many places and incorporation of such material is not evident in whole rock CO_2 contents or in initial strontium values, which would tend to be lowered by incorporation of carbonate.

Snee (1978) suggested possible explanations for the lack of consistent trends with time based on studies in the southeastern portions of the batholith, such as changes in the physical conditions at the magma source with time, tapping of different zones of a single magma chamber or formation of different magmas at different levels in the crust.

Strontium data supports a multi-source model for the Pioneer rocks. Trends in mineral chemistry in major plutons suggest that exposed levels represent evolution of one or more (if more, quite similar) magmas largely by differentiation. Pressure quenches may account for the distribution of porphyritic rocks.

Crystallization sequences based on petrographic observations suggest that 1) plagioclase was a liquidus phase for all of the plutonic rocks of the batholith, followed by onset of crystallization of mafic silicates, 2) quartz and alkali feldspar for granodiorite, and 3) alkali feldspar and quartz for granites.

In recent years, comparisons of observed sequences of crystallization for natural rocks with experimentally derived sequences for synthetic granitic rock compositions have been used to estimate water contents of granitic magmas. Whitney (1975) investigated relations in the system $CaAl_2Si_2O_8$-$NaAlSi_3O_8$-$KAlSi_3O_8$-SiO_2 as a function of P, T and water content. Naney (1977) added Fe and Mg to the same system and found

that for a given composition and pressure, the order of crystallization varied as a function of water content. Fig. 42 is modified from Naney's diagrams for 2 kbar crystallization sequences for granodiorite and granite compositions. For the granodiorite compositon, alkali feldspar crystallizes before quartz for low water contents (1.0 weight percent), but at water contents of 3.0% and greater, quartz precedes alkali feldspar. At 3.0% water, orthopyroxene and biotite were the only mafic silicate minerals encountered whereas at higher water contents, hornblende crystallized. For the granite composition, alkali feldspar precedes quartz at all water contents, but biotite preceded alkali feldspar only at 3.5% water.

Although Naney's bulk compositions are not directly comparable to Pioneer rocks, inferred sequences of crystallization agree with experimental data and suggest that Pioneer granodiorite and granite magmas contained moderate (>2 wt%) amounts of water.

Evidence of late magmatic-metamorphic reactions, such as chloritization of biotite and hornblende, formation of sericite and saussurite in feldspars, exists in Pioneer rocks; however, there is no evidence for a pervasive alteration event. Coarse muscovite can be interpreted as a primary magmatic phase or as a subsolidus alteration product. Similarly, epidote, which is particularly abundant in Cretaceous granite, is probably of deuteric origin. Naney and Swanson (1980) reported epidote as a stable phase encountered in crystallization experiments on Fe-Mg bearing granite systems, at magmatic temperatures (600°C). Magmatic epidote has been reported for the Ecstall pluton in the Coast Range of Canada (Chorlton and Martin, 1978) and Whitney and

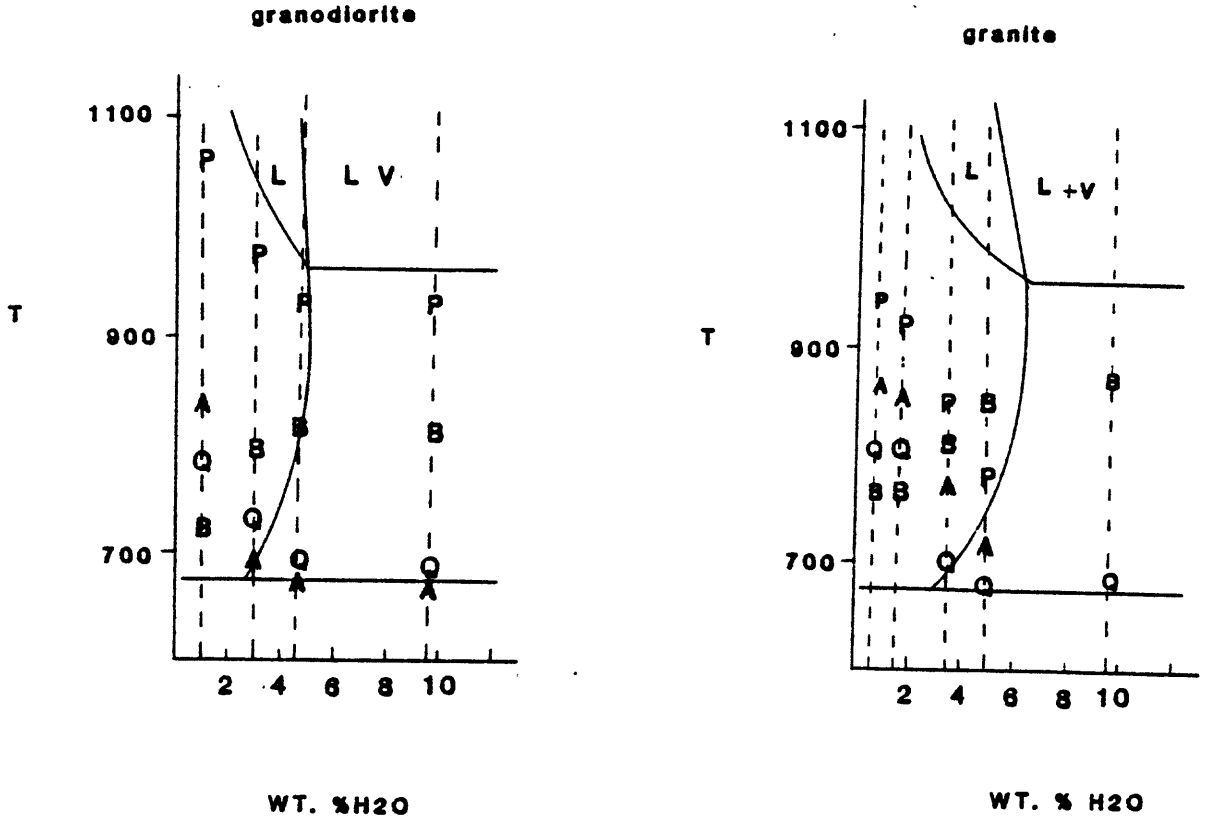

Figure 42. Crystallization sequences for synthetic granite and granodiorite compositions as a function of T and $\%H_2O$ at 2 kbar. Diagrams modified from Naney (1977).

V:vapor	L:liquid
P:plagioclase	A:alkali feldspar
B:biotite	Q:quartz

others (1976) suggested a late magmatic origin for muscovite and epidote in the Stone Mountain Granite by reactions such as

$$4\text{anorthite} + \text{K-feldspar} + 2H_2O = 2\text{clinozoisite} + \text{muscovite} + 2\text{quartz}$$

and

$$6\text{anorthite} + 2\text{K-feldspar} + \text{annite} + 7/2H_2O + 3/4O_2 = 3\ \text{epidote} + 3\text{muscovite} + 3\ \text{quartz}.$$

Crystallization of Stone Mountain granite took place at higher pressures (~ 12 km depth) than pressures inferred for solidification of Pioneer magmas. The association of epidote with chlorite in biotite in Pioneer rocks however, lends support to a subsolidus origin for epidote. Granular sphene, which appears to be compositionally distinct from euhedral sphene is commonly observed with epidote in a given biotite grain.

In recent years, two major trends of thought on the nature of calc-alkalic complexes have arisen in the literature based largely on detailed petrologic studies in Australia and Japan.

The Australian school of thought, led by Chappell and White (1974) contends that granitic rocks (granitoids) may be classified in terms of the nature of their source rocks as I-type (igneous source for magma) or S-type (sedimentary source). Chemical and mineralogical criteria for separating the two types are cited in Table XVI.

The Pioneer rocks cannot be neatly assigned to either category. An I-type character is suggested by wide range of silica, linear variation diagrams, low δO^{18} values (written communication, S. O'Neil), and lack of association with regionally metamorphosed rocks whereas S-type character is suggested by high (>0.710) initial strontium values and

presence of muscovite. The amount of normative corundum in Pioneer rocks ranges from 0 to 2.6%; Na_2O varies from 2.4 to 4.5 wt%. Garnet and aluminum silicate minerals, which are key S-type minerals, are not observed.

In a paper describing granitoid genesis as a product of metamorphism, White and Chappell (1977) presented a molar plot of Al-Na-K:Ca:Fe^{+2} + Mg for whole rock chemical data which neatly separated I- and S-type rocks in Australia. Plotted in these terms, Fig. 43, the Pioneer rocks clearly lie in the I-type region of the diagram.

Despite the obvious utility of these criteria in describing other plutonic assemblages, the Pioneer rocks defy any attempts to propose a simple, consistent model.

The Japanese school of granite classification, proposed by Ishihara (1977), divides rocks observed in the granite belts that span Japan into a "magnetite" and an "ilmenite" series, characterized chiefly by the presence or absence of magnetite. Other criteria used to separate the two series are noted in Table XVII. Ishihara considered oxygen fugacity to be the most important factor leading to formation of one series or the other. Although total iron (whole rock) contents were the same for both groups of rocks, ferric/ferrous ratios differ. Oxygen fugacity conditions aproximating those defined by the nickel-bunsenite buffer are considered as the boundary between the two series. Ishihara noted the association of molybdenite, scheelite-gold deposits, and porphyry coppers with rocks meeting the criteria for the "magnetite" series, whereas "ilmenite" series rocks are associated with tin and wolframite greisen mineralization. He proposed that the presence of

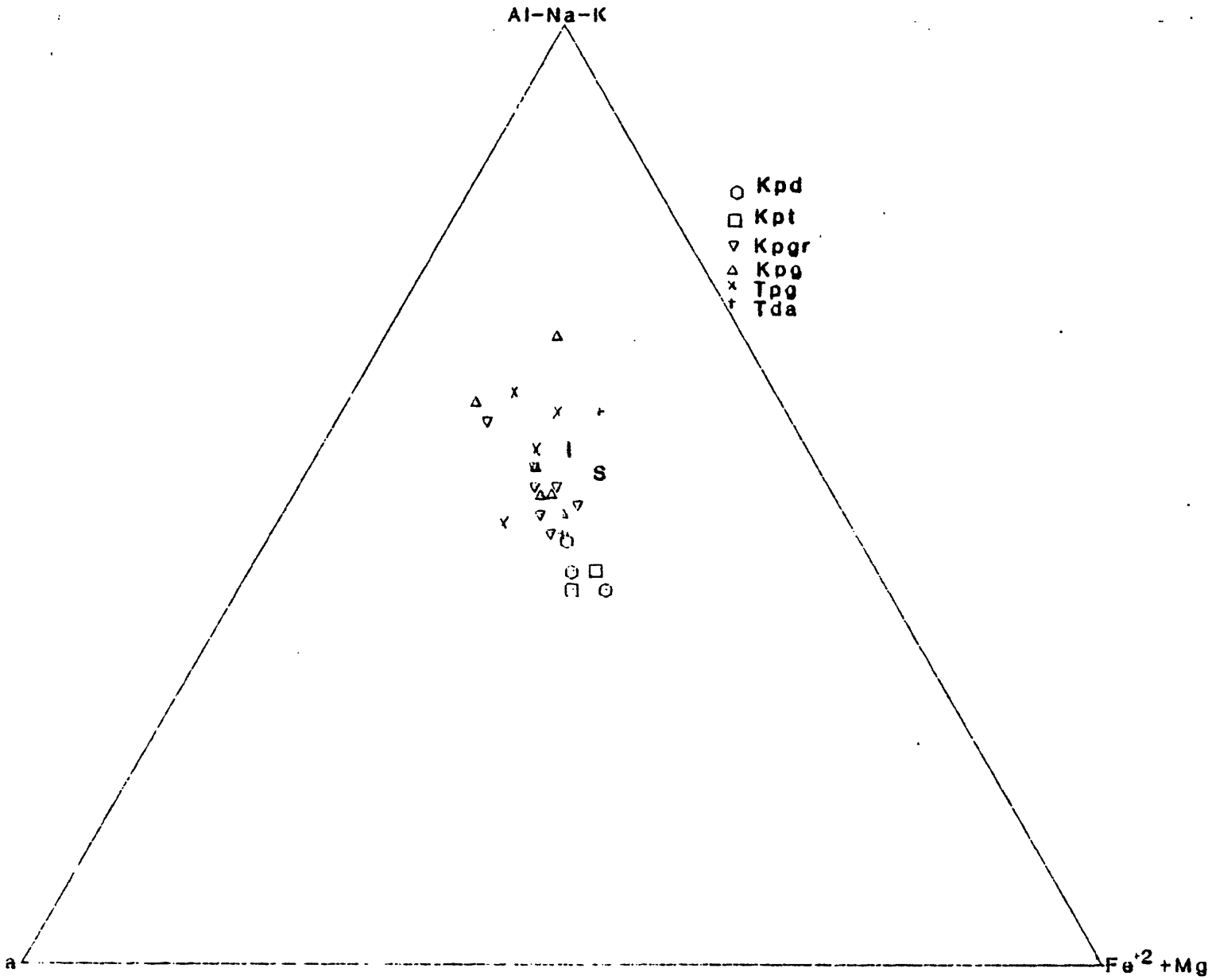

Figure 43. Molar Al-Na-K, Ca, Fe^{+2} + Mg diagram for Pioneer rocks. White and Chappell's "I" and "S" type granite compositions (1977) are plotted for reference.

carbonaceous material in shallow crustal environments contributes to the relatively reducing conditions that give rise to the ilmenite series rocks whereas magnetite series rocks are generated from deeper sources.

Considered in these terms, the Pioneer rocks belong to the "magnetite" series: magnetite is found in all rocks, biotite compositions plot near or above conditions defined by the nickel-bunsenite buffer, associated mineralization is of the scheelite-molybdenite type, and pyrite is the common sulfide mineral.

Table XVI. Characteristics of I- and S-type granitoids

I-type	S-type
Wide range of SiO_2	High SiO_2
<1% normative corundum	>1% normative corundum
Linear major element variation diagrams	Irregular variation diagrams
Low initial strontium .704-.706	High initial strontium >.708
low $\delta^{18}O$ <10	High $\delta^{18}O$ >10
High Na_2O >3.2	Low Na_2O <3.2
	Peraluminous minerals
Not associated with regional metamorphism	Commonly associated with regional metamorphism and migmatites
	Molecular $Al_2O_3/Na_2O + K_2O + CaO$ >1.1

Table XVII.

"Magnetite" Series	"Ilmenite" Series
Magnetite present	Magnetite absent
0.1-2% opaque oxide minerals	<0.1% opaque oxide minerals
Hematite replacing magnetite	
Sulfide = Pyrite	Sulfide = Pyrrhotite
Sphene common	
Epidote	
High Fe^{+3}/Fe^{+2} for biotite	Low Fe^{+3}/Fe^{+2} for biotite
High Mg/Fe for biotite	Low Mg/Fe for biotite

Table XVIII.

Rock Unit	Sample	%SiO_2	Na_2O+K_2O	Slab Modal Mafics	Fe/Fe+Mg Biotite	Fe/Fe+Mg Hornblende	Maximum An in Plagioclase	Mineralogy*
Kpt	M547-1	61.10	6.30	24	.52	.38-.50	An 53	bt, hb, mt, sp
Kpgr	Farlin Gulch	65.50	5.70	13.9	.39-.42	.29-.37	An 49	bt, hb, mt, sp
	Ivanhoe Pit	65.70	5.60	13.4, 15.3	.42-.47	.35-.40	An 44	bt, hb, mt, sp
Near Kpg Contact	M881-1	66.40	7.00	8.4	.44	.40-.41		ht, bt, mt, sp
	M121-1	65.50	7.20	10.6	.43-.44	.35-.44	An 45	hb, bt, mt, sp
Kpg	M1293-1	68.40	6.70	12.5	.41-.50	.41-.45		hb, bt, mt, sp
	BHS	72.80	6.60	4.7	.45-.50		An 45	bt, mt, sp
Tpg	M500-1	73.00	7.70	8.8	.57-.59		An 26	bt, mu, mt, ilm

*+ plagioclase
Kspar quartz

Conclusions

Pertinent changes in rock mineralogy and chemistry and mineral chemistry are summarized in Table XVIII. Results of this study demonstrate that

1) modal, chemical and mineralogic data show changes within given map units

2) mineral compositions record both magmatic and subsolidus reequilibration conditions; zoning in plagioclase and hornblende, related to changes in bulk composition and decreasing temperatures are preserved; alkali feldspars are all Or-rich and do not record magmatic temperatures (<700°C)

3) values of oxygen fugacity were relatively high throughout the crystallization of Cretaceous rocks as evidenced by the abundance of sphene and absence of ilmenite

4) Paleocene rocks have a distinct mineralogy and may have crystallized partly or entirely under different conditions from those that prevailed during crystallization of the Cretaceous rocks.

References

Abrecht, Jurgen and Hewitt, D.A., 1980, Ti-substitution in synthetic Fe-biotites: Geological Society of America Abstracts with Programs, v. 12, no. 7, p. 377.

Albee, A.L. and Ray, L., 1970, Correction factors for electron probe microanalysis of silicates, oxides, carbonates, phosphates and sulfates: Analytical Chemistry, v. 42, p. 1408-1414.

Anderson, J.L., 1980, Mineral equilibria and crystallization conditions in the late Precambrian Wolf River rapakivi massif, Wisconsin: American Journal of Science, v. 280, p. 289-332.

Bailey, J.C., 1977, Fluorine in granitic rocks and melts, a review: Chemical Geology, v. 19, p. 1-42.

Barker, F., Wones, D.R., Sharp, W.N. and Desborough, J.A., 1975, The Peak Peak batholith, Colorado Front Range, and a model for the origin of the gabbro-anorthosite-syenite-potassic granite suite: Precambrin Research, v. 2, p. 97-160.

Barriere, Michel and Cotton, Joseph, 1979, Biotites and associated minerals as markers of magmatic fractionation and deuteric equilibration in granites: Contributions to Mineralogy and Petrology, v. 70, p. 183-192.

Barth, T.F.W., 1934, Polymorphic phenomena and crystal structure: American Journal of Science, v. 5, p. 273.

Bateman, P.C. and Chappell, B.W., 1979, Crystallization, fractionation, and solidification of the Tuolumne Intrusive Series, Yosemite Natioanl Park, California: Geological Society of America Bulletin, Part I, v. 90, p. 465-482.

Bence, A.E. and Albee, A.L., 1968, Empirical correction factors for the electron microanalysis of silicates and oxides: Journal of Geology, v. 76, p. 382-408.

Benoit, W.R., 1971, Vertical zoning and differentiation in granitic rocks - Central Flint Creek Range, Montana: M.S. Thesis, University of Montana, Missoula,Montana, 53 p.

Berger, B.R., Breit, G.N., Siems, D.F., Welsch, E.P., and Speckman, W.S., 1979, A geochemical survey of mineral deposits and stream deposits in the East Pioneer Wilderness Study Area, Beaverhead County, Montana: U.S. Geological Survey Open-file Report 79-1079.

Berger, B.R., Van der Voort, J.L., Siems, D.F., and Welsch, E.P., 1979, Geochemical exploration studies in the Dillon, Montana-Idaho 1° x 2° quadrangle: Geochemical reconnaissance of mining districts in the southern Pioneer Mountains and vicinity, Beaverhead County,

Montana: U.S. Geological Open-file Report 79-1426.

Borg, I.Y., 1967, On conventional calculations of amphible formulae from chemical analyses with inaccurate $H_2O^{(+)}$ and F determinations: Mineralogical Magazine, v. 36, p. 583-590.

Bowen, R.W., 1971, Graphical normative analysis program (Program number C542): U.S. Geological Survey Open-file Report.

Bradfish, L.J., 1979, Petrogenesis of the Tea Cup Granodiorite, Pinal County, Arizona: M.S. thesis, University of Arizona.

Buddington, A.F., 1959, Granite emplacement with special reference to North America: Geological Society of America Bulletin, v. 70, p. 671-747.

Buddington, A.F. and Lindsley, D.H., 1964, Iron titanium oxide minerals and synthetic equivalents: Journal of Petrology, v. 5, p. 310-357.

Burnham, C.W., Holloway, J.R., and Davis, N.F., 1969, Thermodynamic properties of water to 1000°C and 10000 bars: Geological Society of America Special Paper 132.

Chappell, B.W., 1979, Granites as images of their source rocks: Geological Society of America Abstracts with Programs, v. 11, p. 400.

Chappell, B.W. and White, A.J.R., 1974, Two contrasting granite types: Pacific Geology, v. 8, p. 173-174.

Chatterjee, N.D. and Johannes, W., 1974, Thermal stability and standard thermodynamic properties of synthetic $2M_1$-muscovite, $KAl_2[AlSi_3O_{10}(OH)_2]$: Contributions to Mineralogy and Petrology, v. 48, p. 89-114.

Chorlton, L.B. and Martin, R.F., 1978, The effect of boron on the granite solidus: Canadian Mineralogist, V. 16, pt. 2, p. 239-245.

Collins, B.I., 1975, A petrochemical model for the tungsten-bearing skarns in the Pioneer Mountains, Montana: Unpublished Ph. D. thesis, University of Montana, 140 p.

-----, 1977, Formation of scheelite-bearing and scheelite-barren skarns at Lost Creek, Pioneer Mountains, Montana: Economic Geology, v. 72, p.1505-1522.

Crawford, M.L., 1966, Optical properties of metamorphic albite: American Mineralogist, v. 51, p. 523-524.

Czamanske, G.K., Ishihara, Shunso, and Atkin, S.A., 1981, Chemistry of rock-forming minerals of the Cretaceous-Paleocene Batholith in southwestern Japan and implications for magma genesis (in press).

Czamanske, G.K. and Mihalik, P., 1972, Oxidation during magmatic differentiation, Finnmarka complex, Oslo area, Norway: Part I, The opaque oxides: Journal of Petrology, v. 13, p.493-509.

Czamanske, G.K. and Wones, D.R., 1973, Oxidation during magmatic differentiation, Finnmarka complex, Oslo area, Norway: Part 2, The mafic silicates: Journal of Petrology, v. 14, p. 349-380.

Czamanske, G.K., Wones, D.R., and Eichelberger, J.C., 1977, Mineralogy petrology of the intrusive complex of the Pliny Range,New Hampshire: American Journal of Science, v. 277, p. 1073-1123.

Davis, G.A., Anderson, J.L., Frost, E.G., and Shackleford, T.J., 1979, Regional Miocene detachment faulting and Early Tertiary (?) mylonitization, WhippleBuckskin-Rawhide Mountains, southeastern California and western Arizona: Text accompanying Field Guide, Geological Society of America, Annual Meeting

Deer, W.A., Howie, R.A., and Zussman, J., 1963, Rock Forming Minerals, Volume 3, Sheet Silicates: Longmans, Green, and Company,Ltd., London, 270 p.

Dodge, F.C.W. and Moore, J.G., 1968, Occurrence and composition of biotites from the Cartridge Pass Pluton of the Sierra Nevada Batholith, California: U.S. Geological Survey Professional Paper 600-B, p. B6-B10.

Dodge, F.C.W., Papike, J.J., and Mays, R.E., 1968, Hornblendes from granitic rocks of the central Sierra Nevada batholith, California: Journal of Petrology, v. 9, p. 378-410.

Dodge, F.C.W. and Ross, D.C., 1971, Coexisting hornblendes and biotites from granitic rocks near the San Andreas fault, California: Journal of Geology, v. 79, p. 158-172.

Dodge, F.C.W., Smith, V.C., and Mays,R.E., 1969, Biotites from granitic rocks of the central Sierra Nevada batholith, California: Journal of Petrology, v. 10, p. 250-271.

Doe, B.R., Tilling, R.I., Hedge, C.E., and Klepper, M.R., 1968, Lead and strontium isotope studies of the Boulder Batholith, Southwestern Montana: Economic Geology, v. 63, p. 884-906.

Doolan, B.L., Zen, E-an, Bence, A.E., 1978, Highly aluminous hornblendes: compositions and occurrences from southwestern Massachusetts: American Mineralogist, v. 63, p. 1088-1099.

Ernst, W.G., 1968, Amphiboles: New York: Springer-Verlag, New York.

Fleischer, Michael, 1971, Glossary of Mineral Species: Mineralogical Record, Inc., Bowie, Maryland.

Gorbatschev, R., 1977, The influence of some compositional relations on the partitioning of Fe and Mg between biotite and Ca-amphibole: Neues Jahrbuch fur Mineralogie Abh., v. 130, pt. 1-2, p. 3-11.

Greenland, L.P., Gottfried, David, and Tilling, R.I., 1968, Distribution of manganese between coexisting biotite and hornblende in plutonic rocks: Geochimica et Cosmochimica Acta, v. 32, 9. 1149-1163.

Haggerty, S.E., 1976, Opaque mineral oxides in terrestrial igneous rocks: in Oxide Minerals, Mineralogical Society of America Short Course Notes, v. 3, Southern Printing Company, Blacksburg, Va.

Haskin, G.N., 1978, The application of trace elements to the petrogenesis of igneous rocks of granitic composition: Earth and Planetary Science Letters, v. 38, p. 26-43.

Helz, R.T., 1973, Phase relations of basalts in their melting range at P_{H2O}= 5 kb as a function of oxygen fugacity Part I. Mafic phases: Journal of Petrology, v. 14, pt. 2, p. 249-302.

Hewitt, D.A. and Wones, D.R., 1975, Physical properties of some synthetic Fe-Mg-Al trioctahedral biotites: American Mineralogist, v. 60, p. 854-862.

Higgins, J.B. and Ribbe, P.H., 1976, The crystal chemistry and space groups of natural and synthetic titanites: American Mineralogist: v. 61, p. 878-888.

Hutchinson, R.M., 1956, Structural geology of the Browne Lake area, Beaverhead County, Montana: Geological Society of America Bulletin, v. 67, p. 1796-1797.

Hunt, J.A. and Kerrick, D.M., 1977, The stability of sphene: experimental redetermination and geologic implications: Geochimica et Cosmochimica Acta, v. 41, p. 279-288.

Hyndman, D.W., 1972, Petrology of igneous and metamorphic rocks: Mc-Graw Hill,New York.

Ishihara, S., 1977, The magnetite-series and ilmenite-series granitic rocks: Mining Geology, v. 27, p. 293-305.

James, R.S. and Hamilton, D.L., 1969, Phase relations in the system $NaAlSi_3O_8$-$KAlSi_3O_8$-$CaAl_2Si_2O_8$-SiO_2 at 1 kilobar water vapour pressure: Contributions to Mineralogy and Petrology, v. 21, p. 111-141.

Karlstrom, T.N.V., 1948, Geology and ore deposits of the Hecla mining district, Beaverhead County, Montana: Montana Bureau of Mines and Geology Memoir 25, 87 p.

Larsen, E.S., Jr. and Draisin, W.M., 1950, Composition of the minerals in the rocks of the southern California Batholith: Report of the 18th International Geological Congress, Great Britain, 1948, part 2, p. 66-79.

Leake, B.E., 1978, Nomenclature of amphiboles: Canadian Mineralogist, v. 16, p. 501-520.

Luth, W.C., 1969, The systems $NaAlSi_3O_8$-SiO_2 and $KAlSi_3O_8$-SiO_2 at 20 kb and the relationship between H_2O content, P_{H2O} and P_T in granitic magmas: American Journal of Science, v. 276-A, p. 325-342.

Luth, W.C., Jahns, R.H., and Tuttle, O.F., 1964, The granite system at pressures of 4 to 10 kilobars: Journal of Geophysical Research, v. 69, p. 759-773.

Maxwell, J.A., 1968, Rock and mineral analysis: Interscience Publishers, John Wiley and Sons, New York, 584 p.

Miller, C.F., Stoddard, E.F., Bradfish, L.J. and Dollase, W.A., 1981, Composition of plutonic muscovite: genetic implications: Canadian Mineralogist, v. 19, p. 25-34.

Moxham, R.L., 1965, Distribution of minor elements in coexisting hornblendes and biotites: Canadian Mineralogist, v. 8, p.204-240.

Munoz, J.L. and Ludington, S.D., 1974, Fluoride-hydroxyl exchange in biotite: American Journal of Science, v. 274, p. 369-413.

Munoz, J.L. and Lundington, S.D., 1977, Fluorine-hydroxyl exchange in synthetic muscovite and its application to muscovite-biotite assemblages: American Mineralogist, v. 62, p. 304-308.

Myers, W.B.,1952, Geology and mineral deposits of the northwest quarter Willis quadrangle and adjacent Browne's Lake area, Beaverhead County, Montana: U.S. Geological Survey Open-file Report 147, 46p.

Naney, M.T., 1977, Phase equilibria and crystallization in iron- and magnesium-bearing granitic systems: Ph.D. dissertation, Stanford University, 229 p.

Naney, M.T. and Swanson, S.E., 1980, The effect of Fe and Mg on crystallization in granite systems: American Mineralogist, v. 65, p. 639-653.

Nockolds, S.R., 1947, The relation between chemical composition and paragenesis in the biotite micas of igneous rocks: American Journal of Science, v. 245, no. 7, p. 401-420.

Parsons, Ian and Boyd, R., 1971, Distribution of potassium feldspar polymorphs in intrusive sequences: Mineralogical Magazine, v. 38, p. 259-311.

Pattee, E.C., 1960, Tungsten resources of Montana: deposits of the Mount Torrey batholith, Beaverhead County, Montana: U.S. Bureau of Mines Report of Investigations 5552, 41 p.

Peacock, M.A., 1931, Classification of igneous rock series: Journal of Geology, v. 39, p. 54-67.

Pearson, R.C. and Berger, B.R., 1980, Geology and geochemistry of some hydrothermally altered rocks, Pioneer Mountains, Beaverhead County, Montana: U.S. Geological Survey Open-file Report 80-706.

Robert, J.L., 1976, Titanium solubility in synthetic phlogopite solid solutions: Chemical Geology, v. 17, p. 213-226.

Robinson, P., Ross, M. and Jaffe, H.W., 1971, Composition of the anthophyllite- gedrite series, comparisons of gedrite and hornblende, and the anthophyllite-gedrite solvus: American Mineralogist, v. 56, p. 1005-1041.

Rutherford, M.J., 1969, An experimental determination of iron biotite-alkali feldspar equilibria: Journal of Petrology, v. 10, p. 381-408.

Schmidt, E.A. and Worthington, J.E., 1977, Geology and mineralization of the Cannivan Gulch molybdenum deposit, Beaverhead County, Montana: Geological Association of Canada, Programs with Abstracts, v. 2, p. 46.

Shapiro, Leonard, 1956, Rapid analysis of silicate rocks: U.S. Geological Survey Bulletin 1036-C.

Snee, L.W. and Sutter, J.F., 1978, Areal distribution, petrography, and K/Ar dating of the southern portion of the Pioneer Batholith, southwestern Montana: Geological Society of America Abstracts with Programs, v. 10, p. 238.

Snee, L.W., 1978, Petrography, K-Ar ages, and field relations of the igneous rocks of part of the Pioneer Batholith, southwestern Montana: M.S. Thesis, Ohio State University.

Stewart, D.B. and Wright, T.L., 1974, Al/Si order and symmetry of natural alkali feldspars, and the relationship of strained cell parameters to bulk composition: Bulletin de la Societe francaise de Mineralogie et de Cristallographie, v. 97, p. 356-377.

Stormer, J.C., Jr., 1975, A practical two-feldspar geothermomter: American Mineralogist, v. 60, pt. 7-8, p. 667-674.

Streckeisen, A.L., 1973, Plutonic rocks: Classification and nomenclature recommended by the IUGS Subcommission on the Systematics of Igneous Rocks: Geotimes, v. 18, no. 10, p. 26-30.

Theodosis, S.D., 1956, The geology of the Melrose area, Beaverhead and Silver Bow Counties, Montana: Ph. D. thesis, Indiana University, 118 p.

Thompson, A.B., 1974, Calculation of muscovite-paragonite-alkali feldspar phase relations: Contributions to Mineralogy and Petrology, v. 44, p. 173-194.

Tilling, R.I., 1968, Zonal distribution of variations in structural state within the Rader Creek Pluton, Boulder Batholith, Montana: Journal of Petrology, v. 9, p. 331-358.

-----, 1973, Boulder Batholith, Montana: a product of two contemporaneous but chemically distinct magma series: Geological Society of America Bulletin, v. 84, p. 3879-3900.

Tuttle, O.F. and Bowen, N.L., 1958, Origin of granite in the light of experimental studies in the system $NaAlSi_3O_8$-$KAlSi_3O_8$-SiO_2-H_2O: Geological Society of America Memoir 74, 153 p.

Turner, F.J. and Verhoogan, John, 1960, Igneous and metamorphic petrology: McGraw-Hill, New York, 694 p.

Velde, B., 1965, Phengite micas: synthesis, stability and natural occurrence: American Journal of Science, v. 263, p. 886-913.

Verhoogan, J., 1962, Oxidation of iron titanium oxides in igneous rocks: Journal of Geology, v. 70, p. 168-181.

-----, 1962, Distribution of titanium between silicates and oxides in igneous rocks: American Journal of Science, v. 260, p. 211.

Washington, H.S., 1917, Chemical analyses of igneous rocks: U.S. Geological Survey Professional Paper 99, 1201 p.

White, J.R. and Chappell, B.W., 1977, Ultramatamorphism and granitoid genesis: Tectonophysics, v. 43, p. 7-22.

Whitney, J.A. and Stormer, J.C., Jr., 1976, Geothermometry and geobarometry in epizonal granitic intrusions: a comparison of Fe-Ti oxides and coexisting feldspars: American Mineralogist, v. 61, no. 7-8, p. 751-761.

-----, 1977, Two-feldspar geothermometry, geobarometry in mesozonal granitic intrusions: three examples from the Piedmont of Georgia: Contributions to Mineralogy and Petrology, v. 63, p. 51-64.

-----, 1977, The distribution of $NaAlSi_3O_8$ between coexisting microcline and plagioclase and its effect on geothermometric calculations: American Mineralogist, v. 62, p. 687-691.

Whitney, J.A., Jones, L.M., and Walker, R.L., 1976, Age and origin of the Stone Mountain Granite, Lithonia district, Georgia: Geological Society of America Bulletin, v. 87, p. 1067-1077.

Wise, W.S. and Eugster, H.P., 1964, Celadonite: Synthesis, thermal stability and occurrence: American Mineralogist, v. 49, p. 1031-1083.

Wones, D.R., 1980, Contributions of crystallography, mineralogy and petrology to the geology of the Lucerne pluton, Hancock County, Maine: American Mineralogist, v.65, p. 411-437.

-----, 1981, A reexamination of the significance of sphene-magnetite-quartz assemblages in granitic rocks: American Mineralogist (in press).

Wones, D.R. and Eugster, H.P., 1965, Stability of biotite: Experiment, theory, and application: American Mineralogist, v. 50, p. 1228-1272.

Wright, T.L., 1974, Presentation and interpretation of chemical data for igenous rocks: Contributions to Mineralogy and Petrology, v. 48, p. 233-248.

Wright, T.L., 1968, X-ray and optical study of alkali feldspar: II. An x-ray method for determining the composition and structural state from measurement of 2 values for three reflections: American Mineralogist, v. 53, p. 88-104.

Wright, T.L. and Stewart, D.B., 1968, X-ray and optical study of alkali feldspar: I. Determination of composition and structural state from refined unit-cell parameters and 2V: American Mineralogist, v. 53, p. 38-87.

Wyllie, P.J. and Tuttle, O.F., 1961, Experimental investigation of silicate systems containing two volatile components. Part II. The effects of NH_3 and HF, in addition to H_2O, on the melting temperatures of albite and granite: American Journal of Science, v. 259, p. 128-143.

-----, 1964, Experimental investigation of silicate systems containing two volatile components. Part III. The effects of SO_3, P_2O_5, HCl and Li_2O, in addition to H_2O, on the melting temperatures of albite and granite: American Journal of Science, v. 262, p. 930-939.

Yoder, H.S. and Eugster, H.P., 1955, Synthetic and natural muscovites: Geochimica et Cosmochimica Acta, v. 8, p. 225-280.

Zen, E-an, 1977, Some regional tectonic problems inferred from the Pioneer Mountains, Montana: Geological Society of America Abstracts with Programs, v. 9, p.779.

-----, 1980, some possible reactions for deriving muscovite granite

from calc-alkalic granite and granodiorite melts: Geological Society of America Abstracts with Programs, v. 12, no. 7, p. 554.

Zen, E-an, 1981, Metamorphic mineral assemblages of slightly calcic pelitic rocks in and around the Taconic Allocthon, southwestern Massachusetts and adjacent Connecticut and New York: U.S. Geological Survey Professional Paper 1113, 128 p.

Zen, E-an, Arth, J.G., and Marvin, R.F., 1980, Petrology, age and some isotope geochemistry of the Cretaceous and Paleocene intrusive rocks, Pioneer Batholith, southwest Montana: Geological Society of America Abstracts with Programs, v. 12, no. 6, p. 309.

Zen, E-an, Hammarstrom, J.M., Marvin, R.F., and Arth, J.G., 1979, Tertiary volcanic rocks, Pioneer Mountains, southwestern Montana: Geological Society of America Abstracts with Programs, v. 11, no. 6, p. 306.

Zen, E-an, Marvin, R.F., and Mehnert, H.H., 1975, Preliminary petrographic, chemical, and age data on some intrusive and associated contact metamorphic rocks, Pioneer Mountains, southwestern Montana: Geological Society of America Bulletin, v. 86, p. 367-370.

Appendix I

The complete set of microprobe analyses for Kpgr sample WC (coded 333) is given on the following two pages. Three hornblende grains from a single thin section are represented.

Grain 1: points a11-a17

Grain 2: points a21-a22

Grain 3: points a31-a33

Where points were specifically chosen to analyse cores or rims, the location of the point within the grain is noted at the bottom of the table.

Due to heterogeneity of hornblendes in Pioneer rocks, averages were not considered meaningful.

Ferric iron is computed as 27% $Fe^{+3}/Fe^{+3} + Fe^{+2}$. Theoretical water content is assumed (2 OH per formula unit). The following elements were not analysed: Ba, Cl, F, S, Cr, P.

	KPGR 333 HBLD a 13	KPGR 333 HBLD a 14	KPGR 333 HBLD a 15	KPGR 333 HBLD a 16	KPGR 333 HBLD a 17	KPGR 333 HBLD a 21
SiO2	50.82	48.31	48.37	49.53	49.82	46.58
Al2O3	3.31	4.87	4.58	4.17	4.30	6.27
Fe2O3	3.79	4.11	4.03	3.84	3.88	4.37
FeO	9.23	9.99	9.80	9.34	9.45	10.64
MgO	15.23	14.30	14.55	14.82	15.14	13.12
CaO	14.34	13.55	13.66	13.60	13.80	13.66
Na2O	0.40	0.99	0.59	0.60	0.67	0.89
K2O	0.20	0.53	0.42	0.33	0.40	0.79
H2O	0.00	0.00	0.00	0.00	0.00	0.00
TiO2	0.23	0.76	0.62	0.63	0.76	1.05
P2O5	0.00	0.00	0.00	0.00	0.00	0.00
MnO	1.07	1.30	1.32	1.26	1.38	1.01
BaO	0.00	0.00	0.00	0.00	0.00	0.00
Cl	0.00	0.00	0.00	0.00	0.00	0.00
F	0.00	0.00	0.00	0.00	0.00	0.00
S	0.00	0.00	0.00	0.00	0.00	0.00
Cr2O3	0.00	0.00	0.00	0.00	0.00	0.00
SUM	98.63	98.71	97.93	98.12	99.60	98.39
Cl=O	0.00	0.00	0.00	0.00	0.00	0.00
F=O	0.00	0.00	0.00	0.00	0.00	0.00
SUM	98.63	98.71	97.93	98.12	99.60	98.39
H2O calc	2.08	2.05	2.04	2.06	2.09	2.03
SUM	100.71	100.76	99.98	100.18	101.68	100.42
CATIONS ON THE BASIS OF 23 OXYGENS						
Si	7.336	7.050	7.096	7.208	7.157	6.864
Al(iv)	0.563	0.838	0.792	0.715	0.728	1.089
T=	7.899	7.888	7.888	7.923	7.886	7.953
Al(vi)	0.000	0.000	0.000	0.000	0.000	0.000
Fe(iii)	0.412	0.451	0.444	0.420	0.420	0.485
Fe(ii)	1.115	1.220	1.202	1.137	1.135	1.312
Mg	3.277	3.110	3.181	3.214	3.242	2.881
Ti	0.025	0.083	0.068	0.069	0.082	0.116
Mn	0.131	0.136	0.104	0.155	0.122	0.126
M1-M3=	4.959	5.000	5.000	4.996	5.000	4.921
Mn	0.000	0.025	0.060	0.000	0.046	0.000
Fe(ii)	0.000	0.000	0.000	0.000	0.000	0.000
Mg	0.000	0.000	0.000	0.000	0.000	0.000
Ca	2.000	1.975	1.940	2.000	1.954	2.000
Na	0.000	0.000	0.000	0.000	0.000	0.000
M4=	2.000	2.000	2.000	2.000	2.000	2.000
Na	0.112	0.280	0.168	0.169	0.187	0.254
K	0.037	0.099	0.079	0.061	0.073	0.149
Ca	0.218	0.144	0.207	0.121	0.171	0.157
A=	0.367	0.523	0.453	0.351	0.431	0.560
CATSUM	15.226	15.411	15.341	15.271	15.316	15.434
F	0.000	0.000	0.000	0.000	0.000	0.000
CL	0.000	0.000	0.000	0.000	0.000	0.000
OHcalc	2.000	2.000	2.000	2.000	2.000	2.000
ANSUM	2.000	2.000	2.000	2.000	2.000	2.000
Fe/Fe+Mg	0.32	0.35	0.34	0.33	0.32	0.38

	KPGR 333 HBLD a 22	KPGR 333 HBLD a 31	KPGR 333 HBLD a 32	KPGR 333 HBLD a 33	KPGR 333 HBLD a 11	KPGR 333 HBLD a 12
SiO2	46.08	46.29	47.13	45.92	48.89	48.45
Al2O3	6.28	6.37	5.25	5.82	4.37	4.14
Fe2O3	4.38	4.20	3.94	4.22	3.86	3.90
FeO	10.65	10.22	9.59	10.26	9.39	9.49
MgO	13.19	13.48	14.36	13.77	14.87	14.76
CaO	13.39	13.73	13.76	13.67	14.07	13.71
Na2O	0.73	0.80	0.57	0.92	0.82	0.87
K2O	0.74	0.67	0.53	0.69	0.41	0.43
H2O	0.00	0.00	0.00	0.00	0.00	0.00
TiO2	1.14	1.10	0.69	1.08	0.64	0.58
P2O5	0.00	0.00	0.00	0.00	0.00	0.00
MnO	0.86	1.00	1.07	1.01	0.95	1.18
BaO	0.00	0.00	0.00	0.00	0.00	0.00
Cl	0.00	0.00	0.00	0.00	0.00	0.00
F	0.00	0.00	0.00	0.00	0.00	0.00
S	0.00	0.00	0.00	0.00	0.00	0.00
Cr2O3	0.00	0.00	0.00	0.00	0.00	0.00
SUM	97.44	97.86	96.89	97.36	98.27	97.53
Cl=O	0.00	0.00	0.00	0.00	0.00	0.00
F=O	0.00	0.00	0.00	0.00	0.00	0.00
SUM	97.44	97.86	96.89	97.36	98.27	97.53
H2O calc	2.02	2.03	2.02	2.01	2.06	2.04
SUM	99.45	99.89	98.91	99.37	100.32	99.57
CATIONS ON THE BASIS OF		23 OXYGENS				
Si	6.849	6.841	6.994	6.838	7.127	7.132
Al(iv)	1.100	1.110	0.918	1.022	0.751	0.718
T=	7.950	7.950	7.912	7.860	7.878	7.850
Al(vi)	0.000	0.000	0.000	0.000	0.000	0.000
Fe(iii)	0.490	0.467	0.440	0.473	0.423	0.432
Fe(ii)	1.324	1.263	1.190	1.278	1.145	1.168
Mg	2.922	2.969	3.176	3.056	3.231	3.238
Ti	0.127	0.122	0.077	0.121	0.070	0.064
Mn	0.108	0.125	0.117	0.072	0.117	0.098
M1-M3=	4.971	4.946	5.000	5.000	4.986	5.000
Mn	0.000	0.000	0.018	0.055	0.000	0.050
Fe(ii)	0.000	0.000	0.000	0.000	0.000	0.000
Mg	0.000	0.000	0.000	0.000	0.000	0.000
Ca	2.000	2.000	1.982	1.945	2.000	1.950
Na	0.000	0.000	0.000	0.000	0.000	0.000
M4=	2.000	2.000	2.000	2.000	2.000	2.000
Na	0.210	0.229	0.164	0.266	0.232	0.248
K	0.140	0.126	0.100	0.131	0.076	0.085
Ca	0.133	0.174	0.206	0.236	0.198	0.212
A=	0.483	0.530	0.470	0.633	0.506	0.545
CATSUM	15.404	15.426	15.382	15.492	15.370	15.395
F	0.000	0.000	0.000	0.000	0.000	0.000
CL	0.000	0.000	0.000	0.000	0.000	0.000
OHcalc	2.000	2.000	2.000	2.000	2.000	2.000
ANSUM	2.000	2.000	2.000	2.000	2.000	2.000
Fe/Fe+Mg	0.38	0.37 rim	0.34 core	0.36	0.33	0.33

Appendix II

Complete microprobe analyses for Kpgr sample IVP (coded 869) are given on the following pages. Nine analyses, representing 5 grains are included. Average biotite composition for the rock is cited in Table X. Two columns are listed for each analysis: the first column represents the actual micorprobe analysis where all iron is computed as FeO and the second column lists the same analysis with 17% total iron computed as Fe_2O_3. Both F and Cl were analyses for all points. P, Ba, S and Cr were not analysed. Letters in column headings identify the 5 different biotite grains (A-E). Rim vs. core analyses are indicated at the bottom of the tables.

	KPGR 869 BIOT c 1	KPGR 869 BIOT c 1	KPGR 869 BIOT d 11	KPGR 869 BIOT d 11	KPGR 869 BIOT d 12	KPGR 869 BIOT d 12
SiO_2	36.92	36.92	36.64	36.64	35.87	35.87
Al_2O_3	14.78	14.78	14.93	14.93	14.43	14.43
Fe_2O_3	0.00	3.60	0.00	3.34	0.00	3.30
FeO	19.05	15.81	17.69	14.68	17.46	14.49
MgO	11.82	11.82	12.44	12.44	13.18	13.18
CaO	0.16	0.16	0.06	0.06	0.14	0.14
Na_2O	0.13	0.13	0.13	0.13	0.22	0.22
K_2O	8.90	8.90	8.96	8.96	9.12	9.12
H_2O	0.00	0.00	0.00	0.00	0.00	0.00
TiO_2	3.45	3.45	3.47	3.47	3.04	3.04
P_2O_5	0.00	0.00	0.00	0.00	0.00	0.00
MnO	0.58	0.58	0.66	0.66	0.54	0.54
BaO	0.00	0.00	0.00	0.00	0.00	0.00
Cl	0.02	0.02	0.02	0.02	0.03	0.03
F	0.29	0.29	0.30	0.30	0.33	0.33
S	0.00	0.00	0.00	0.00	0.00	0.00
Cr_2O_3	0.00	0.00	0.00	0.00	0.00	0.00
SUM	96.10	96.46	95.30	95.63	94.36	94.69
Cl=0	0.00	0.00	0.00	0.00	0.01	0.01
F=0	0.12	0.12	0.13	0.13	0.14	0.14
SUM	95.97	96.33	95.17	95.50	94.21	94.54
H_2O calc	3.81	3.85	3.80	3.83	3.73	3.76
SUM	99.79	100.18	98.97	99.33	97.94	98.30
CATIONS ON THE BASIS OF 11 OXYGENS						
Si	2.797	2.772	2.785	2.761	2.765	2.741
Al(iv)	1.203	1.228	1.215	1.239	1.235	1.259
T=	4.000	4.000	4.000	4.000	4.000	4.000
Al(vi)	0.118	0.080	0.123	0.088	0.076	0.041
Fe(iii)	0.000	0.203	0.000	0.189	0.000	0.190
Fe(ii)	1.207	0.993	1.125	0.925	1.126	0.926
Mg	1.335	1.322	1.409	1.397	1.514	1.501
Ti	0.197	0.195	0.198	0.197	0.176	0.175
P	0.000	0.000	0.000	0.000	0.000	0.000
Mn	0.037	0.037	0.042	0.042	0.035	0.035
Cr	0.000	0.000	0.000	0.000	0.000	0.000
M=	2.893	2.830	2.898	2.839	2.927	2.867
Ca	0.013	0.013	0.005	0.005	0.012	0.011
Na	0.019	0.019	0.019	0.019	0.033	0.033
K	0.860	0.852	0.869	0.862	0.897	0.889
Ba	0.000	0.000	0.000	0.000	0.000	0.000
A=	0.892	0.884	0.893	0.885	0.941	0.933
CATSUM	7.786	7.714	7.791	7.724	7.868	7.800
F	0.069	0.069	0.072	0.072	0.080	0.080
Cl	0.003	0.003	0.003	0.003	0.004	0.004
H_2O calc	1.928	1.929	1.925	1.926	1.916	1.916
ANSUM	2.000	2.000	2.000	2.000	2.000	2.000
Fe/Fe+Mg	0.47	0.47	0.44	0.44	0.43	0.43

	KPGR 869 BIOT a 11	KPGR 869 BIOT a 11	KPGR 869 BIOT b 1	KPGR 869 BIOT b 1	KPGR 869 BIOT e 1	KPGR 869 BIOT e 1
SiO_2	35.68	35.68	35.92	35.92	36.98	36.98
Al_2O_3	14.93	14.93	14.84	14.84	13.98	13.98
Fe_2O_3	0.00	3.26	0.00	3.27	0.00	3.43
FeO	17.28	14.34	17.32	14.38	18.16	15.07
MgO	12.02	12.02	11.48	11.48	12.14	12.14
CaO	0.02	0.02	0.09	0.09	0.10	0.10
Na_2O	0.03	0.03	0.11	0.11	0.21	0.21
K_2O	9.28	9.28	8.89	8.89	9.38	9.38
H_2O	0.00	0.00	0.00	0.00	0.00	0.00
TiO_2	3.53	3.53	3.87	3.87	3.87	3.87
P_2O_5	0.00	0.00	0.00	0.00	0.00	0.00
MnO	0.46	0.46	0.73	0.73	0.42	0.42
BaO	0.00	0.00	0.00	0.00	0.00	0.00
Cl	0.00	0.00	0.02	0.02	0.04	0.04
F	0.24	0.24	0.44	0.44	0.32	0.32
S	0.00	0.00	0.00	0.00	0.00	0.00
Cr_2O_3	0.00	0.00	0.00	0.00	0.00	0.00
SUM	93.47	93.80	93.71	94.04	95.60	95.94
Cl=0	0.00	0.00	0.00	0.00	0.01	0.01
F=0	0.10	0.10	0.19	0.19	0.13	0.13
SUM	93.37	93.70	93.52	93.85	95.46	95.80
H_2O calc	3.75	3.78	3.66	3.69	3.77	3.81
SUM	97.12	97.48	97.18	97.54	99.23	99.61
CATIONS ON THE BASIS OF 11 OXYGENS						
Si	2.768	2.744	2.783	2.759	2.816	2.791
Al(iv)	1.232	1.256	1.217	1.241	1.184	1.209
T=	4.000	4.000	4.000	4.000	4.000	4.000
Al(vi)	0.133	0.098	0.138	0.103	0.072	0.036
Fe(iii)	0.000	0.189	0.000	0.189	0.000	0.195
Fe(ii)	1.121	0.923	1.122	0.923	1.157	0.952
Mg	1.390	1.378	1.325	1.314	1.378	1.366
Ti	0.206	0.204	0.225	0.224	0.222	0.220
P	0.000	0.000	0.000	0.000	0.000	0.000
Mn	0.030	0.030	0.048	0.047	0.027	0.027
Cr	0.000	0.000	0.000	0.000	0.000	0.000
M=	2.880	2.821	2.859	2.800	2.855	2.794
Ca	0.002	0.002	0.007	0.007	0.008	0.008
Na	0.005	0.004	0.017	0.016	0.031	0.031
K	0.918	0.911	0.879	0.871	0.911	0.903
Ba	0.000	0.000	0.000	0.000	0.000	0.000
A=	0.925	0.917	0.903	0.895	0.951	0.942
CATSUM	7.805	7.738	7.762	7.895	7.806	7.736
F	0.059	0.058	0.108	0.107	0.077	0.076
Cl	0.000	0.000	0.003	0.003	0.005	0.005
H_2O calc	1.941	1.942	1.890	1.891	1.918	1.918
ANSUM	2.000	2.000	2.000	2.000	2.000	2.000
Fe/Fe+Mg	0.45	0.45	0.46	0.46	0.46	0.46

	KPGR 869 BIOT d 13	KPGR 869 BIOT d 13	KPGR 869 BIOT c 11	KPGR 869 BIOT c 11	KPGR 869 BIOT c 12	KPGR 869 BIOT c 12
SiO_2	37.46	37.46	36.50	36.50	37.52	37.52
Al_2O_3	15.05	15.05	14.46	14.46	14.27	14.27
Fe_2O_3	0.00	3.32	0.00	3.37	0.00	3.34
FeO	17.60	14.61	17.82	14.79	17.71	14.70
MgO	13.02	13.02	12.84	12.84	12.83	12.83
CaO	0.07	0.07	0.07	0.07	0.10	0.10
Na_2O	0.10	0.10	0.10	0.10	0.22	0.22
K_2O	9.08	9.08	9.30	9.30	9.29	9.29
H_2O	0.00	0.00	0.00	0.00	0.00	0.00
TiO_2	3.60	3.60	3.44	3.44	3.20	3.20
P_2O_5	0.00	0.00	0.00	0.00	0.00	0.00
MnO	0.63	0.63	0.57	0.57	0.55	0.55
BaO	0.02	0.02	0.00	0.00	0.00	0.00
Cl	0.16	0.16	0.00	0.00	0.07	0.07
F	0.00	0.00	0.16	0.16	0.21	0.21
S	0.00	0.00	0.00	0.00	0.00	0.00
Cr_2O_3	0.00	0.00	0.00	0.00	0.00	0.00
SUM	96.79	97.12	95.26	95.60	95.97	96.30
Cl=0	0.04	0.04	0.00	0.00	0.02	0.02
F=0	0.00	0.00	0.07	0.07	0.09	0.09
SUM	96.75	97.09	95.19	95.53	95.87	96.20
H_2O calc	3.98	4.02	3.86	3.89	3.85	3.89
SUM	100.74	101.10	99.05	99.42	99.72	100.09
CATIONS ON THE BASIS OF 11 OXYGENS						
Si	2.792	2.769	2.781	2.757	2.832	2.808
Al(iv)	1.208	1.231	1.219	1.243	1.168	1.192
T=	4.000	4.000	4.000	4.000	4.000	4.000
Al(vi)	0.115	0.080	0.080	0.044	0.102	0.067
Fe(iii)	0.000	0.185	0.000	0.191	0.000	0.188
Fe(ii)	1.097	0.903	1.136	0.934	1.118	0.920
Mg	1.446	1.434	1.458	1.445	1.443	1.431
Ti	0.202	0.200	0.197	0.195	0.182	0.180
P	0.000	0.000	0.000	0.000	0.000	0.000
Mn	0.040	0.039	0.037	0.036	0.035	0.035
Cr	0.000	0.000	0.000	0.000	0.000	0.000
M=	2.900	2.842	2.907	2.847	2.880	2.821
Ca	0.006	0.006	0.006	0.006	0.008	0.008
Na	0.014	0.014	0.015	0.015	0.032	0.032
K	0.863	0.856	0.904	0.896	0.895	0.887
Ba	0.001	0.001	0.000	0.000	0.000	0.000
A=	0.884	0.877	0.925	0.916	0.935	0.927
CATSUM	7.784	7.718	7.832	7.764	7.815	7.748
F	0.000	0.000	0.039	0.038	0.050	0.050
Cl	0.020	0.020	0.000	0.000	0.009	0.009
H_2O calc	1.980	1.980	1.961	1.962	1.941	1.941
ANSUM	2.000	2.000	2.000	2.000	2.000	2.000
Fe/Fe+Mg	0.43	0.43	0.44	0.44	0.44	0.44

Appendix III

The complete set of microprobe analyses for Tpg sample BLM9800[1] is given on the following pages. Two columns are given for each analysis: the first column treats total iron as FeO as determined by microprobe analysis and the second column repeats the analysis with Fe_2O_3 computed as 66% of the total iron to show the effect of Fe^{+3} on the mineral formula. Theoretical water contents are computed as OH = 2.00 -F-Cl.

Five muscovite grains are represented. Duplicate analyses for points b11 and b12 represent two separate microprobe sessions--one included analysis for fluorine, the other did not.

Averages 1 standard deviation for 3 "primary" and 2 "secondary" muscovites are given below.

	Primary (pts b 11,12 b 41,42 e 11,12)		Secondary (pts d1) X1	
SiO_2	45.61	0.44	46.11	0.08
Al_2O_3	32.19	1.00	32.79	0.75
FeO	4.32	0.53	4.03	0.93
MgO	0.87	0.21	0.78	0.25
CaO	0.06	0.06	0.05	0.05
Na_2O	0.46	0.12	0.29	0.04
K_2O	10.07	0.28	10.40	0.08
TiO_2	0.78	0.11	0.36	0.06
MnO	0.09	0.08	0	
F	0.23	0.14	0.36	0.06
	94.68		95.17	

	TPG 9800 MUSC b 11	TPG 9800 MUSC b 11	TPG 9800 MUSC b 12	TPG 9800 MUSC b 12	TPG 9800 MUSC b 41	TPG 9800 MUSC b 41
SiO2	45.02	45.02	45.53	45.53	45.93	45.93
Al2O3	31.60	31.60	31.80	31.80	31.11	31.11
Fe2O3	0.00	3.20	0.00	3.26	0.00	3.64
FeO	4.37	1.49	4.45	1.51	4.96	1.69
MgO	0.82	0.82	0.76	0.76	1.07	1.07
CaO	0.00	0.00	0.00	0.00	0.00	0.00
Na2O	0.54	0.54	0.41	0.41	0.49	0.49
K2O	10.32	10.32	9.74	9.74	10.40	10.40
H2O	0.00	0.00	0.00	0.00	0.00	0.00
TiO2	0.89	0.89	0.87	0.87	0.72	0.72
P2O5	0.00	0.00	0.00	0.00	0.00	0.00
MnO	0.13	0.13	0.19	0.19	0.00	0.00
BaO	0.00	0.00	0.00	0.00	0.00	0.00
Cl	0.00	0.00	0.00	0.00	0.00	0.00
F	0.00	0.00	0.00	0.00	0.00	0.00
S	0.00	0.00	0.00	0.00	0.00	0.00
Cr2O3	0.00	0.00	0.00	0.00	0.00	0.00
SUM	93.69	94.01	93.75	94.08	94.68	95.04
Cl=O	0.00	0.00	0.00	0.00	0.00	0.00
F=O	0.00	0.00	0.00	0.00	0.00	0.00
SUM	93.69	94.01	93.75	94.08	94.68	95.04
H2O calc	4.34	4.38	4.37	4.40	4.38	4.42
SUM	98.03	98.39	98.12	98.48	99.06	99.46
CATIONS ON THE BASIS OF 11 OXYGENS						
Si	3.108	3.084	3.126	3.102	3.142	3.115
Al(iv)	0.892	0.916	0.874	0.898	0.858	0.885
T=	4.000	4.000	4.000	4.000	4.000	4.000
Al(vi)	1.679	1.637	1.699	1.656	1.651	1.603
Fe(iii)	0.000	0.165	0.000	0.167	0.000	0.186
Fe(ii)	0.252	0.085	0.255	0.086	0.284	0.096
Mg	0.084	0.084	0.078	0.077	0.109	0.108
Ti	0.046	0.046	0.045	0.045	0.037	0.037
P	0.000	0.000	0.000	0.000	0.000	0.000
Mn	0.008	0.008	0.011	0.011	0.000	0.000
Cr	0.000	0.000	0.000	0.000	0.000	0.000
M=	2.070	2.024	2.089	2.042	2.080	2.029
Ca	0.000	0.000	0.000	0.000	0.000	0.000
Na	0.072	0.072	0.055	0.054	0.065	0.064
K	0.909	0.902	0.853	0.847	0.908	0.900
Ba	0.000	0.000	0.000	0.000	0.000	0.000
A=	0.981	0.974	0.908	0.901	0.973	0.964
CATSUM	7.051	6.998	6.996	6.943	7.053	6.994
F	0.000	0.000	0.000	0.000	0.000	0.000
Cl	0.000	0.000	0.000	0.000	0.000	0.000
H2O calc	2.000	2.000	2.000	2.000	2.000	2.000
ANSUM	2.000	2.000	2.000	2.000	2.000	2.000
Na/K	0.08	0.08	0.06	0.06	0.07	0.07

	TPG 9800 MUSC b 11	TPG 9800 MUSC b 11	TPG 9800 MUSC b 12	TPG 9800 MUSC b 12	TPG 9800 MUSC b 42	TPG 9800 MUSC b 42
SiO2	45.75	45.75	45.77	45.77	45.73	45.73
Al2O3	32.21	32.21	33.54	33.54	30.94	30.94
Fe2O3	0.00	3.07	0.00	2.65	0.00	3.78
FeO	4.13	1.42	3.38	1.32	5.16	1.75
MgO	0.79	0.79	0.89	0.89	1.27	1.27
CaO	0.04	0.04	0.15	0.15	0.11	0.11
Na2O	0.51	0.51	0.46	0.46	0.22	0.22
K2O	10.05	10.05	9.81	9.81	10.44	10.44
H2O	0.00	0.00	0.00	0.00	0.00	0.00
TiO2	0.84	0.84	0.90	0.90	0.65	0.65
P2O5	0.00	0.00	0.00	0.00	0.00	0.00
MnO	0.06	0.06	0.19	0.19	0.01	0.01
BaO	0.00	0.00	0.00	0.00	0.00	0.00
Cl	0.00	0.00	0.00	0.00	0.00	0.00
F	0.12	0.12	0.38	0.38	0.08	0.08
S	0.00	0.00	0.00	0.00	0.00	0.00
Cr2O3	0.00	0.00	0.00	0.00	0.00	0.00
SUM	94.55	94.86	95.97	96.25	94.61	94.99
Cl=O	0.00	0.00	0.00	0.00	0.00	0.00
F=O	0.05	0.05	0.16	0.16	0.03	0.03
SUM	94.50	94.81	95.81	96.09	94.58	94.95
H2O calc	4.34	4.37	4.28	4.31	4.33	4.37
SUM	98.84	99.18	100.09	100.41	98.91	99.33
CATIONS ON THE BASIS OF 11 OXYGENS						
Si	3.118	3.096	3.074	3.054	3.137	3.109
Al(iv)	0.882	0.904	0.926	0.946	0.863	0.891
T=	4.000	4.000	4.000	4.000	4.000	4.000
Al(vi)	1.706	1.666	1.729	1.692	1.639	1.589
Fe(iii)	0.000	0.156	0.000	0.143	0.000	0.194
Fe(ii)	0.238	0.080	0.218	0.074	0.296	0.100
Mg	0.080	0.080	0.089	0.088	0.130	0.129
Ti	0.043	0.043	0.045	0.045	0.034	0.033
P	0.000	0.000	0.000	0.000	0.000	0.000
Mn	0.003	0.003	0.011	0.011	0.001	0.001
Cr	0.000	0.000	0.000	0.000	0.000	0.000
M=	2.071	2.028	2.092	2.053	2.099	2.045
Ca	0.003	0.003	0.011	0.011	0.008	0.008
Na	0.067	0.067	0.060	0.060	0.029	0.029
K	0.874	0.868	0.840	0.835	0.914	0.906
Ba	0.000	0.000	0.000	0.000	0.000	0.000
A=	0.944	0.937	0.911	0.905	0.951	0.943
CATSUM	7.015	6.966	7.003	6.958	7.050	6.988
F	0.026	0.026	0.081	0.080	0.017	0.017
Cl	0.000	0.000	0.000	0.000	0.000	0.000
H2O calc	1.974	1.974	1.919	1.920	1.983	1.983
ANSUM	2.000	2.000	2.000	2.000	2.000	2.000
Na/K	0.08	0.08	0.07	0.07	0.03	0.03

	TPG 9800 MUSC e 11	TPG 9800 MUSC e 11	TPG 9800 MUSC e 12	TPG 9800 MUSC e 12	TPG 9800 MUSC d 1	TPG 9800 MUSC d 1
SiO2	46.22	46.22	44.91	44.91	46.17	46.17
Al2O3	33.32	33.32	33.01	33.01	32.26	32.26
Fe2O3	0.00	2.87	0.00	2.69	0.00	3.44
FeO	3.92	1.33	3.67	1.25	4.69	1.59
MgO	0.63	0.63	0.69	0.69	0.96	0.96
CaO	0.15	0.15	0.01	0.01	0.00	0.00
Na2O	0.56	0.56	0.53	0.53	0.32	0.32
K2O	9.82	9.82	9.97	9.97	10.45	10.45
H2O	0.00	0.00	0.00	0.00	0.00	0.00
TiO2	0.73	0.73	0.62	0.62	0.40	0.40
P2O5	0.00	0.00	0.00	0.00	0.00	0.00
MnO	0.14	0.14	0.00	0.00	0.00	0.00
BaO	0.00	0.00	0.00	0.00	0.00	0.00
Cl	0.00	0.00	0.00	0.00	0.00	0.00
F	0.21	0.21	0.37	0.37	0.32	0.32
S	0.00	0.00	0.00	0.00	0.00	0.00
Cr2O3	0.00	0.00	0.00	0.00	0.00	0.00
SUM	95.70	95.99	93.78	94.05	95.57	95.91
Cl=O	0.00	0.00	0.00	0.00	0.00	0.00
F=O	0.09	0.09	0.16	0.16	0.13	0.13
SUM	95.61	95.90	93.62	93.89	95.44	95.78
H2O calc	4.36	4.39	4.19	4.22	4.27	4.31
SUM	99.98	100.29	97.81	98.11	99.71	100.09
CATIONS ON THE BASIS OF 11 OXYGENS						
Si	3.105	3.084	3.085	3.066	3.129	3.104
Al(iv)	0.895	0.916	0.915	0.934	0.871	0.896
T=	4.000	4.000	4.000	4.000	4.000	4.000
Al(vi)	1.743	1.705	1.759	1.723	1.706	1.661
Fe(iii)	0.000	0.144	0.000	0.138	0.000	0.174
Fe(ii)	0.220	0.074	0.211	0.071	0.266	0.090
Mg	0.063	0.063	0.071	0.070	0.097	0.096
Ti	0.037	0.037	0.032	0.032	0.020	0.020
P	0.000	0.000	0.000	0.000	0.000	0.000
Mn	0.008	0.008	0.000	0.000	0.000	0.000
Cr	0.000	0.000	0.000	0.000	0.000	0.000
M=	2.071	2.031	2.073	2.035	2.089	2.041
Ca	0.011	0.011	0.001	0.001	0.000	0.000
Na	0.073	0.072	0.071	0.070	0.042	0.042
K	0.842	0.836	0.874	0.868	0.903	0.896
Ba	0.000	0.000	0.000	0.000	0.000	0.000
A=	0.925	0.919	0.945	0.939	0.946	0.938
CATSUM	6.996	6.951	7.018	6.974	7.035	6.979
F	0.045	0.044	0.080	0.080	0.069	0.068
Cl	0.000	0.000	0.000	0.000	0.000	0.000
H2O calc	1.955	1.956	1.920	1.920	1.931	1.932
ANSUM	2.000	2.000	2.000	2.000	2.000	2.000
Na/K	0.09	0.09	0.08	0.08	0.05	0.05

	TPG 9800 MUSC x 1	TPG 9800 MUSC x 1
SiO2	46.05	46.05
Al2O3	33.32	33.32
Fe2O3	0.00	2.47
FeO	3.37	1.15
MgO	0.60	0.60
CaO	0.09	0.09
Na2O	0.26	0.26
K2O	10.34	10.34
H2O	0.00	0.00
TiO2	0.32	0.32
P2O5	0.00	0.00
MnO	0.00	0.00
BaO	0.00	0.00
Cl	0.00	0.00
F	0.40	0.40
S	0.00	0.00
Cr2O3	0.00	0.00
SUM	94.75	95.00
Cl=O	0.00	0.00
F=O	0.17	0.17
SUM	94.58	94.83
H2O calc	4.23	4.26
SUM	98.81	99.08
CATIONS ON THE BASIS OF 11 OXYGENS		
Si	3.124	3.106
Al(iv)	0.876	0.894
T=	4.000	4.000
Al(vi)	1.786	1.755
Fe(iii)	0.000	0.125
Fe(ii)	0.191	0.065
Mg	0.061	0.060
Ti	0.016	0.016
P	0.000	0.000
Mn	0.000	0.000
Cr	0.000	0.000
M=	2.057	2.022
Ca	0.007	0.007
Na	0.034	0.034
K	0.895	0.890
Ba	0.000	0.000
A=	0.936	0.930
CATSUM	6.992	6.952
F	0.086	0.085
Cl	0.000	0.000
H2O calc	1.914	1.915
ANSUM	2.000	2.000
Na/K	0.04	0.04